CRANFIELD UNIVERSITY

Xiaoheng Jiang

The impact of process variables and wear characteristics on the cutting tool performance using Finite Element Analysis

SCHOOL OF AEROSPACE, TRANSPORT AND MANUFACTURING

MSc by research
Academic Year: 2015 - 2016

Supervisors: Dr Konstantinos Salonitis & Dr Sue Impey

SEPTEMBER 2016

CRANFIELD UNIVERSITY

SCHOOL OF AEROSPACE, TRANSPORT AND MANUFACTURING

MSc by research

Academic Year 2015 - 2016

Xiaoheng Jiang

The impact of process variables and wear characteristics on the cutting tool performance using Finite Element Analysis

Supervisors: Dr Konstantinos Salonitis & Dr Sue Impey

SEPTEMBER 2016

ABSTRACT

The frequent failure of cutting tool in the cutting process may cause a huge loss of money and time especially for hard to machine materials such as titanium alloys. Thus this study is mainly focused on the impact of wear characteristics and process variables on the cutting tool which is ignored by most of researchers. A thermo-mechanical finite element model of orthogonal metal cutting with segment chip formation is presented. This model can be used to predict the process performance in the form of cutting force, temperature distribution and stress distribution as a function of process parameters. Ls-dyna is adopted as the finite element package due to its ability in solving dynamic problems. Ti-6Al-4V is the workpiece material due to its excellent physical property and very hard to machine. This thesis uses the Johnson-Cook constitutive model to represent the flow stress of workpiece material and the Johnson-Cook damage model to simulate the failure of the workpiece elements. The impacts of process variables and tool wear are investigated through changing the value of the variables and tool geometry.

It is found that flank wear length has a linear relationship with the cutting force which is useful for predicting the cutting tool performance. Increasing the crater wear will in some degree diminishes the cutting force and temperature. A chip breakage will also happen in some cases of crater wear.

Through these findings, the relationship between flank wear and cutting power is established which can be used as the guidance in the workshop for changing the tools. The distribution of temperature and stress on the cutting tool in different cutting conditions can be adopted to predict the most possible position forming cutting tool wear.

Keywords: FEM, cutting temperature, Ls-dyna, Ti-6Al-4V, flank wear, crater wear, cutting power

ACKNOWLEDGEMENTS

I would like to express my deep sense of gratitude to Dr Konstantinos Salonitis and Dr Sue Impey for their excellent supervision and patience during my research process in Cranfield University. They teach me a lot of methods needed for doing a research project. It is more important than specific knowledge and will benefit me for a life time.

I am very much thankful to Dr Jorn Mehnen and Dr Chris Sansom for their genius suggestions in my review processes. Their ideas are essential for my research process and the final thesis writing.

I also thank Mr Ben Labo, the employee of Livermore Software Technology Corp. (LSTC), with his help on the Ls-dyna, the simulation process becomes much easier.

It is my privilege to thank my wife Mrs Yongyu Wang and my parents for their love and constant encouragement throughout my research period.

Finally, I would like to give my sincere thanks to my company the Commercial Aircraft Corporation of China, Ltd. and China Scholarship Council for having sponsored and supported my stay in Cranfield University.

TABLE OF CONTENTS

LIST OF FIGURES

LIST OF TABLES

LIST OF ABBREVIATIONS

ALE	Arbitrary Lagrangian–Eulerian
BUE	Build-up edge
DOE	Design of experiments
FEA	Finite Element Analysis
FEM	Finite Element Method
RSM	Response surface methodology

1 Introduction

1.1 The background of the research

Since the development of the CNC machining technology, metal cutting industry has become a significant sector both in the developed and developing countries. It is not only widely used in high technology industries such as automotive engine, robot and aerospace, but also in some ordinary products such as the gears in the bicycle. Rhodes [1] mentioned that the manufacturing industry accounted for 10% or £150.7 billion economic output of UK and employed around 2.6 million people in 2013. Metal cutting sector was about 11% of the total manufacturing industry. Jablonowski and Eigel-Miller [2] pointed out that in 2012 the machine-tool output value by 28 principal producing countries in the world was $94.3 billion. Thus, it is vital to investigate the metal cutting process to create more value for the society.

The metal cutting process is usually consisted of cutting machine, fixture, tool holder, cutting tool and workpiece. Generally, the cutting machine, fixture and tool holder can be used for a long time and still have acceptable accuracy. For cutting tool, the failure of it may not only lead to the rejection of the final part and waste of the time waiting for the tool to be discarded or repaired but also cause the break down of the expensive cutting machine even interrupting the whole production line. Thus, the cutting tool has to be replaced before the end of its life in order to get the designed dimensional accuracy and surface finishing since the happening of cutting tool wear in the cutting process. Salonitis & Kolios [3] mentioned that only 50–80 % of the expected tool life is typically used according to [4].

Thus, it is very important to understand metal cutting process including the types of cutting tool wear the causes of tool wear, and the mechanisms behind them. After that, the impacts of various cutting parameters and the cutting tool wear on the cutting tool should be investigated.

Many methods can be applied to study the impacts of various cutting parameters and the cutting tool wear.

People acquire some results from the experiments in the first place. These are very helpful to understand the whole cutting process. However,

experiments can be very expensive and time consuming, especially for machining process. Workpiece material may be damaged, the machine is occupied, people have to spend a lot of time observing the process and recording the data. The most frustrating thing is that when a small cutting condition (such as cutting speed) is changed, the experiment's results cannot be adopted anymore.

Modelling of the cutting process is another way to investigate the metal cutting. Markopoulos [5] introduced the brief history of the developing of modelling methods. In the original thoughts, researchers were trying to use theoretic and modelling methods to estimate the performance of the cutting process and find out solutions for realistic problems in the workshop without any experimental work. Around 1900s, simplified analytical models started publishing. In 1950s, modelling methods took the leading place for understanding machining mechanism and investigating the cutting process. In the early 1970s, papers using Finite Element Method (FEM) on machining process modelling began to publish in scientific journals. Through the development of computing ability and commercial FEM software, FEM method has become the favourite modelling tool for researchers in the cutting area. By using the finite element methods, basic knowledge about the machining mechanisms is acquired. Researchers can learn the process parameters such as temperature, strain, stress, cutting force from the model and predict the quality of the product conveniently.

In this thesis, an orthogonal metal cutting model is established using finite element method. In chapter two, literature review will be carried out to understand the previous work and find out the research gap for the thesis. In chapter three, aims and objectives will be emphasized. Research methodology will be explained in the following chapter. Fundamental knowledge for modelling metal cutting process are presented in chapter five. In chapter six, present cutting model is explained. Model validation will be carried out in chapter seven. Results and discussion are presented in chapter eight. In the final chapter, the conclusion of the study is given.

1.2 Aim and objectives of the research

Due to the importance of the cutting tool in the machining process and the absence of papers on the impacts of process variables and wear characteristics on the cutting tool, the aim of the present thesis will be:

Investigating the impacts that various process parameters and tool wear characteristics have on the cutting tool and link the wear evolution with measurable machine tool metrics.

The objectives of the research are to:

1. Develop a cutting model using commercial FE package to predict the cutting process variables (such as cutting temperature, forces etc.)
2. Validate the FE model using experiment results from the published literatures
3. Predict the effects of cutting speed, depth, tool edge radius and wear geometry on the cutting force, stress and temperature distribution mainly on cutting tool
4. Establish the relationship between flank wear and machine power, in order to predict a critical spindle power value for changing the cutting tool

1.3 Research methodology

The research process will follow 5 phases which is shown in Figure 1-1.

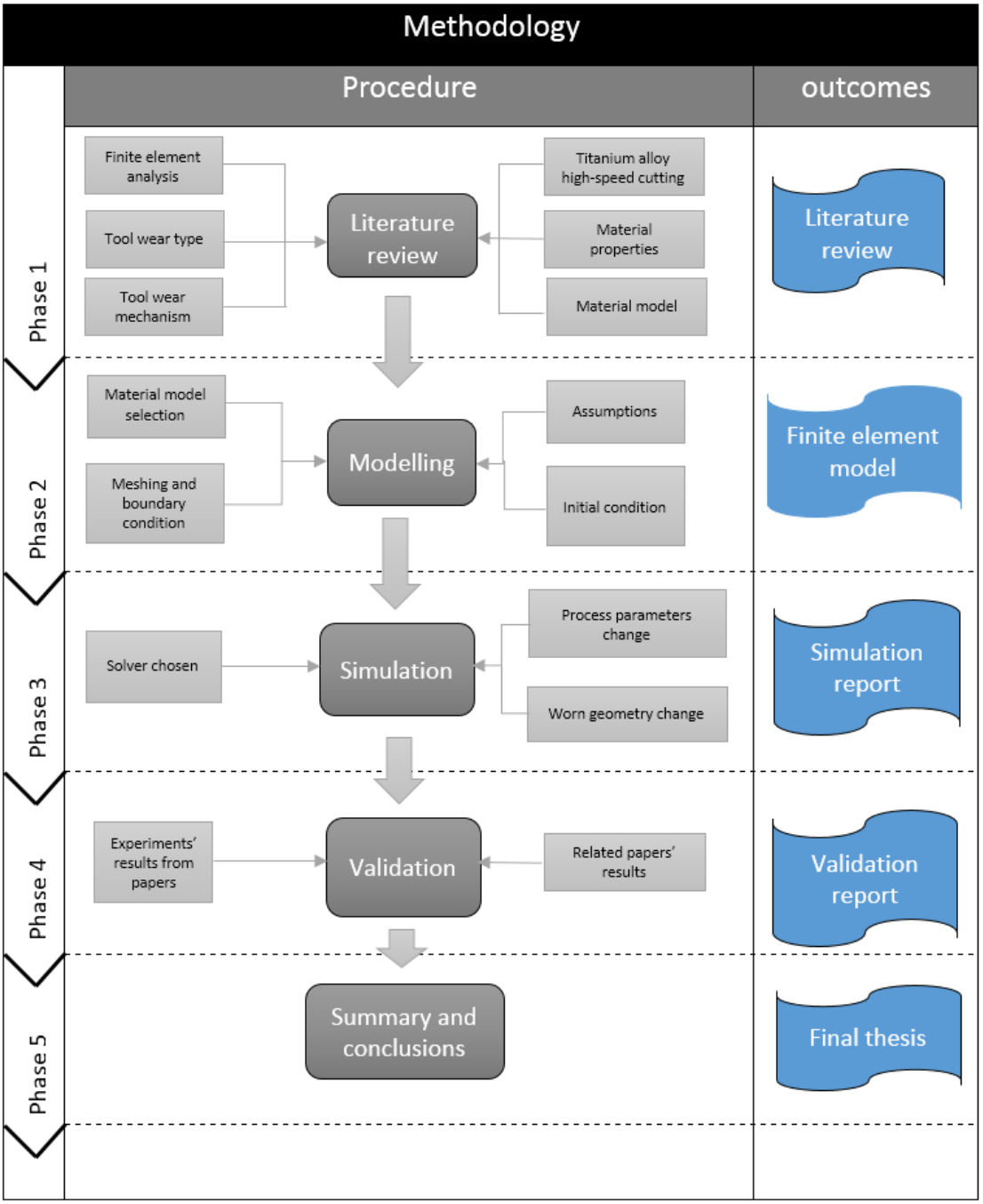

Figure 1-1 Research methodology

In the phase 1, literature review will be done mainly about the software, the material model and the tool wear background information. In this phase, the most important thing is to get a general idea about the research gap, aims, objectives, and way to finish this project.

In the phase 2, tool wear model will be built through the commercial finite element software Ls-dyna. In this progress, material model, structure meshing, remeshing process, code development and separation criterial are needed to be considered. Some assumption will be made in this phase in order to simplify the model. But the most important thing is to make sure the accuracy of this simplified model. The model has to be validated through some experiments or tests done by other papers by comparing the simulation results. So the modelling process may be updated in some cases. The modelling phase is the most significant in all these five phases.

In phase 3, the simulation process will be done. The simulation plan needs to be carried out. Process parameters and the tool wear geometry will be changed in order to investigate the impact. Each simulation instant may be time consuming, and a lot of simulation will be needed in this phase. Choosing the suitable information for comparing is another challenge in the simulation process. Some basic skills may help to analysis the results such as office skills.

In phase 4, validating the model using the experimental results from published papers is the main work. Parameters must be chosen carefully in order to keep the same as the experiments. The results may be different from the experiments. Revising the model should be done until an acceptable result is achieved.

Finally, in phase 5, the whole progress will be summarized, some great ideas and drawbacks will be concluded in the final paper. Using less information to present the whole process is not only a challenge but also a basic skill for a qualified researcher.

2 Literature review

In this chapter, the previous work on cutting tool wear and finite element method will be reviewed. Research gap will be defined in the end according to the key findings in the present papers.

A total of 180 papers were selected through the keywords: FEM, FEA, cutting tool wear, wear evolution, tool life, titanium alloy, wear mechanism, explicit, implicit, analytical model, slip line, shear plane and ls-dyna. The papers are chosen from journals such as International Journal of Advanced Manufacturing Technology, Journal of Materials Processing Technology, Procedia CIRP, International Journal of Machine Tools and Manufacture, Wear, Journal of the Mechanics and Physics of Solids, CIRP Annals - Manufacturing Technology, Procedia Engineering.

According to the stage of development, the work on cutting tool wear and modelling can be classified into five groups: fundamental knowledge such as types of tool wear and the mechanisms behind them, the elements influencing tool wear, tool life and wear evolution models, analytical models and the finite element method.

2.1 The tool wear types and tool wear mechanisms

Stephenson and Agapiou [6] identified 10 principle types of tool wear according to the influencing regions on the tool: flank wear, crater wear, notch wear, nose radius wear, thermal or mechanism fatigue crack, build-up edge (BUE), plastic deformation, edge chipping, chip hammering and tool fracture. The shape and position of flank wear and crater wear are shown in Figure 2-1.

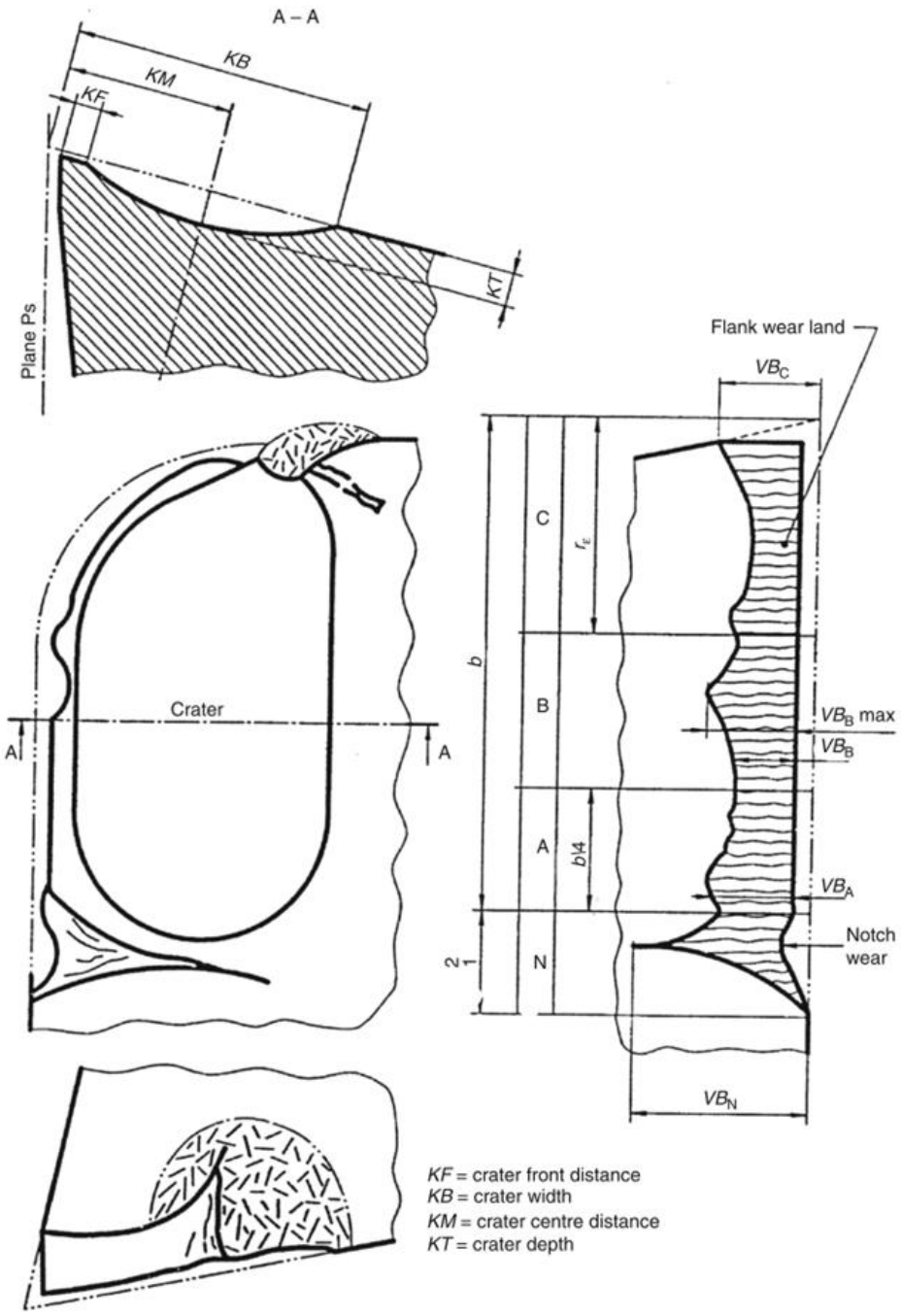

Figure 2-1 Flank wear and crater wear [7]

Because of its predictable and consistent properties, flank wear become the most desirable tool failure mode. Its evolution can be explained as Figure 2-2 which illustrated in [3].

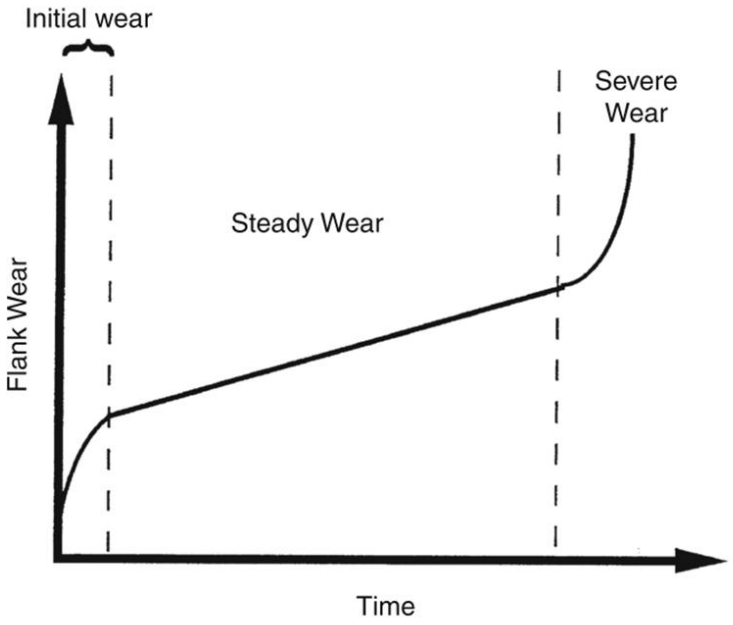

Figure 2-2 Tool wear evolution [8]

The cutting edge of the tool becomes rounded at the beginning. Then a stable period is reached when the flank wear increases linear with the time. However, after a critical value of wear land is reached, the flank wear increases rapidly [8].

The physical mechanisms that produce various types of wear depend on the materials of workpiece and cutting tool, geometry of cutting tool, surface finish and the cutting conditions.

Salonitis and Kolios [3] draw a brief conclusion about tool wear mechanism for different wear types in Figure 2-3.

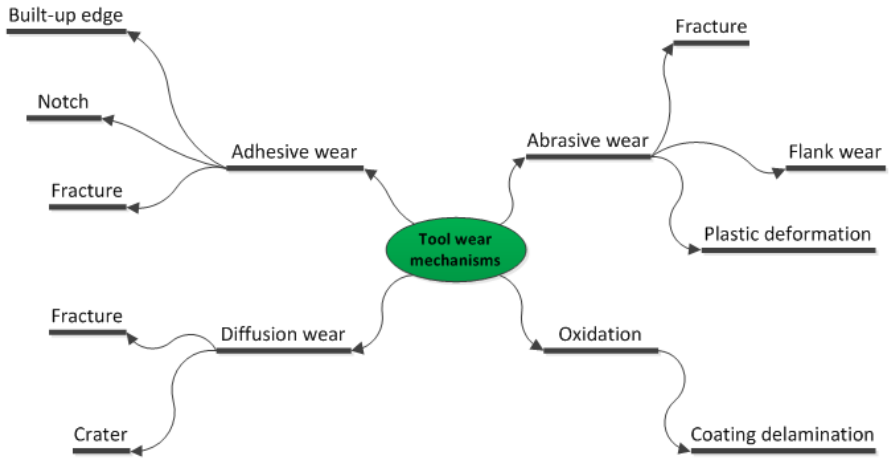

Figure 2-3 Tool wear mechanism for different wear types [3]

Wang et al. [8] explained each wear mechanism carefully and provided methods to prevent certain type of wear. It is mentioned that using one equation to describe both adhesive and abrasive wear is possible [9].

$$\mathrm{V} = \frac{K_w N L_s}{H} \qquad (2\text{-}1)$$

Where V is the volume of material worn away, K_w is the wear coefficient, N is the force normal to the sliding interface, L_s is the slid distance, and H is the penetration hardness of the tool.

This equation shows some effective methods of controlling wear due to adhesive and abrasive wear mechanisms.

Increasing the hardness H of the cutting tool is the simplest way. Choosing a material with higher hardness and coating the surface of the cutting tool are both effective way to prevent wear. Other than that, reducing cutting force, which is N, can also decrease wear rate under these conditions. Decreasing cutting speed is another way to diminish the wear rate. The cutting speed has two major effects on the tool wear rate. First of all, the sliding distance L_s has a positive relationship with the cutting speed. Secondly, the temperature raises on the cutting tool as the increasing the cutting speed which reduces the hardness of the tool [8].

Plastic deformation of the cutting tool edge is also caused by this thermal softening phenomenon [8].

2.2 The elements influencing tool wear

Yen et al. [10] summarised the elements influencing cutting tool wear in four major groups, as show in Figure 2-4.

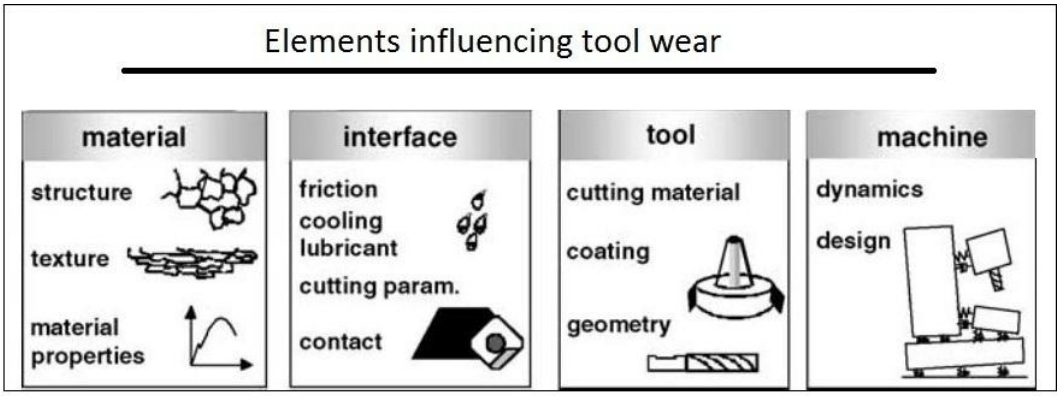

Figure 2-4 Four major elements influencing tool wear in machining process [10].

Almost all of these elements have been deeply investigated. Machine problem will not be mentioned in this part because most of the problems are referred to maintenance. Sahin et al. [11] paid attention to the effects of material structures on the tool wear and surface roughness in the turning of Al_2O_3 particle-reinforced aluminum alloy composite. Flank wear of the cutting tool is investigated from different particle sizes and cutting speed. Arulkirubakaran et al. [12] employed the surface finishing on the rake faces in machining Ti-6Al-4V alloy using numerical simulation software deform 3D. A larger reduction in cutting force, temperature generation and tool wear were exhibited in the direction perpendicular to chip flow when using the cutting tools with surface textures

The friction in the metal cutting process is very complicated. Li [13] focused on the basic aspects of friction modelling in cutting and the influence of friction modelling on numerical simulation process. Cooling and lubrication could reduce the temperature in the cutting zone, thus prolong the cutting tool

life. However, the cycle of heat and cooling on the cutting tool will cause thermal fatigue, and eventually lead to failure.

Cutting tool life empirical models can provide some clues to the importance of cutting parameters. Taylor's equation is the first cutting tool life model. It can be expressed as the simple relationship between cutting speed (V) and tool life (T) [14]:

$$VT^n = C \tag{2-2}$$

Where n and C are constants. The exact number depends on feed, depth of cut, workpiece material, and cutting tool material. From Taylor's equation, cutting speed plays an important role in the machining process. Due to its limitation, Taylor's equation was changed into different kinds of forms where other cutting parameters are considered. One of these examples is [15]:

$$VT^n f^m d^p = C \tag{2-3}$$

Where V is the cutting speed, T is the tool life, f is the feed rate, and d is the depth of cut. Constants n,m, p and C depend on the characteristics of the process and are experimentally derived. Davis [16] compared the properties of different cutting tool materials in Figure 2-5 and suggested about the tool selection methodology shown as Figure 2-6 which is very useful for the manufacturing engineers.

Parameter	Carbon and low–medium alloy steels	High speed steels	Cast cobalt alloys	Carbides: Cemented	Carbides: Coated	Ceramics	Polycrystalline cBN	Diamond
hot hardness	———	———	increasing →	→	→	→	→	
toughness	———	———	decreasing →	→	→	→	→	
impact strength	———	———	decreasing →	→	→	→	→	
wear resistance	———	———	increasing →	→	→	→	→	
chipping resistance	———	———	decreasing →	→	→	→	→	
cutting speed	———	———	increasing →	→	→	→	→	
depth of cut	light to medium	light to heavy	light to heavy	light to heavy	light to heavy	light to heavy	light to heavy	very light for single crystal diamond
finish obtainable	rough	rough	rough	good	good	very good	very good	excellent
method of processing	wrought	wrought, cast, HIP sintering	cast and HIP sintering	cold pressing and sintering	CVD PVD	cold pressing and sinter-ing or HIP	high pressure–high tempera-ture sintering	high pressure–high tempera-ture sintering
fabrication	machining and grinding	machining and grinding	grinding	grinding or as molded		grinding	grinding and polishing	grinding and polishing
thermal shock resistance	———	———	———	decreasing →	→	→	→	
tool material cost	———	———	increasing →	→	→	→	→	

Figure 2-5 Properties of cutting tool materials [16]

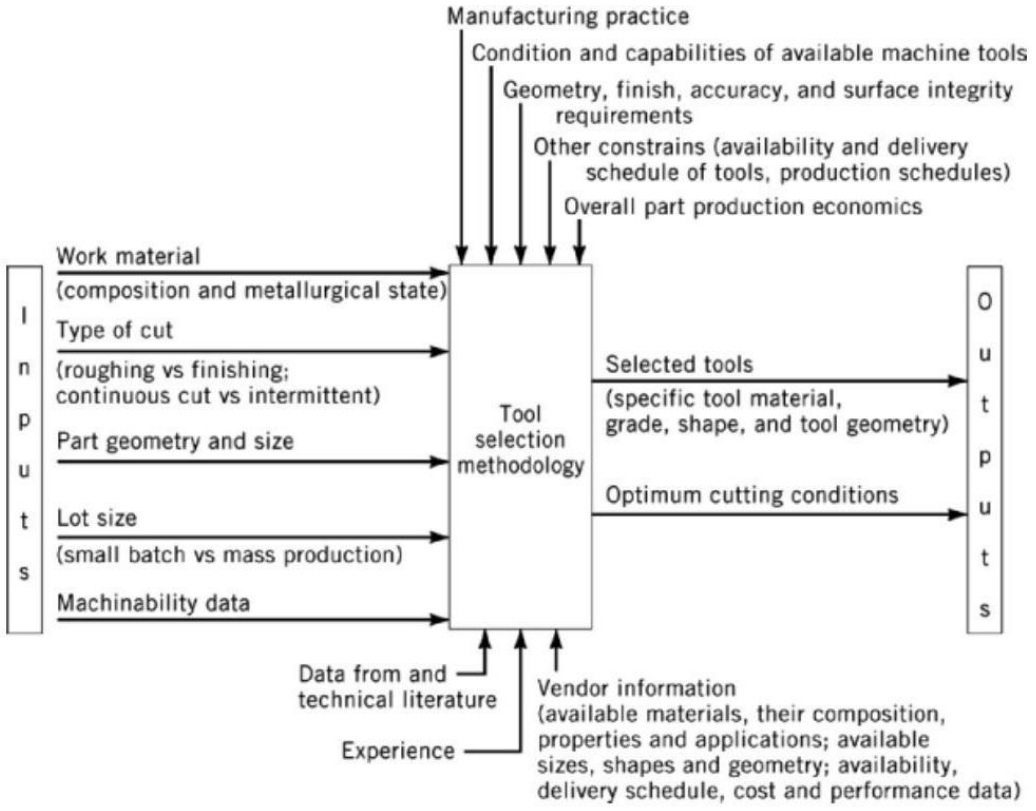

Figure 2-6 Methodology for cutting tool selection [16]

Lo [17] investigated the effect of rake angle on the cutting forces and chip formation. The findings indicated the negative correlation between rake angle and cutting force and equivalent stress. The increasing of rake angel will also decrease the strength of the cutting tool. A balanced point should be found according to the workpiece material. The geometry of the cutting tool has a closed relationship with the chip formation, temperature distribution and stress distribution. In return, they will affect the tool wear evolution.

2.3 Tool life and wear evolution models

Arranging cutting experiments under different conditions (such as feed rate, cutting speed) is the normal method to acquire the data for building the tool wear model. Design of experiments (DOE) and response surface methodology (RSM) are two optimization techniques for analyzing the tool wear data [10].

Attanasio et al. [18] applied the RSM technique to establish the models for predicting flank wear (VB) and crater depth (KT). The AISI 1045 steel bars is the workpiece material and uncoated tungsten carbide (WC) is the cutting tool material under turning process. The models were expressed as:

$$VB(V_c, f, t) = (-0.70199 + 0.00836V_c + 1.88679f + 0.00723t - 0.00002{V_c}^2 - 3.89975f^2 - 0.00288t^2 - 0.001697V_c f + 0.00015V_c t + 0.02176ft)^2 \quad (2\text{-}4)$$

$$KT(V_c, f, t) = exp(-3.2648 - 0.0367V_c + 5.6378f + 0.4999t + 0.0001{V_c}^2 + 11.0695f^2 - 0.0483t^2 + 0.01257V_c f + 0.0005V_c t + 0.1929ft)^2 \quad (2\text{-}5)$$

Where V_c is the cutting speed, f is the feed rate, t is the cutting time.

Camargo et al. [19] also adopted the RSM technology to investigate the difference between the full wear model and the reduced wear model when considering the effect of cutting speed and feed rate.

However, a lot of experiments will be required to achieve a relative accurate empirical model. Although it costs a lot of money and time, the final results may only can be used in a narrow area, such as the specific workpiece material and cutting tool material.

Cutting tool life model is another kind of empirical model used to predict the cutting tool performance in the cutting process. Taylor's equation is the most famous one and has already been introduced in the section 2.2. Despite the simplicity of the cutting tool life model, the constants in the life model can only be acquired from experiments. The limitation on cutting conditions is another drawback of these kind of models. Furthermore, as for the managers of a manufacturing company, cutting tool wear evolution is more interesting to them. Due to this, some wear rate models were built in the recent few decades.

Ceretti et al. [20] found out the constants through experiments based on the abrasive wear model suggested by [21], which is given by:

$$Z_{AB} = K_1 \frac{p^{a_1} v_c^{b_1} \Delta t}{H_d^{c_1}} \quad (2\text{-}6)$$

Where Z_{AB} is the abrasive wear depth, $K_1$is the coefficient determined by experiments, p is the local pressure, v_c is the local sliding velocity, Δt is the incremental time interval, H_d is the cutting tool hardness, a_1, b_1, c_1 are the experimental constants.

Takeyama and Murata gave out an abrasive wear and diffusive wear rate model in [22]:

$$\frac{dW}{dt} = G(V, f) + Dexp(-\frac{E}{RT}) \quad (2\text{-}7)$$

Where G, D is constants, $\frac{dW}{dt}$ is the wear rate volume loss per unit contact area per unit time, V is the cutting speed, E is the process activation energy, R is the universal gas constant, T is the cutting temperature.

Usui et al. considered adhesive wear in [23]:

$$\frac{dW}{dt} = A\sigma_n v_s \exp(^{-B}/_{T}) \quad (2\text{-}8)$$

Where$A$, B are the constants, $\sigma_n$is the normal stress, v_s is the sliding velocity, T is the cutting temperature.

Luo et. Al [24] combined the abrasive wear rate from [25] and diffusive wear from [26]:

$$\frac{dw}{dt} = \frac{A}{H} \frac{F_f}{Vf} V_s + Bexp(\frac{-E}{RT_f}) \quad (2\text{-}9)$$

Where $\frac{dw}{dt}$ is the flank wear rate, A is the abrasive wear constant, H is the hardness of the cutting tool material, F_f is the feed force, V is the cutting speed, f is the feed rate, V_s is the sliding speed, B is the diffusive wear constant, E, R, T_f are process activation energy, universal gas constant and cutting temperature in the tool flank zone, respectively.

This model is the enhancement of the model of Takeyama and Murata.

Pálmai [27] concluded the tool wear rate models which is shown in Table 2-1.

Table 2-1 Tool wear rate models

Shaw and Dirke (1956) $\mathrm{V} = \mathrm{k}\frac{F_n}{3\sigma_y}L$
Trigger and Chao (1956) $\mathrm{k} = k_1 exp - \frac{E}{RT}$
Takeyama, Murata (1963) $\frac{dW}{dt} = G(V,f) + Dexp(-\frac{E}{RT})$
Usui et. al (1984) $\frac{dW}{dt} = A\sigma_n v_s \exp(^{-B}/_{T})$
Zhao et. al (2002) $\mathrm{VB} = k_3\left(\frac{2v_c}{b^2\tan\alpha_c}\right)^{\frac{1}{3}}\left(\frac{F_t t_c}{H(T)}\right)^{\frac{1}{3}}$ $H(T) = c_1T^3 + c_2T^2 + c_3T + c_4 \quad (c_1, c_2, c_3, c_4 \; are \; constants)$
Luo et. al (2005) $\frac{dw}{dt} = \frac{A}{H}\frac{F_f}{Vf}V_s + Bexp(\frac{-E}{RT_f})$
Astakhov (2006) $h_s = \frac{dh_r}{dS} = \frac{(h_r - h_{r-i})100}{(l-l_i)f}$
Attanasio et. al (2008) $\frac{dW}{dt} = D(T)exp\left(-\frac{E}{RT}\right)$ $D(T) = d_1T^3 + d_2T^2 + d_3T + d_4 \quad d_1, d_2, d_3, d_4 \; are \; constants$

The empirical model is a powerful tool when a new finite element model using this model is validated by the experiments. These models can be used directly by the manufacturing companies.

2.4 Analytical models

Analytical models are mathematical models which have a closed form solution. These models are usually adopted by the numerical models to describe the condition of a system.

However, this is by no way means to say that numerical models are superior to the analytical models. In some simple system, the solution in the analytical model is fairly transparent, but for more complex systems, the analytical solution can be very complicated. For those used to the mathematics, the analytical model can provide a concise preview of a model's behavior which is hidden in the numerical solution. On the other hand, numerical model could show out the graphs of important process parameters changing along with the time which are essential for people to understand.

Since analytical model is the foundation of a numerical model, continuing working on the analytical model is vital. Even though, it can be sure that no analytical model in cutting process is universally accepted or employed. However, the analytical models in many papers reveal the mechanics of machining and should be considered as the prospective models before moving on to numerical or any other kinds of machining modeling. Two typical analytical models will be discussed in following: shear plane models and slip-line models.

2.4.1 Shear plane models

Ernst and Merchant had done a great work on the shear plane models [28]. The idea is the chip will be formed along a single plane inclined at the shear angle. The formation of a continuous chip can be illustrated by a simple model of a stack of cards. In the equilibrium analysis, the chip is regarded as the rigid body and the shear stress is the same as the material flow stress along the shear plane [5].

The Merchant’s circle force diagram is used to calculate the forces on the chip-tool interface and across the shear plane. As Show in Figure 2-7

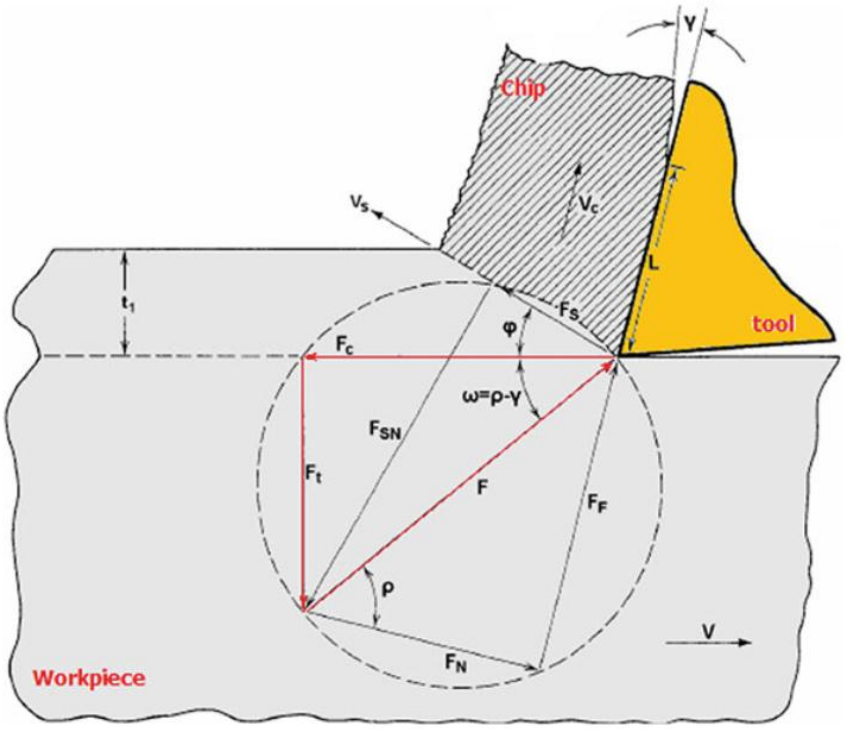

Figure 2-7 Merchant's circle [28]

All forces are concentrating on the tool tip. The resultant force F can be resolved in two components: the force normal to the tool face (F_N) and force along the tool face (F_F). On the other hand, it can be decomposed into F_{SN} and F_S which are normal and along the shear plane respectively. Furthermore, it can be represented by the cutting force F_c and the thrust force F_t. Finally, the shear angle φ , rake angle γ , the mean friction angle between chip and tool ρ are shown.

Suppose μ is the mean friction coefficient, then ρ and μ can be related in the equation:

$$\rho = \arctan(\mu) = \arctan({}^{F_F}/_{F_N}) \qquad (2\text{-}10)$$

According to the upper bound condition, a shear angle needs to be found to reduce cutting work to a minimum. The work done is proportion to the cutting force, thus the relationship between the cutting force with the shear angle needs to be found and then using the differential method to obtain the equation when Fc is a minimum.

From the Merchant circle, the relationship between cutting force F_c and resultant force F is apparent:

$$F_c = F\cos(\rho - \gamma) \quad (2\text{-}11)$$

On the other hand, shear force along the shear plane can be expressed in two ways:

$$F_s = F\cos(\varphi + \rho - \gamma) \quad (2\text{-}12)$$

$$F_s = \tau_s A_s = \frac{\tau_s A_c}{\sin\varphi} \quad (2\text{-}13)$$

Where τ_s is the shear strength of the workpiece material on the shear plane, A_s is the cross-sectional area of the shear plane and A_c is the cross-sectional area of the un-deformed chip.

From the equation (2-12) and (2-13), the resultant force can be written:

$$F = \frac{\tau_s A_c}{\sin\varphi} \cdot \frac{1}{\cos(\varphi+\rho-\gamma)} \quad (2\text{-}14)$$

So the cutting force can be concluded as:

$$F_c = \frac{\tau_s A_c}{\sin\varphi} \cdot \frac{\cos(\rho-\gamma)}{\cos(\varphi+\rho-\gamma)} \quad (2\text{-}15)$$

The cutting force is the function of shear angle, using the differential method, and in order to minimize the cutting force, the differential equation equal to zero. Then:

$$2\varphi + \rho - \gamma = {}^{\pi}/_{2} \quad (2\text{-}16)$$

It is a brief equation to predict the shear angle but cannot be validated by experiments. Merchant considered the normal stress of the shear plane σ_s will affects the shear stress τ_s. In the modified model, a new relation is shown as:

$$\tau_s = \tau_0 + k\sigma_s \quad (2\text{-}17)$$

Where k is the constant and regarded as the slope between τ and σ.

According to this new theory, the final equation is:

$$2\varphi + \rho - \gamma = C \quad (2\text{-}18)$$

Where C is the constant depend on the workpiece material.

2.4.2 Slip-line models

A slip-line is a line usually curved and along which the shear stress is the maximum. A complete set of slip-lines in the plastic region form a slip-line field.

For classic slip-line field models, in order to simplify the governing equations, several assumptions are made:

- Plane-strain deformation: the model can be only used in the orthogonal metal cutting.
- Rigid-plastic work material: The material shows no elastic deformation and shear flow stress does not change with strain, strain-rate, and temperature.
- Quasi-static loading: A static load is time independent. Note that a quasi-static condition for one structure may not quasi-static for another.
- No temperature changes and no body force

There are two rules that the slip-line field theory must follow in order to construct a slip-line field for a particular case [5]:

First of all, the boundary between a part of a material that is plastically loaded and another that has not yielded is a slip-line.

Another rule is that slip-lines must intersect with free surfaces at $45°$.

Lee and Shaffer use the above rules and assumptions to build the slip-line field as shown in Figure 2-8

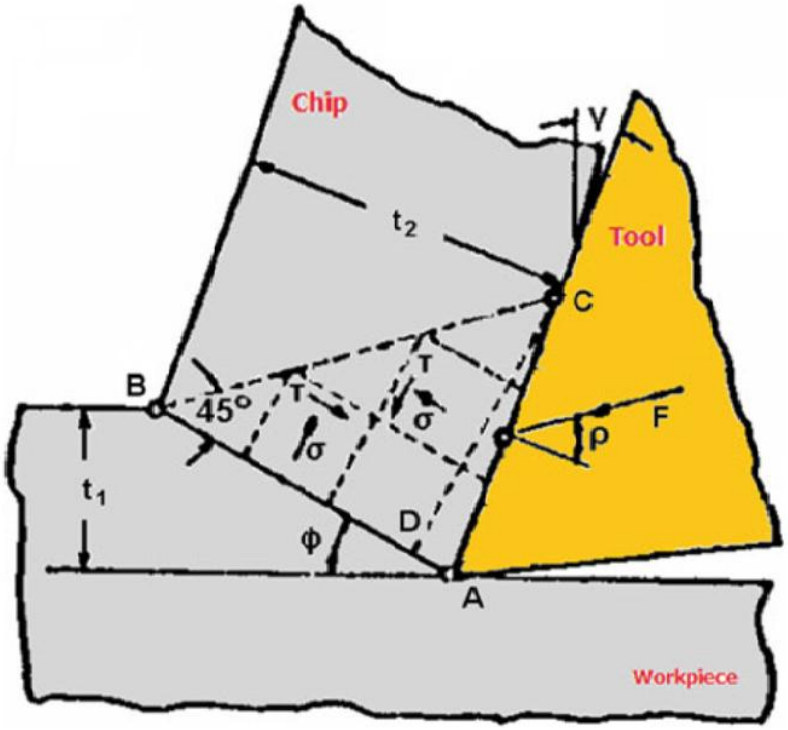

Figure 2-8 Lee and Shaffer's slip-line theory for orthogonal cutting [29]

In the Figure 2-8, ABC is the deformation zone, shear plane AB is one of the slip-line because the maximum shear stress occurs along this plane. BC is regarded as the free surface since no cutting force act after BC, so according the second rule, angle ABC is equal to $\pi/4$.

On the other hand, normal stresses will meet two boundaries at ρ and $\rho + \pi/2$

The shear angle can be expressed as:

$$\emptyset + \rho - \gamma = \pi/4 \qquad (2\text{-}19)$$

However, if the rake angle equal to zero and the mean angle of friction between chip and tool is $\pi/4$, then the shear angle will be zero which is not possible.

Fang [30] developed a new slip-line model for machining with a rounded-edge tool. This new model has 27 slip-line sub-regions and everyone has its physical meaning. See Figure 2-9

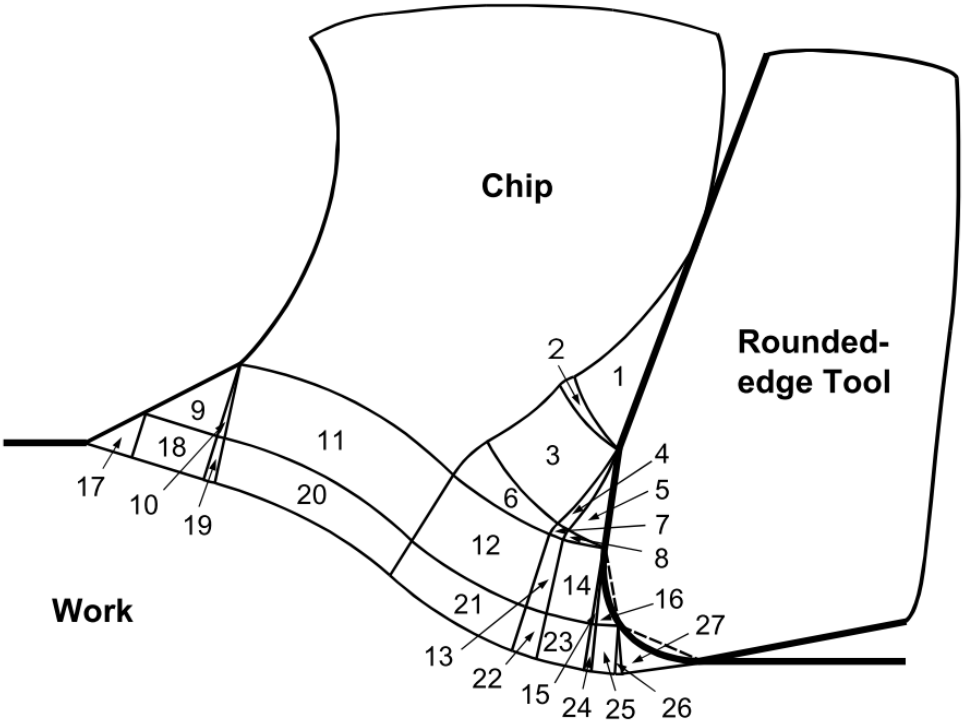

Figure 2-9 Fang's model [30]

Furthermore, the model can explain nine effects that occur in the machining including the size effect and shear zone. Eight groups of machining parameters can be predicted simultaneously including cutting force, chip thickness and shear stain. Eight slip-line models developed during the last six decades such as Merchant's and Lee and Shaffer's can be merged into the new model. See Figure 2-10

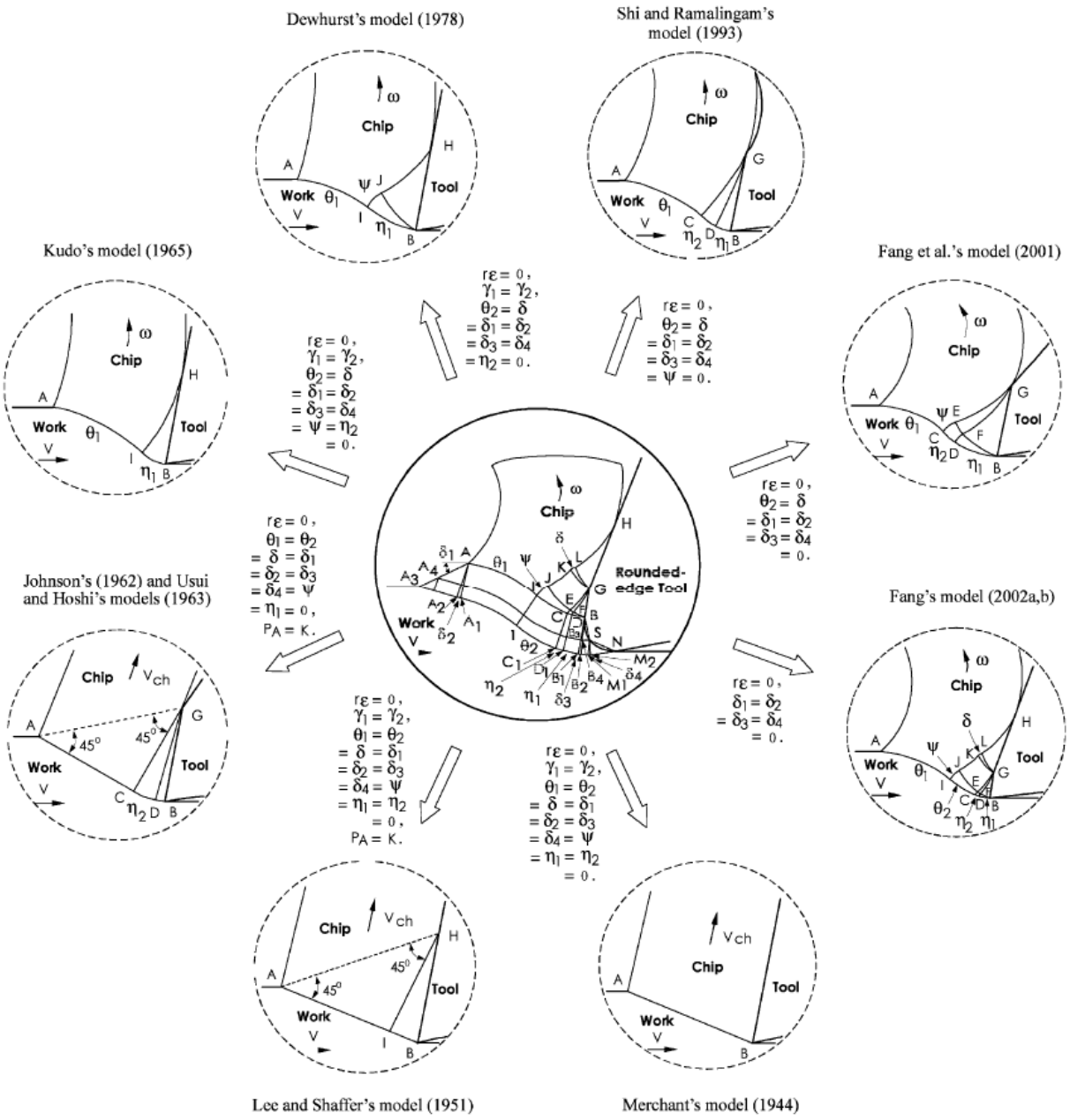

Figure 2-10 Eight special cases of new slip-line model [30]

Arrazola et.al [31] made a conclusion about analytical models and gave out the equations for calculating the main cutting parameters which is a good guidance for new learners to understand the modelling process.

2.5 Finite element method

Finite element method is widely used for investigating the cutting process due to its flexibility and efficiency. Four purposes can be distinguished in the published papers: impacts on workpiece material including the residual stress, chip formation process, strain, stress and temperature distribution in the workpiece; effects on the cutting tool such as tool wear, temperature distribution on the cutting tool and cutting tool design; building the finite element model such as different workpiece material models, friction models; others.

Abboud et al. [32] studied the effect of feed rate and cutting speed on residual stresses in titanium alloy Ti-6Al-4V using the orthogonal model. Arulkirubakaran et al. [33] made an attempt to reduce detrimental effects on titanium alloy Ti-6Al-4V using surface textures on rake face of the tool. Ceretti et al. [20] investigated the influence of some cutting parameter such as cutting speed, rake angel in a plane strain cutting process using FE code DEFORM 2D. Chiappini et al. [34] studied of the mechanics of chip formation in spindle speed variation(SSV) machining. Hadzley et al. [35] studied the effect of coolant pressure on chip formation, cutting force and cutting temperature. A reduced cutting force and temperature was witnessed due to the increasing of the coolant pressure. Kalyan and Samuel [36] developed a FE model to study the effect of cutting edge chamfer on high speed turning of AlMgSi (Al 6061 T6) alloy and validated by experiments. Lei et al. [37] simulated continuous chip formation for 1020 steel under a plane strain condition with a new material constitutive model using finite element method. Li et al. [38] investigated the effects of crater wear on the cutting process using Abaqus by change the geometry of the cutting tool. A significant impact of crater wear size on the chip formation and contact stresses is observed. List et al. [39] examined the strain and strain rate variations in the primary shear zone and investigated the distribution of velocity. Liu and Melkote [40] investigated the relationship between cutting tool edge radius and size effect by developing finite element model on Al5083-H116 alloy under orthogonal cutting condition. Lo [17] investigated the effect of tool rake angle on cutting

force, chip geometry, stress distribution, residual stress and surface quality of the workpiece material. Mamalis et al. [41] presented a coupled thermo-mechanical orthogonal cutting model using commercial finite element package MARC to simulate continuous chip formation under plane-strain condition. Maranhão and Paulo Davim [42] built a thermal and mechanical model for AISI 316, determined the effect of the friction coefficient on important process parameters such as temperature and stress along the tool-chip interface. Shet and Deng [43] developed an orthogonal metal cutting model to investigate the residual stress and strain distribution using FEM in the workpiece under plane strain conditions. Thepsonthi and Özel [44] studied the effect of cutting tool wear on process variables when milling on Ti-6Al-4V.

Filice et al. [45] proposed an effective FE model including both flank and crater wear using polynomial method. Hosseinkhani [46] built a finite element model using Abaqus to investigate the change of contact stress, plastic deformation and temperature distribution based on different worn cutting tool geometry. It is shown that the flank wear size has the larger impact on the tertiary deformation region than the other two. The highest temperature point on the cutting tool transferred from rake face to flank face due to the flank wear. Kumar et al. [47] constructed an optimal design method of end mill cutters for milling Titanium alloy Ti-6Al-4V using FE analysis. Salvatore et al. [48] presented a new method for predicting tool wear evolution during cutting process. Yen et al. [10] developed a methodology to simulate the cutting tool life and wear evolution under orthogonal cutting condition using FEM.

Lin and Lin [49] established a large deformation thermo-mechanical FE model for oblique cutting process. Liu et al. [50] developed a new constitutive model considering the influencing of micro damage in the workpiece material based on Zerilli–Armstrong (Z-A) model. Owen and Vaz [51] presented a FE model about the effect of adiabatic strain concentration on the failure of material using adaptive method. Özel [52] developed an orthogonal cutting model to simulate the continuous chip formation based on updated Lagrangian FE formulation and investigated the stress distributions on the

cutting tool under different friction models. Patil et al. [53] studied the influence of ultrasonic assisted turning (UAT) using 2D FE transient simulation in DEFORM framework, this method seemed improving all except the surface roughness comparing with continue turning process. Umbrello [54] investigated the machining of Ti-6Al-4V for both conventional and high speed cutting regimes using finite element analysis (FEA). Wang et al. [55] proposed a new approach to predict optimal machining conditions for most energy-efficient machining of Ti-6Al-4V.

Bil et al. [56] compared various finite element packages such as MSC. Marc, Deform 2D and Thirdwave AdvantEdge using an orthogonal cutting model and found out that no model can acquire acceptable results for all process parameters.

2.6 Key findings and research gap

It can be concluded from the papers that:

- Most of the published papers are focused on the effects on workpiece material.
- Cutting tool wear evolution and temperature distribution are commonly investigated in papers.
- Cutting tool is usually regarded as a rigid body in the simulation process.

Although almost all the aspects of cutting process are studied using FEM, the effects of various cutting parameters such as cutting speed, tool edge radius, cutting depth and tool wear on the cutting tool are neglected by most researchers. On the other hand, the wear evolution models and tool life models cannot be used in the workshop efficiently and conveniently. Machining power maybe the choice. In this thesis, these two aspects will be investigated.

3 Finite element simulation of metal cutting

3.1 Introduction

Experiments, analytical models and finite element methods are commonly adopted in metal cutting research area. At the beginning, experiments were the most widely used method to study the impacts of various cutting process parameters. However, it is very expensive and time consuming. Analytical models were adopted to predict the cutting tool life and the mechanisms behind the cutting process such as chip formation and size effect. It helps a lot but cannot be used for complicated cutting conditions. Finite element method becomes predominant in the cutting process research area due to the development of computer technology and commercial finite element software. Various parameters and characteristics of the cutting process such as temperature and stress distribution, strain, cutting force can be predicted which may be hard to obtain through experiments or analytical methods.

In order to build a simulation model using FEM, the following aspects need to be considered:

- Select a suitable finite element package according to the explicit and implicit method and motion description method
- Choice of workpiece material
- Workpiece material constitutive model and damage model
- Chip formation and separation criteria
- Friction model

The reasons can be listed as:

- Only a few finite element codes can be used for dynamic process such as cutting process.
- Workpiece material should be chosen according to the requirement in the company.
- The workpiece material model should represent the flow stress under high strain, strain rate and temperature. The damage model

is part of the material property which need to be considered carefully.

- Chip formation has a close relationship with the surface quality, tool life and machining stability.
- Friction is quite complicated in the contact face between cutting tool and the chip. Reflecting the true friction condition is vital to the simulation accuracy.

3.2 The selection of finite element package

There are many finite element codes existing in the market which can be used in engineering area. In order to find the right one for the cutting process, two important concepts must be clarified in the first place: explicit and implicit method and motion description method.

3.2.1 Explicit and implicit

3.2.1.1 Explicit and implicit solution method

Explicit use central different formula to solve the (t + Δt) using information at the time t [57], while in implicit solution the condition of (t + Δt) determine the state of (t + Δt) [58]. Backward Euler method is an example of implicit time integration scheme, while forward Euler method or central difference are examples of explicit time integration schemes.

Backward Euler method is according to backward difference approximation [59], and can be expressed as

$$y_{t+\Delta t} = y_t + hf(y_{t+\Delta t}, x_{t+\Delta t}) \quad (5\text{-}1)$$

Which confirms the statement that the condition of (t + Δt) determine the state of (t + Δt).

Forward Euler method uses forward difference approximation, as shown below

$$y_{t+\Delta t} = y_t + hf(y_t, x_t) \quad (5\text{-}2)$$

It is clearly shown that, the information at the time (t + Δt) depends on the condition of the time t.

Another explicit time integration scheme is central difference method. See Figure 5-1.

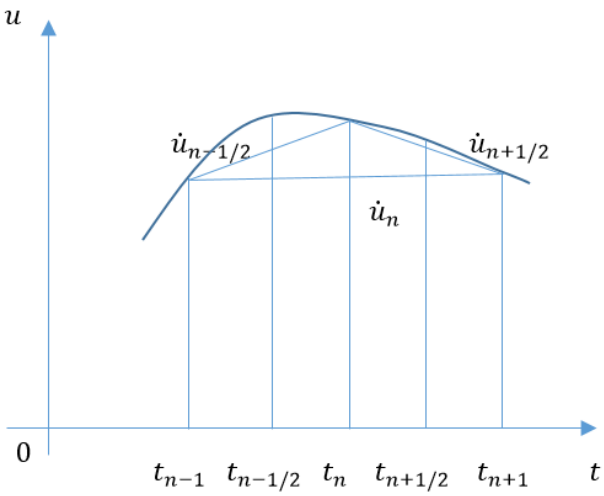

Figure 5-1 Explicit time scheme (every time distance is $\Delta t/2$)

Central different formula can be displayed as:

$$\dot{u}_n = \frac{1}{2\Delta t}(u_{n+1} - u_{n-1}) \tag{5-3}$$

$$\ddot{u}_n = \frac{1}{\Delta t}\left(\dot{u}_{n+\frac{1}{2}} - \dot{u}_{n-\frac{1}{2}}\right) = \frac{1}{\Delta t}\left(\frac{u_{n+1}-u_n}{\Delta t} - \frac{u_n-u_{n-1}}{\Delta t}\right) = \frac{1}{\Delta t^2}(u_{n+1} + u_{n-1} - 2u_n) \tag{5-4}$$

When consider linear dynamic situation, equilibrium at time t_n:

$$M\ddot{u}_n + C\dot{u}_n + Ku_n = R \tag{5-5}$$

Put (5-3), (5-4) into (5-5),

$$\left(M + \frac{\Delta t}{2}C\right)u_{n+1} = \Delta t^2 R - (\Delta t^2 K - 2M)u_n - (M - \frac{\Delta t}{2}C)u_{n-1} \tag{5-6}$$

Where u is the displacement vector, $\dot{u}$ is the velocity vector, $\ddot{u}$ is the acceleration vector, R is vector of the applied load, M is the mass matrix, C is the damping matrix, and K is the stiffness matrix.

It also shows that the situation of (t + Δt) rely on the condition of the time t.

3.2.1.2 Iterative scheme

The implicit procedure uses the Newton-Raphson method to do the automatic iteration [60]. The main idea can be seen from Figure 5-2

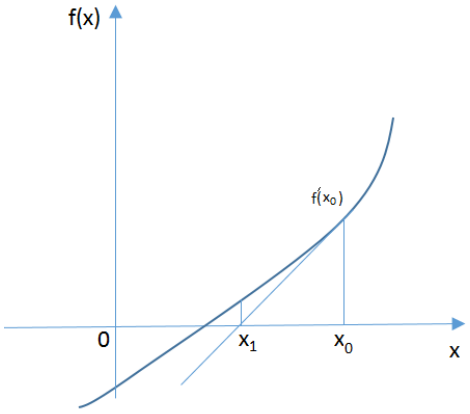

Figure 5-2 Newton-Raphson iterative method

$$f'(x_0) = \frac{f(x_0)}{x_0 - x_1} \tag{5-7}$$

$$x_1 = x_0 - \frac{f(x_0)}{f'(x_0)} \tag{5-8}$$

This process will repeat as

$$x_{n+1} = x_n - \frac{f(x_n)}{f'(x_n)} \tag{5-9}$$

Until x_{n+1}, x_n are close enough to each other.

On the other hand, explicit procedure demands no iteration, and during each time increment, the change of time rates is considered constant. Unlike implicit solver, the stability of explicit integration relies on the highest eigenvalue of the system (ω_{max}) [61], and time step should meet the equation below:

$$\Delta t \leq \frac{2}{\omega_{max}} (\sqrt{1 + \varepsilon^2} - \varepsilon) \tag{5-10}$$

Where ε is the critical damping fraction, this ensure that the time step Δt is smaller than the time of elastic wave passes one mesh.

In non-linear situation, implicit solver may need many iterations for an increment, smaller time steps will be used and convergence may be impossible [58]. As shown above, the convergence of explicit only depends

on Δt.

3.2.1.3 Choice in cutting process

In the cutting process, large deformation occurs in the workpiece material. Large deformation is regarded as geometrical nonlinearity [62]. Both implicit and explicit methods can be used in nonlinear situations [60]. Rebelo et al. [63] argue that 2D problems are suitable for implicit method, and complicated contact problems should use explicit methods for efficiency. Implicit method can suffer converging problem during large deformation processes and surface contact problems ([58] in [61,63,64,65]). Due to the converging issue, explicit is the better choice tackling the contact and large deformation problem. Harewood [58] argues that minimizing the time step will increase the computer running time and may result in divergence. The drawback of explicit method is stability and short time duration, decreasing the time step and limit the kinematic energy are possible solutions [58]. Yang et al. [61] also argue that for high-speed dynamic events, explicit solver is more suited.

Based on these findings, this thesis will use the explicit method to solve the finite element model in manufacturing process.

3.2.2 Description of motion

Traditionally speaking, in structure mechanics, Lagrangian description is adopted to solve the deformation problems [66]. The movement of each individual node is solved as a function of the material coordinates and time. Comparing with the pure Eulerian approach, the only need to satisfy fewer governing equations [66]. This is mainly due to the simple way to track the forming process when using the pure Lagrangian approach [66].

However, a large deformation of the material may happen in the cutting area without frequent remeshing operations. Remeshing process is conducted to acquire accepted accuracy for the simulation even though it will need a long computing time [66]. However, in pure Lagrangian approach, it is difficult to describe the boundaries of sharp edges or corners since the edge may move during the simulation process. [66].

Eulerian description is widely used in fluid dynamics [67]. The movement

of the elements is regarded as the relationship between spatial coordinate and time [68]. In the Eulerian description, reference mesh is adopted to trace the movement of material without any distortion [68]. However, if two or more materials exist in the Eulerian domain, numerical diffusion may occur [68].

Because of the advantages and disadvantages of each method, a new technology occurs to combine these two which is known as Arbitrary Lagrangian–Eulerian (ALE) description. Donea et al. [67] present a one-dimensional picture about the difference of these three descriptions. Show as Figure 5-3.

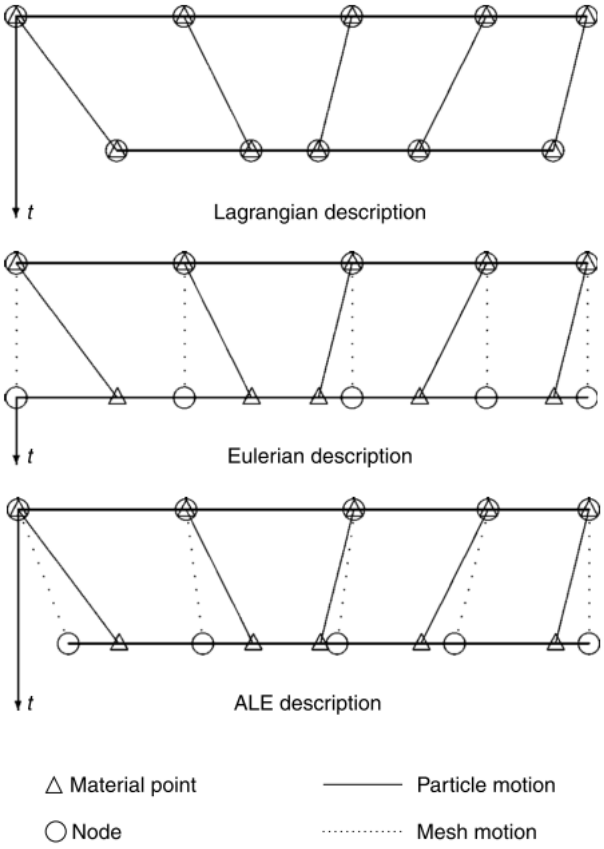

Figure 5-3 One dimensional example of lagrangian, Eulerian and ALE mesh and particle motion [67]

Khoei et al. [69] divided the uncoupled ALE solution into 3 different phases: Material (Lagrangian) phase, Smoothing phase and Convection (Eulerian) phase. The Lagrangian phase is used to acquire the convergence

at each time step. The Eulerian phase was adopted to get a regular mesh configuration. In the first place, the nodal positions were relocated arbitrarily regardless of the FE mesh. In the smoothing phase, nodes' coordinate value was updated according to the setting of level which may different from the previous one.

Donea et al. [67] argued that in ALE, any mesh-smoothing algorithm can be used once the topology is fixed to improve the shape of the elements.

Lagrangian description is used in this simple model.

3.2.3 Selection of Finite element package

More and more commercial FE codes are developed to simulate the physical world in engineering field.

For metal cutting simulation, packages like Abaqus, AdvantEdge, Deform 2D/3D and Ls-dyna using explicit and Lagrangian description are widely used both in research area and industrial field. Software mainly using the implicit method such as ANSYS cannot be used to simulate the metal cutting process.

Pop and Bianca [70] have made a conclusion about the most widely used finite element package from 1995 to 2013. The result is shown Figure 4-4:

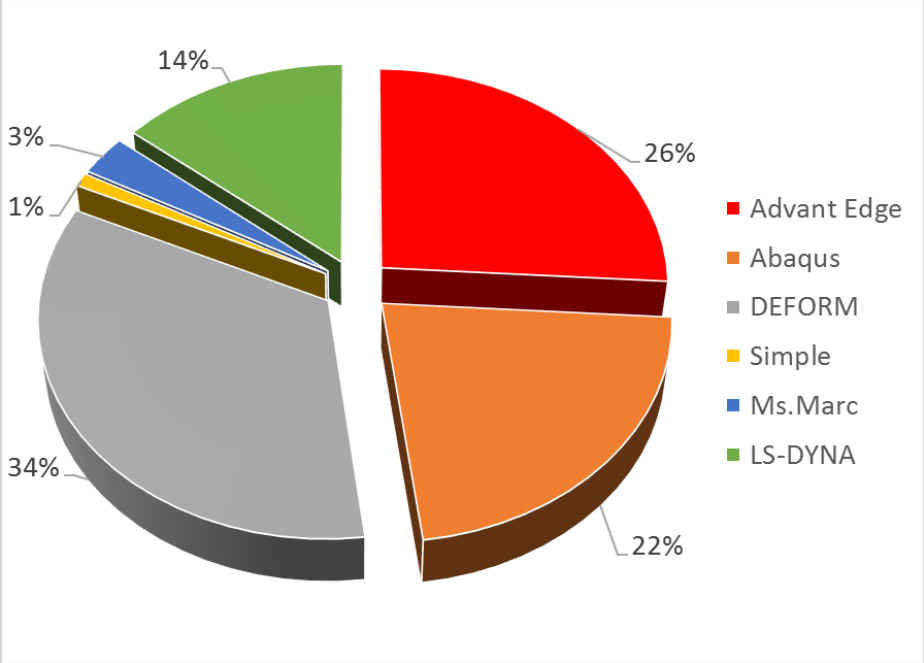

Figure 5-4 The usage ratio of different finite element packages [70]

Instead of talking about the differences between those packages which have already mentioned in the work of Kilicaslan [71], an example will be given for each popular package.

Deform 2D/3D, which is regarded as the most popular FE software for metal cutting in the industry field, was first released in 1989 as the 2D workstation version. In 1993, DEFORM-3D was released based on engineering workstations to solve full three dimensional problems.

Kohir and Dundur [72] used the DEFORM 2D to investigate the influence of flank wear on the cutting force, stress and temperature distribution.

Temperature distribution in the workpiece and cutting tool is shown in Figure 5-5

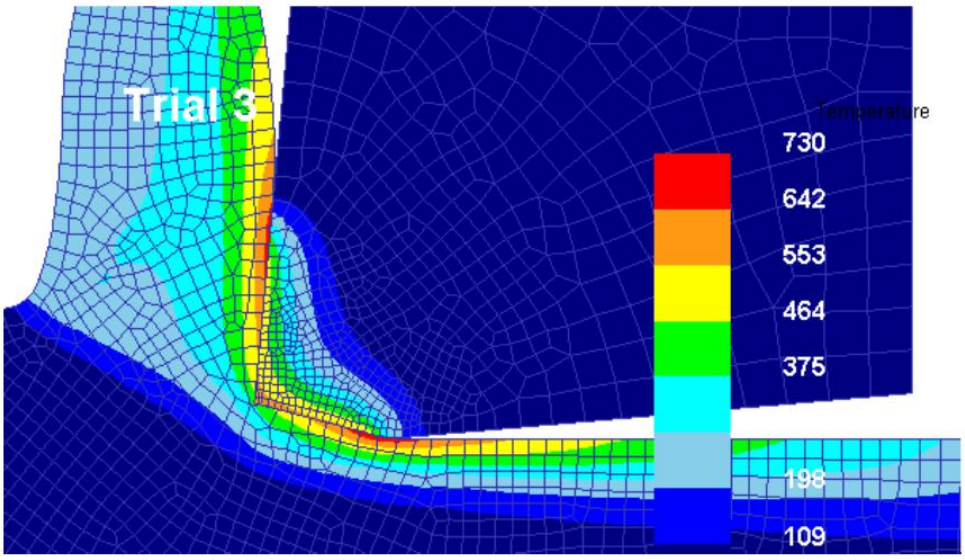

Figure 5-5 Temperature distribution when flank wear inclination=12°，wear land=2mm [72]

AdvantEdge uses a virtual testing environment to understand the inner causes of the tool performance and improve the cutting tool design. Temperature and stress analysis due to tool wear is a strong point of this code.

Maranhão and Paulo Davim [42] use the AdvantEdge to investigate the

effect of the friction coefficient on the tool-chip interface in the cutting process.

The result of maximum shear stress in cutting tool, workpiece material and chip can be seen below in Figure 5-6:

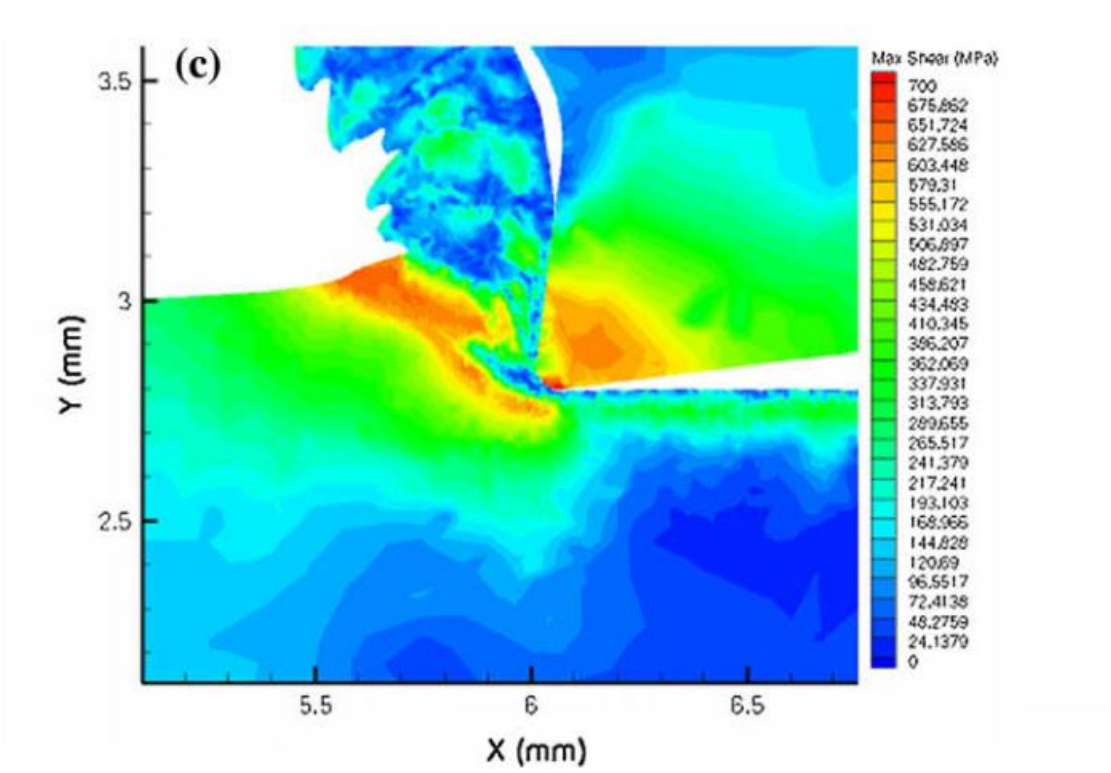

Figure 5-6 Maximum shear stress in the tool and workpiece [42]

Abaqus is firstly released in 1978 and suited for finite element analysis (FEA). It is widely used in campus and research institutions mainly because its capacity in material modelling and customization.

Hosseinkhani and Ng [46] build an ALE model based on ABAQUS/Explicit. The model was validated by experiment results. the influence of tool wear on process variables were investigated.

Temperature distribution on cutting tool, workpiece and chip can be seen in Figure 5-7

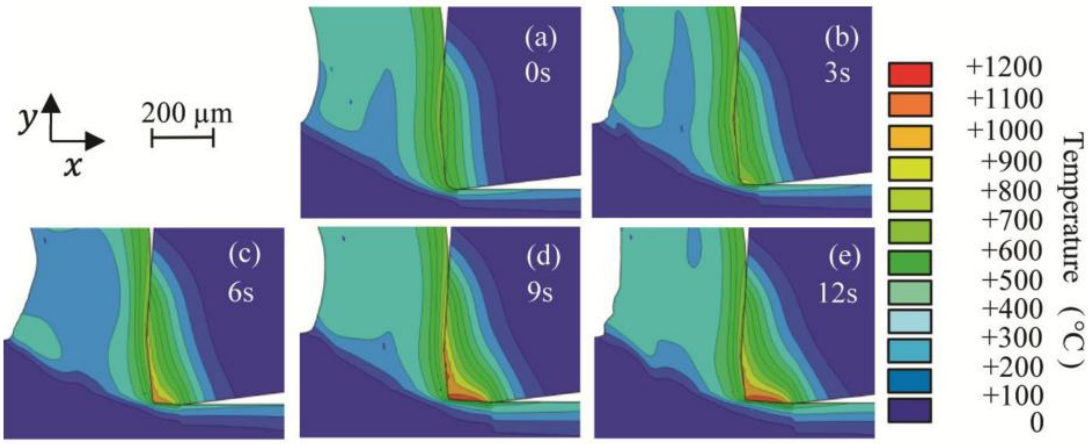

Figure 5-7 Temperature distribution on cutting tool, workpiece and chip [46]

Ls-dyna uses explicit time scheme to simulate the complex nonlinear and dynamic problems. It is naturally suitable for cutting, crash and forming problems. However, Ls-dyna cannot do remeshing in the tool and workpiece contact area while cutting which affects the results in metal cutting simulations.

Zouhar and Piska [73] studied the effect of tool edge radius and rake angle on process parameters using Ls-dyna.

The stress distribution due to different rake angle can be seen in Figure 5-8

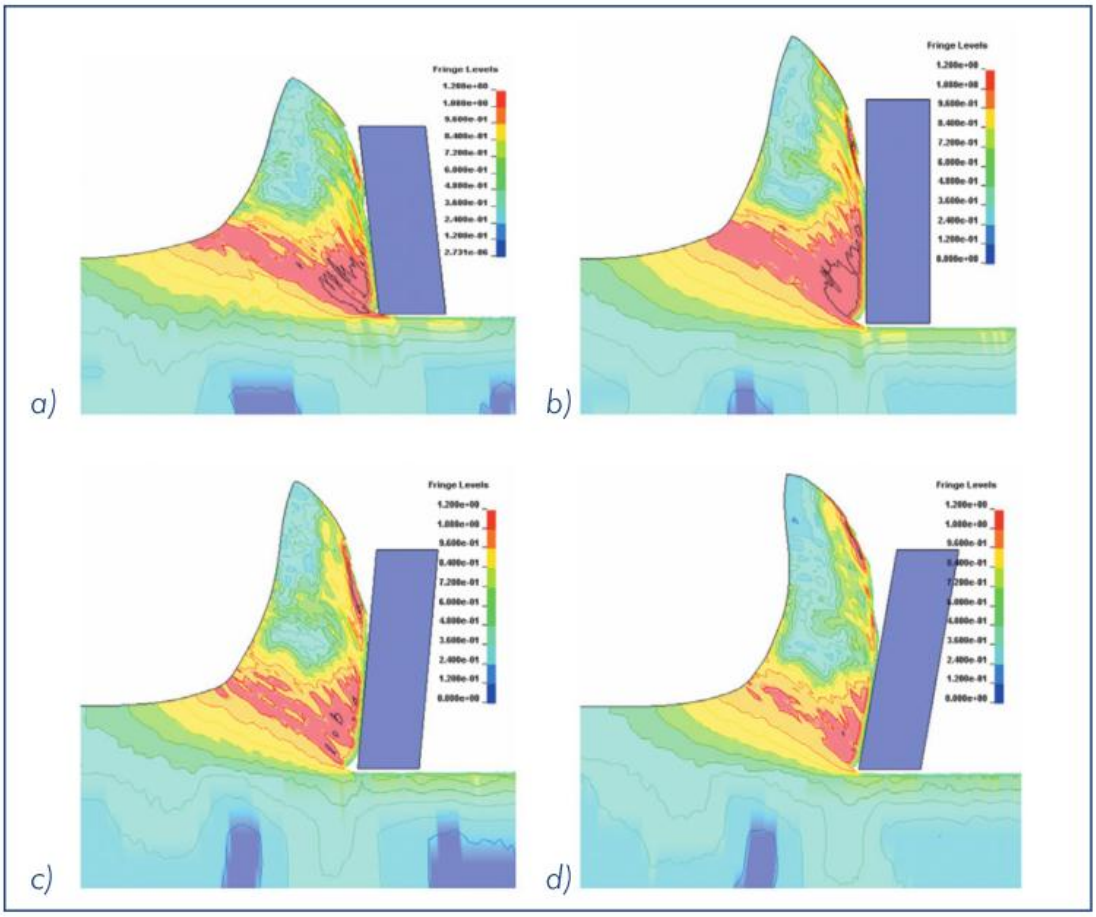

Figure 5-8 Von Mises stress field for tool with different rake angle a) -5 °b) 0 ° c) 5 °d) 10 ° [73]

As one of these commercial FE packages, Ls-dyna is chosen for this thesis because of its ability in solving dynamic problems and accessibility to the author on campus. This software is used to investigate the effect of cutting tool wear on cutting force, temperature and stress distribution.

3.3 Workpiece material and different models for modelling

3.3.1 The chosen of workpiece material

In this thesis, Ti-6Al-4V is chosen as the workpiece material mainly due to the following reasons:

Firstly, the excellent physical properties of Ti-6Al-4V. The property of three different widely used alloys in aerospace is presented in Table 5-1

Properties	Ti-6Al-4V	Aluminum 7075 Alloy	AISI 4340 Alloy Steel
Density (g/cm3)	4.43	2.8	7.85
Melting point (°C)	1674	483	1427
Tensile strength (MPa)	≥ 895	220	745
Yield strength (MPa)	≥ 828	95	470
Elastic modulus (GPa)	105-116	70-80	190-210
Poisson's ratio	0.31	0.33	0.27-0.30
Thermal expansion (μm/m°C)	9	23.2	12.3
Thermal conductivity (W/mK)	6.60	130	44.5
Specific Strength(strength to weight ratio) (KN.m/Kg)	208	78.5	94.9

Table 5-1 The physical property of three different alloys [74]

The property of Ti-6Al-4V can be concluded as:

- Relative low density. The density of Ti-6AL-4V is bigger than aluminium 7075 alloy but smaller than AISI 4340 alloy.
- High Melting point. The Melting point is the highest of these three material and means that the parts made of Ti-6AL-4V can work at a relative high temperature like turbine blades.
- High strength. The Tensile and Yield strength is much higher than the other two materials.
- Small thermal expansion and conductivity. Under high temperature, the structure will still keep its function if it is made of Ti-6AL-4V.
- High specific strength. This parameter is very important in the aerospace area. It means the strength per kilogramme. Ti-6AL-4V has a quite high specific strength. In order to satisfy the designed strength, less material

can be used for Ti-6AL-4V. Thus less fuel will be consumed for an airplane if Ti-6AL-4V is used rather than other two materials.

Secondly, it is used more and more in aerospace. The components of the material in Boeing 777 and Boeing 787 are shown in Figure 4-9 and Figure 4-10 respectively.

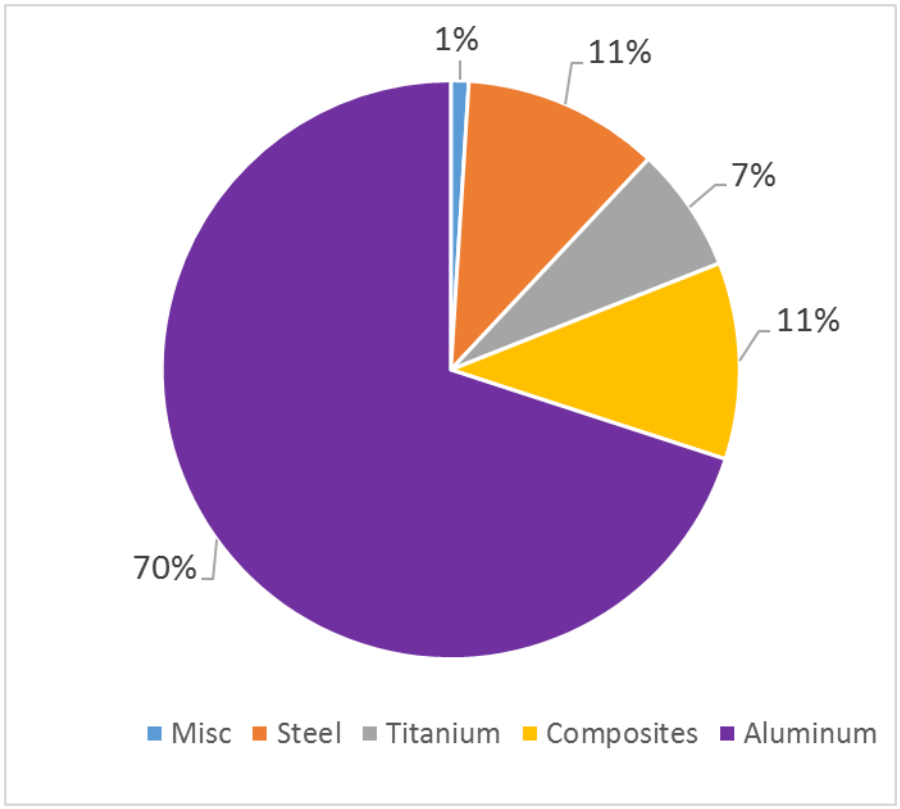

Figure 5-9 The weight ratio for different materials in Boeing 777 [75]

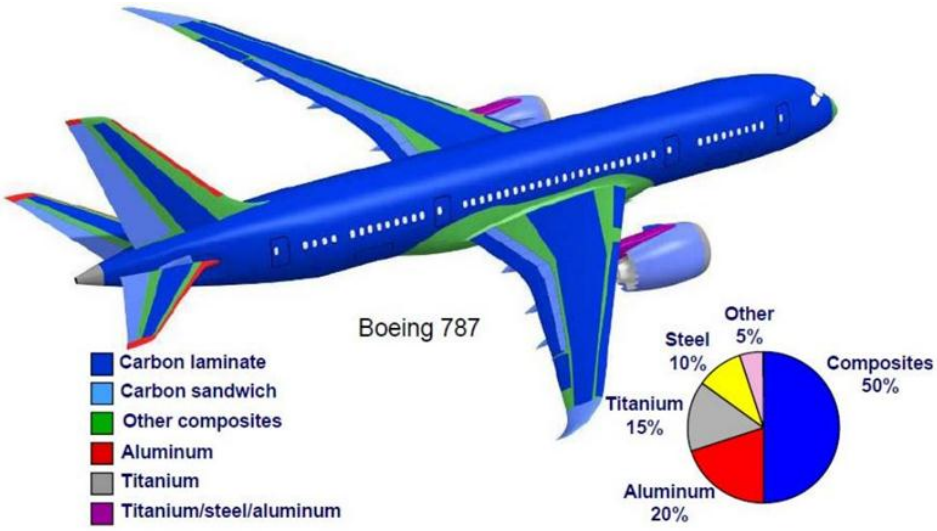

Figure 5-10 The weight ratio for different materials in Boeing 787 [76]

In Boeing 777 which was introduced in 1993, Titanium alloy is only 7%, for Boeing 787 which was introduced in 2007, the titanium takes 15% of the whole material.

Thirdly, the titanium alloy is very hard to machine. When compared with AISI B1112 steel, the rating for Ti-6Al-4V is only 22, which is regarded as very hard to machine. (The rating for AISI B1112 steel is set as 100.) Shown in Table 5-2.

Table 5-2 The machining easiness of different alloys [77]

Alloy	Type	Condition	Rating
2017	Aluminum Alloy	T4	300
4340	Alloy Steel	A	45
Ti-6Al-4V	Titanium Alloy	A	22

So in this thesis, Ti-6AL-4V is taken as the workpiece material.

3.3.2 The workpiece constitutive model

A workpiece material constitutive model is required to represent the flow stress under high temperature, strain and strain rate condition. [50].

Several researchers have come up with specific constitutive models to represent the material property.

3.3.2.1 The Johnson–Cook (J-C) model

The J-C model is a purely empirical model subjected to large strain by Johnson & Cook in 1983. The model for flow stress, σ, can be expressed as [78]:

$$\sigma = \{A + B\varepsilon^n\}\{1 + Cln\ \dot{\varepsilon}^*\}\{1 - T^{*m}\} \quad (5\text{-}11)$$

Where ε is the equivalent plastic strain, $\dot{\varepsilon}^* = \frac{\dot{\varepsilon}}{\dot{\varepsilon}_0}$ is the dimensionless plastic strain rate for $\dot{\varepsilon}_0 = 1.0\ s^{-1}$ and T^* is the homologous temperature. And $T^* = \frac{T-T_0}{T_m-T_0}$ where $T_0$is the reference temperature and $T_m$is a reference melt temperature. A, B, n, C, m are five material constants. A is the initial yield stress, B is the hardening constant, n is the hardening exponent, C is the strain rate constant, m is the thermal softening exponent.

The J-C model is widely used by many works. Chen et al. [79] used the J-C model to simulate the chip morphology and cutting force of the titanium alloy (Ti–6Al–4V) high-speed machining. The model is validated by experimental results. Thepsonthi and Özel [44] used a modified J-C model to exhibit workpiece flow stress in cutting process, as shown in Equation (5-12):

$$\sigma = \left\{A + B\varepsilon^n\left(\frac{1}{\exp(\varepsilon^a)}\right)\right\}\left\{1 + Cln\ \frac{\dot{\varepsilon}}{\dot{\varepsilon}_0}\right\}\{1 - (\frac{T-T_0}{T_m-T_0})^m\}\{\mathrm{D} + (1 - \mathrm{D})[\tanh(\frac{1}{(\varepsilon+p)^r})]^s\} \quad (5\text{-}12)$$

Where $\mathrm{D} = 1 - (T - T_m)^d$, $\mathrm{p} = (T/T_m)^b$, σ is flow stress, ε is true strain, $\dot{\varepsilon}$ is true strain rate, $\dot{\varepsilon}_0$ is reference true strain rate ($\dot{\varepsilon}_0 = 10^{-5}$). The meaning of other material constants is the same as in the typical J-C model.

Sima & Özel [80] discussed some material constitutive models including the J–C material model and in the end, a modified J-C model was used to simulate the material behaviour of Ti-6Al-4V according to the simulation results.

3.3.2.2 The Steinberg–Cochran–Guinan–Lund (SCGL) model

The Steinberg-Cochran-Guinan-Lund (SCGL) model is a semi-empirical model which was established by Steinberg et al. [81] under high strain-rate

conditions and extended by Steinberg and Lund [82] to low strain-rates and bcc (body-centered-cubic) materials. The flow stress of the material can be expressed as:

$$\sigma_y(\varepsilon_p, \dot{\varepsilon}_p, T) = [\sigma_a\, f(\varepsilon_p) + \sigma_t(\dot{\varepsilon}_p, T)]\frac{\mu(p,T)}{\mu_0};\ \ \sigma_a\, f \le \sigma_{max}\ and\ \sigma_t \le\ \sigma_p \tag{5-13}$$

Where σ_a is the thermal component of the flow stress, $f(\varepsilon_p)$ is a function that represents strain hardening, σ_t is the thermally activated component of the flow stress, $\mu(p,T)$ is the pressure and temperature-dependent shear modulus, and μ_0 is the shear modulus at standard temperature and pressure. σ_{max} is the saturation value of the athermal stress. Peierls stress σ_p.is the saturation of the thermally activated stress.

The Steinberg–Cochran–Guinan shear modulus model [83] is used to calculate the shear modulus .

The strain hardening function f is written as:

$$f(\varepsilon_p) = [1 + \beta(\varepsilon_p + \dot{\varepsilon}_p i)]^n \tag{5-14}$$

Where β , n are work hardening parameters, and $\dot{\varepsilon}_p i$ is the initial equivalent plastic strain.

The thermal component σ_t is got from the following equation ([82], [84]).

$$\dot{\varepsilon}_p = \{\frac{1}{C_1}\exp\left[\frac{2U_k}{k_b T}\left(1 - \frac{\sigma_t}{\sigma_p}\right)^2\right] + \frac{C_2}{\sigma_t}\}^{-1}\ ;\ \sigma_t \le \sigma_p \tag{5-15}$$

Where $2U_k$ is the energy to form a kink-pair in a dislocation segment of length L_d , k_b is the Boltzmann constant, σ_p is the Peierls stress. The constants C_1, C_2 are given by the relations

$$C_1 := \frac{\rho_d L_d a b^2 v}{2\omega^2} \tag{5-16}$$

$$C_2 := \frac{D}{\rho_d b^2} \tag{5-17}$$

Where ρ_d is the dislocation density, L_d is the length of a dislocation segment , a is the distance between Peierls valleys, b is the magnitude of the Burgers vector, v is the Debye frequency, ω is the width of a kink loop, and D is the drag coefficient.

Based on limited experimental evidence and upon robust first-principle calculations of the elastic module for diamond, Orlikowski et al. [85] used the SCGL model without the effect of strain-rate. They performed hydrodynamic 1-D simulations of an isotropic, polycrystalline diamond and have compared them to single crystal diamond experiments as a rough indicator to the model's performance. A good coherence was found.

3.3.2.3 The Zerilli–Armstrong (Z-A) model

The Zerilli–Armstrong (Z-A) model is based on simplified dislocation mechanics that was developed by Zerilli and Armstrong [86], [87], [88]. The general form of the equation for the flow stress is

$$\sigma_y\left(\varepsilon_p, \dot{\varepsilon}_p, T\right) = \sigma_a + B\ exp(-\beta T) + B_0\sqrt{\varepsilon_p}\exp(-\alpha T) \qquad (5\text{-}18)$$

In this model,$\sigma_a$is the athermal component of the flow stress which is given by

$$\sigma_a = \sigma_g + \frac{k_h}{\sqrt{l}} + K\varepsilon_p^n \qquad (5\text{-}19)$$

where σ_g is the contribution due to solutes and initial dislocation density, k_h is the microstructural stress intensity, l is the average grain diameter,K is zero for fcc (Face-centered-cubic) materials,B , B_0 are material constants.

The functional forms of the exponents α and β can be written as:

$$\alpha = \alpha_0 - \alpha_1 \ln\left(\dot{\varepsilon}_p\right) \qquad (5\text{-}20)$$

$$\beta = \beta_0 - \beta_1 \ln\left(\dot{\varepsilon}_p\right) \qquad (5\text{-}21)$$

Where $\alpha_0, \alpha_1, \beta_0, \beta_1$ are material parameters that depend on the type of material (fcc, bcc, hcp (Hexagonal Close Packed) alloys). The Zerilli–Armstrong model had been modified by [89] for better performance at high temperatures.

In order to capture the extremely high strains and strain rates of Ti-6Al-4V, Liu et al. [50] used a modified Z-A model, show as below:

$$\sigma = [\sigma_a + B\ e^{-(\beta_0 - \beta_1 ln\dot{\varepsilon})T} + B_0\sqrt{\varepsilon_r\left(1 - e^{-\frac{\varepsilon}{\varepsilon_r}}\right)}e^{-(\alpha_0 - \alpha_1 ln\dot{\varepsilon})T}][H + (1 - H)(\tanh(\frac{\alpha}{\varepsilon}))^k] \qquad (5\text{-}22)$$

Where the failure function is given by the second bracketed term and is controlled by three strain rate dependent parameters$H$, α and k.

This model is validated by experiments under orthogonal cutting conditions.

3.3.2.4 Evaluation of three models

Banerjee [83] evaluated these three flow stress models on the basis of one-dimensional tension and compression test varying the temperature and strain-rate. The average maximum absolute errors in yield stresses predicted by three flow stress models are exhibited in the Table 5-3.

Table 5-3 Average maximum absolute errors [83]

Condition	Average Max Error (%)		
	J-C model	SCGL model	Z-A model
All Tests	36	64	33
Tension Tests	25	20	19
Compression Tests	45	126	50
High Strain Rate (≥ 100 /s)	29	22	20
Low Strain Rate (< 100 /s)	45	219	76
High Temperature (≥ 800 K)	43	90	40
Low Temperature (< 800 K)	20	20	17
average	34.7	80.1	36.4

The Johnson-Cook model has the lowest average error in all these situations. Thus Johnson-Cook constitutive model is used as the workpiece material constitutive model.

3.3.3 The workpiece damage model

A damage model for cutting process is a part of the Finite Element simulation. It works with the chip separation criteria to simulate the movement of cutting tool and the material before tool tip. Generally, the damage model should contain the damage initiation and damage evolution.

For ductile material, a uniaxial stress–strain curve is used to represent the principle of material behaviour evolution. See Figure 5-11

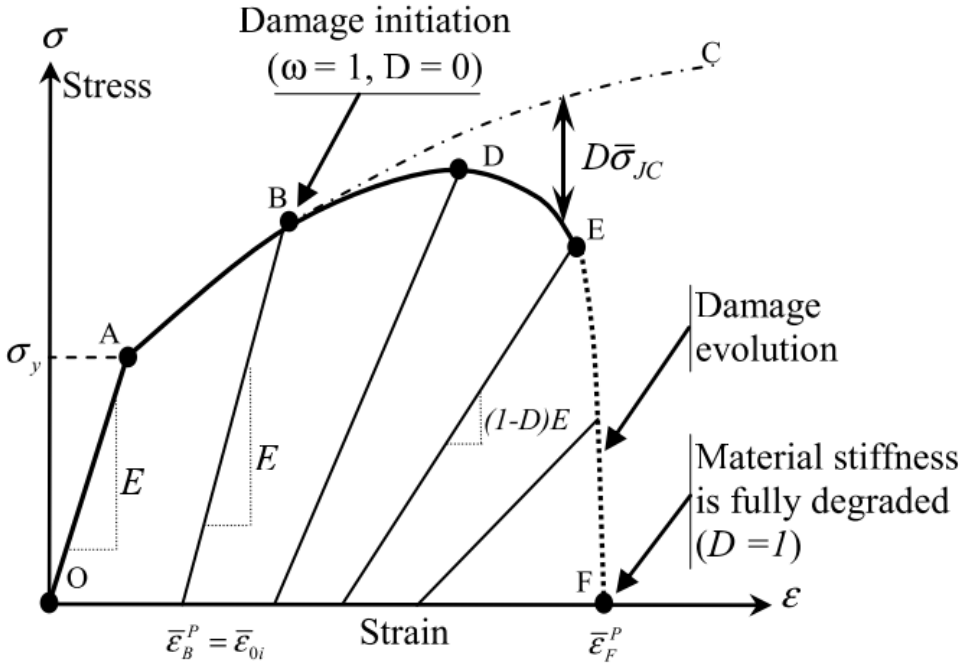

Figure 5-11 Typical uniaxial stress-strain in case of a ductile metal [90]

3.3.3.1 Damage initiation

Damage initiation criterion represents the beginning of the material damage. Johnson-Cook shear failure model will be introduced to analyse the damage initiation in cutting. The strain at fracture can be expressed as [91]:

$$\varepsilon^f = \max([D_1 + D_2 exp D_3 \sigma^*][1 + D_4 ln\dot{\varepsilon}^*][1 + D_5 T^*], EFMIN) \qquad (5\text{-}23)$$

Where D_1 to D_5 are failure parameters, generally from experiments, σ^* is the ratio of pressure divided by effective stress $\sigma^* = \frac{p}{\sigma_{eff}}, \dot{\varepsilon}^* = \begin{cases} \frac{\dot{\bar{\varepsilon}}}{EPSO} \\ \frac{\dot{\bar{\varepsilon}}^p}{EPSO} \end{cases}$, EPSO is the Quasi-static threshold strain rate, $\bar{\varepsilon}^p$ =effective plastic strain, $T^* = \frac{T-T_{room}}{T_{melt}-T_{room}}$. is the homologous temperature.

When a scalar damage parameter ω exceeds 1, the damage is initiated. This parameter is defined as:

$$\omega = \sum_{j=1}^{n} \left(\frac{\Delta\bar{\varepsilon}^p}{\varepsilon f}\right)_j \qquad (5\text{-}24)$$

where $\Delta\bar{\varepsilon}^p$ is the increment of equivalent plastic strain during an increment of loading, j, in each integration point.

According to equation (5-22), the stress triaxiality σ^*, damage may be initiated by strain rate and temperature.

3.3.3.2 Damage evolution

After damage initiation, the Hillerborg's fracture energy was used to control damage evolution. With this method, the damage evolution process became more stable and can capture strain localization using large mesh size [90].

For ductile material, if the damage initiation occurs, the stress–strain relationship can no longer accurately represents the material behaviour.

Hillerborg's fracture energy proposal used a stress–displacement response after damage initiation to decrease the mesh dependency. The fracture energy is then given as [90]:

$$G_f = \int_{\bar{\varepsilon}_B^p}^{\bar{\varepsilon}_F^p} L\bar{\sigma} d\bar{\varepsilon}^p = \int_0^{\bar{u}_F^p} \bar{\sigma} d\,\bar{u}^p \qquad (5\text{-}25)$$

Where $\bar{\varepsilon}_B^p$ and $\bar{\varepsilon}_F^p$ are the equivalent plastic strain at points B and F in Figure 5-11. $\bar{\sigma}$ is the equivalent plastic stress.

Through the definition, G_f introduced the equivalent plastic displacement $\bar{u}^p$ together with the yield stress to control the damage evolution. In the finite element model, characteristic length, L of the element is required to build the stress–displacement relationship.

Element aspect ratio has an effect on the crack behaviour after damage

initiation. Elements which have unit aspect ratio are better choice [90].

The scalar stiffness degradation for the linear damage process is given by:

$$D = \frac{\int_{\bar{\varepsilon}_B^p}^{\bar{\varepsilon}^p} L\bar{\sigma} d\bar{\varepsilon}^p}{G_f} = \frac{\int_0^{\bar{u}^p} \bar{\sigma} d\bar{u}^p}{G_f} \quad (5\text{-}26)$$

Whereas an exponential damage parameter can evolve according to:

$$\mathrm{D} = 1 - \exp(-\int_0^{\bar{u}^p} \frac{\bar{\sigma}}{G_f} d\,\bar{u}^p) \quad (5\text{-}27)$$

The formulation of the model ensured that the energy dissipated is equal to G_f during the damage evolution process. In theory, only at an infinite equivalent plastic displacement, the damage variable D reaches a value of one. In commercial finite element software, D is set as 0.99 or less to keep elements active in simulation. The plastic equivalent stresses in the material is given by:

$$\sigma = (1 - \mathrm{D})\tilde{\sigma} \quad (5\text{-}28)$$

Where $\tilde{\sigma}$ is the effective (or undamaged) stress computed in the current increment. It represents stresses that would exist in the material without damage.

Sui and Feng [92] used the Cockroft and Latham's fracture criterion to explain the material damage process. The criterion can be expressed as:

$$C_i = \int_0^{\varepsilon_f} \sigma\, d\varepsilon \quad (5\text{-}29)$$

Where σ is the maximum flow stress, ε_f is the fracture strain, and C_i is the material constant.

Hambli [93] adopted the Lemaitre damage model to describe the crack initiation and propagation. The damage law is written in an incremental form:

$$\dot{D} = \frac{D_C}{\varepsilon_R - \varepsilon_D}[\frac{2}{3}(1+v) + 3(1-2v)\left(\frac{\sigma_H}{\sigma_{eq}}\right)^2](\varepsilon_{eq})^{2/n} d\dot{\varepsilon}_{eq} \quad (5\text{-}30)$$

Where n is the hardening exponent and v is the Poisson's ratio, ε_D is the threshold logarithmic strain at which damage initiates, ε_R is the logarithmic strain value at fracture and ε_{eq} the logarithmic plastic strain. D_C is the critical damage value at fracture.

3.4 Chip formation process

3.4.1 Introduction

Despite different kinds of traditional machining process like milling, turning, grinding, it is the same process of removing material from a blank to form the chips when a certain chip thickness and depth of cut are reached.

By studying the chip formation process, researchers and engineers can obtain the behaviour of workpiece material under pressure, specific energy (the amount of energy required to remove unit volume of work material) requirement in the machining, cutting tool life and the method to get better surface finish.

The form of the chips mainly depends on:

- The workpiece and cutting tool material
- Cutting conditions (Feed speed, cutting speed, depth of cut and the use of coolant)
- Cutting tool geometry (rake angle, cutting edge angle, tool cutting edge inclination, chip breaker, worn shape)

In this section, the basic mechanism of chip formation for four different types of chip will be discussed in the first place. Types of chip morphology, chip separate criteria, chip forming process and effect of friction model will be clarified.

3.4.2 Chip formation mechanism

In the cutting process, the cutting tool will penetrate into the workpiece material causing elastic and plastic deformation, the stress concentration near the tool tip and the chip deprive from the workpiece. When take a close look at the chip formation process, four types of chip morphology could be identified mainly due to different materials' flow properties. On the other hand, the cutting parameters, geometry of the cutting tool, even the use of coolant will also affect the morphology of the chip.

Generally, there are two ways to distinguish the chip formation process: one is based on the chip morphology, known as continuous chips, lamellar chips, segment chips and discontinuous chips [57], [94] shown in Figure 5-

12; the other is according to the flow property of the workpiece material, such as brittle material and ductile material [95],[96].

In the following sections, chip morphology will be discussed.

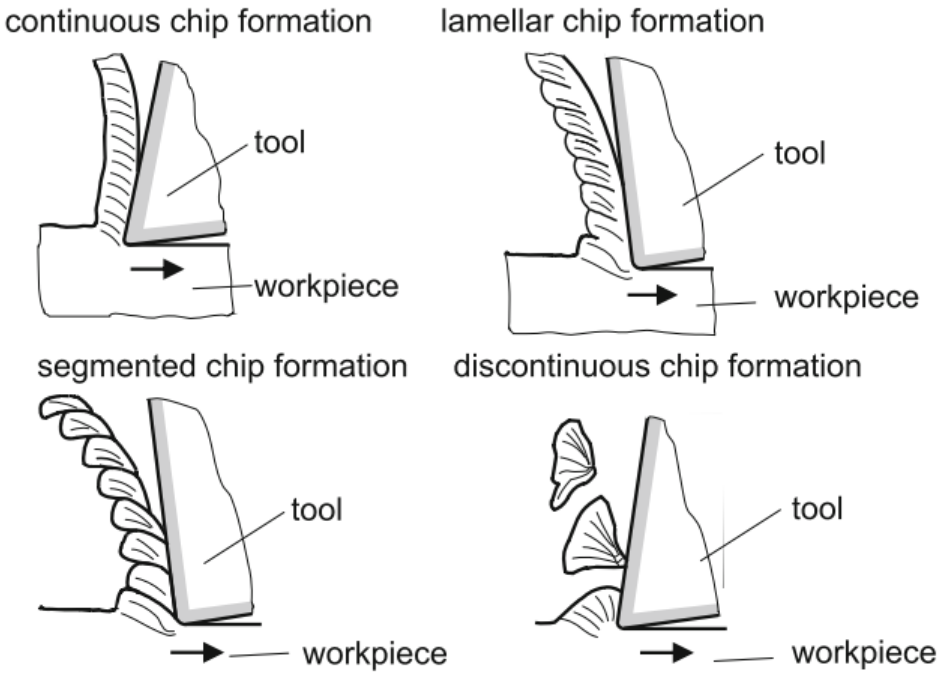

Figure 5-12 Four types of chips [94]

3.4.2.1 Continuous Chips

To form a continuous chip, the maximum shear stress for the material (σ_{max}) is bigger than the maximum shear stress in the deformation zone(σ_0). The stress-strain relationship for ductile material is shown in Figure 5-13.

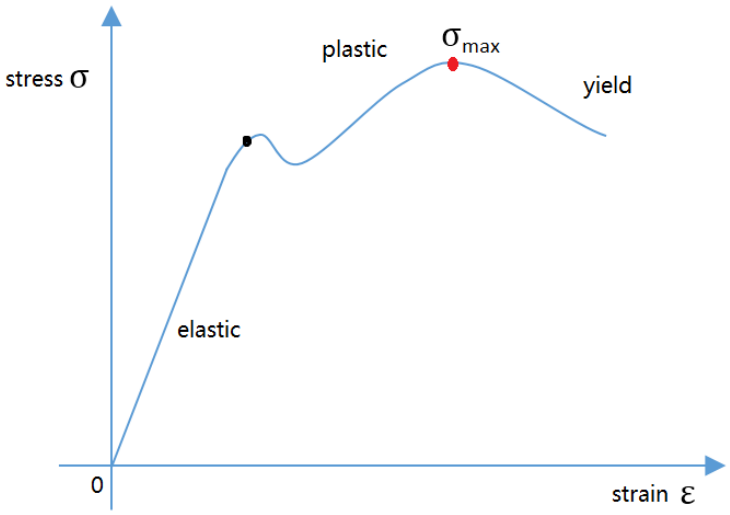

Figure 5-13 Flow stress property

There will be no fracture happening in the cutting area, the microstructure in the cutting zone tend to be uniform and the metal undergoes the continuous plastic deformation due to the compression stress. Then the chip will flow up along the rake face of the cutting tool.

When using a commercial FEM software to simulate this type of chip (as shown in Figure 5-14), the shear zone can be clearly seen.

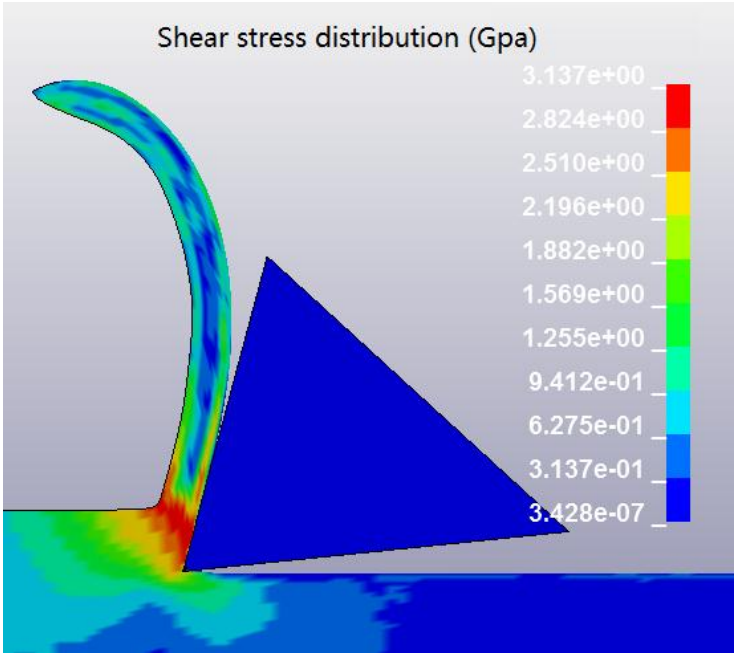

Figure 5-14 Continue chip formation

Almost the same thickness of the chip is obtained throughout and since it is very stable during the cutting, a best surface finish could be expected compare to the other types of chip.

The continuous chip is most likely to form in the following condition:

- Ductile material to withstand the plastic deformation.
- High cutting speed for the smooth flow of the ductile material
- Small chip thickness
- Positive and large rake angle for the material to flow easily
- Sharp cutting edge
- Using coolant and lubricating
- Small friction between the chip and cutting tool surface

However, along the continuous chip, a strong and almost uniform shear stress exists, so it is very hard to break this type of chip and may result the damage of the cutting tool.

3.4.2.2 Lamellar Chips

Lamellar chip is also a result of continuous chip formation process, however, some reasons such as the non-uniform microstructure will cause the happening of cleavages or even the adiabatic shear band which usually occur in the segment chips.

Physically, $\varepsilon_B < \varepsilon_0 < \varepsilon_F$ is necessary to form the lamellar chip, see Figure 5-15

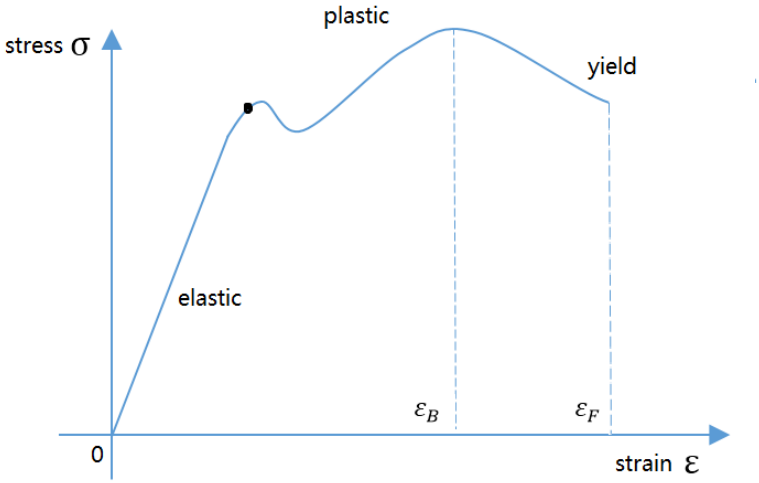

Figure 5-15 Condition for lamellar chip

The lamellar chip is most likely to form in the following condition:

- Ductile material with the strain harden effect
- A high chip formation frequency in KHz range
- High cutting speed
- High feeding speed
- Sharp tool edge
- Positive rake angle

3.4.2.3 Segment Chips

Segment chips consist of elements which break along the shear band and stick together again.

The Segment chip is most likely to form in the following condition:

- Brittle material like cast iron
- Negative rake angle to form a compression stress
- Higher chip thickness
- Relative low cutting speed

However, according to Hua and Shivpuri [97], the chip shift from discontinue to segment when the cutting speed going up when machining Ti-6Al-4V. They argued that as the increasing of the cutting speed, the

maximum stress in the deformation zone changes from the tool tip to the free surface of the deformed chip. The different initiation and propagation of the crack under different cutting speed is the main reason for shifting from the discontinuous chip to segmented chip.

3.4.2.4 Discontinuous Chips

Discontinuous chip occurs when the workpiece material flow behaviour tends to be brittle or a sliding path is predefined because of the inhomogeneous microstructure. The most common material is the cast iron. When the cutting tool penetrate into the workpiece material, the elements of the parts tear apart with each other due to the loose linking with each other.

The Discontinuous chip is most likely to form in the following condition:

- Brittle material in order to form a crack
- Large chip thickness
- Low cutting speed
- Small rake angle

Discontinuous chips can also be formed when choose a suitable chip breaker in the cutting tool or using the coolant in the cutting process even in the ductile material.

3.4.2.5 Experiments to understand the chip-formation process

The real chip formation process is very complicated and have to depend on the experiments to validate the theory.

Three methods are commonly used to investigate the chip formation process.

- Marking rectangular or circular grids on the side of the deformed material. As shown in Figure 5-16.

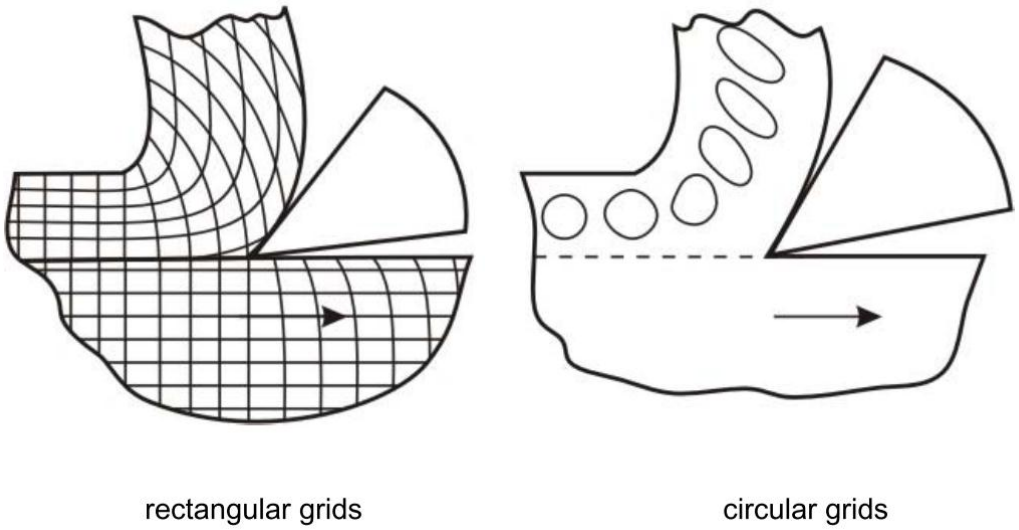

Figure 5-16 Marking grids on the side of the material

- Quick stop or cutting tool dropping to observe the frozen chip morphology
- Using high speed camera fitting with low magnification microscope to catch the chip formation process.

Apart from the experiment method, FEM is widely used and a lot of researchers use commercial FEM software to investigate the mechanism of chip formation and make a great improvement.

Calamaz et al. [98] found out that segmented chips are produced in a wide range of cutting speeds and feeds for the titanium alloy machining.

Sun et al. [99]] figured out that under low cutting speed and large feed rate conditions, both continuous and segmented chip can be observed.

3.4.3 Chip separation criteria

FEM method become more and more popular in investigating the metal cutting process. In order to simulate the chip formation process, a criterion for the chip separation is vital.

No matter what kind of criteria is used, it can be classified as geometrical and physical method [57].

3.4.3.1 Geometrical method

Mabrouki et al [90] divided the geometrical method into two different techniques:

➢ The node separation technique:

A predefined line is adopted to form the chip. Each two nodes on the line are tied together. The tied nodes will separate with each other when the cutting tool approaches, and a pre-defined criterion is met.

Zone-Chin Lin and S.-P. Lo. [100] used this method as the separation criteria. See Figure 4-17.

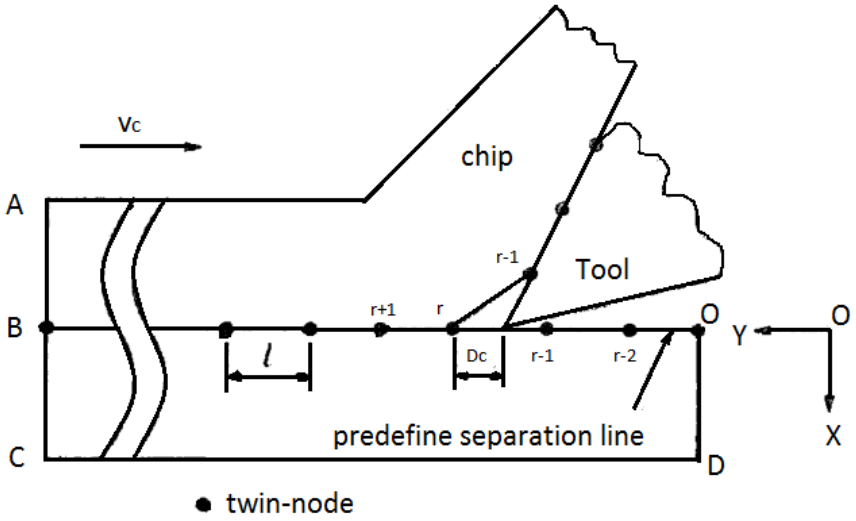

Figure 5-17 Node separation based on critical distance [100]

When the distance between the cutting tool edge and the leading node is equal or smaller than the predefined value D_C , the twin-nodes will separate one by one to form the chip and the machined surface.

When simulate a continuous chip, the critical value D_C must be very small. As the trial and error,

$$D_C = 0.01\ L \sim 0.03L \qquad (5\text{-}31)$$

Where L is the length of the element, to make sure the formation of the continuous chip.

Even though, the critical distance value can be chosen arbitrarily, and no

obvious physical meaning, this method is very easy to handle and understand.

- The element deletion technique:

A predefined sacrificial element zone is laid at the bottom of the chip as the separation layer. When the cutting tool reaches the bottom element, and a given criterion is satisfied, the sacrificial element will be deleted.

Element deletion is based on the equivalent plastic strain or previous material damage. The biggest disadvantage for this method is the loss of material. So the element size in the cutting layer should be as small as possible to reduce the effect of the element deletion.

When a purely ductile material is assumed, an automatic remeshing process can be used for the formation of the chip without a separation criterion.

3.4.3.2 Physical method

In the physical method, a predefined physical parameter will be chosen to judge the separation of nodes in the workpiece [71]. Strain, stress, or strain energy density can be used as the parameter depending on the workpiece material and cutting condition.

It seems that using a physical criteria tend to be more accurate in chip separation process because the connection with the work piece properties. However, deciding the critical value for the real cutting process is still a difficult thing. For example, a simple uniaxial tensile test can be used to measure the strain energy of work piece material, but in actual metal cutting process, the mechanical conditions can be significantly different. Therefore, this parameter can't be used as a critical value. On the other hand, when using effective plastic strain as a critical value, the change between the dynamic state and steady state must take into account. Sometimes, using this value as separation criterion is not a wise choice.

As seen in the Figure 5-18, when the physical value of the node exceeds the I_{KR}, It will separate from the workpiece to form the chip.

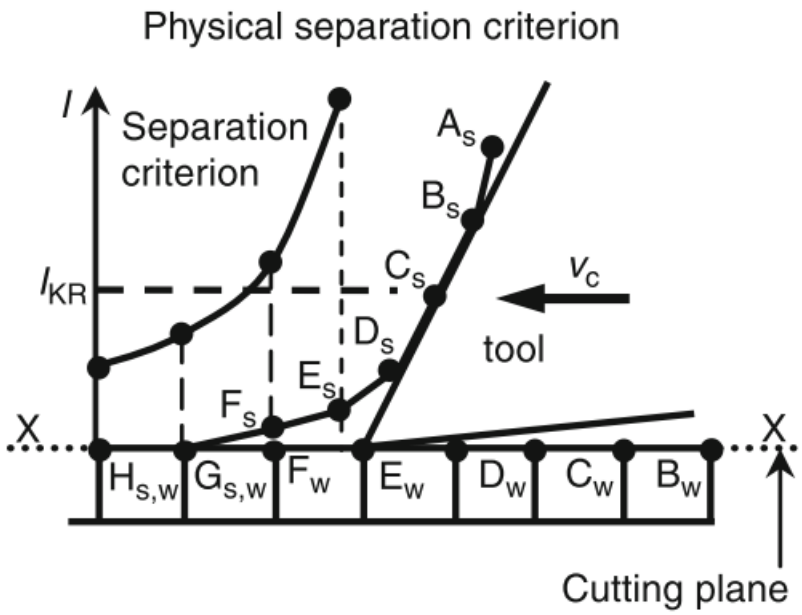

Figure 5-18 Physical separation criteria [57]

3.4.4 Friction model

In metal cutting simulation process, friction model between chip and tool interface has a significant effect on simulation results such as cutting forces, temperature and tool wear. On the other hand, cutting condition and tool geometry will affect the friction between the contact surfaces due to the high normal pressure.

Researchers try to find out the right friction model to represent the actual material flow behavior. Generally, three methods are widely used to determine the friction in the chip and cutting tool surfaces using Finite Element Method.

3.4.4.1 Constant Coulomb (model I)

The friction Law for constant Coulomb were stated by Amonton and Coulomb. These law is:

- The coefficient of the friction is constant in the contact interface and independent of the sliding surface.

This model can be written:

$\tau = \mu \sigma_n$ (5-32)

Where τ is the frictional stress, σ_n is the normal stress and μ is the coefficient of friction.

When normal stress is below a critical value, this law is valid. However, in metal cutting process, the normal stress can be very high and contact surface between tool and chip will increase which is different from the law.

3.4.4.2 Constant Shear (model II)

In Constant shear model, frictional stress on tool rake face is kept constant. The shear stress can be written as:

$\tau = mk$ (5-33)

Where m is friction factor and k is shear flow stress of the work material. In FE simulations, m should be estimated and represent the friction of entire tool-chip interface.

3.4.4.3 Constant Shear in Sticking Zone and Constant Coulomb in Sliding Zone (model III)

The friction on the tool-chip surface can be expressed by normal stress and frictional stress on the tool rake face.

In order to study the detail in the contact surface, two direct measurement methods were mentioned by Özel [52]: the split-tool and photo elastic method. And the split-tool technique has the capacity to obtain the true normal and frictional stress during dry orthogonal cutting.

Usui and Takeyama in [71] measured the normal (σ) stress and shear stress (τ) on the surface of the cutting tool. As shown in Figure 5-19. The shear stress remains constant from A to B, and decreases to zero from B to C. On the other hand, the normal stress decreases to zero from A to C.

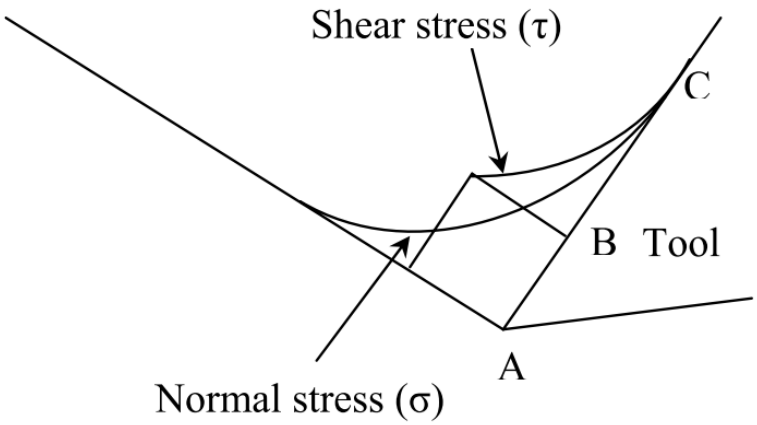

Figure 5-19 Distribution of normal and shear stress on the rake face

In the sticking region AB, normal stress is high enough for metal adhering to the rake face and contact area to total area ratio approaches unity. Plastic deformation occurs in this area. In the sticking region, coefficient of friction varies with the magnitude of the normal load. Through computing, the coefficient of friction is lower in this region than that in sliding friction conditions.

In the sliding region BC, which starts from the end of the sticking region, ends to the separating point between the tool rake face and the chip, the coefficient of friction is constant. So the sliding friction occurs in this area.

This model can be expressed as:

$$\tau_f(x) = \tau_p \; when \;\; 0 < x \leq l_p \qquad (5\text{-}34)$$

$$\tau_f(x) = \mu\sigma_n(x) \; when \;\; l_p < x \leq l_c \qquad (5\text{-}35)$$

Where τ_f is the frictional stress, τ_p is the average flow stress on the contact region, μ is the friction coefficient, σ_n is the normal stress and l_p is the limiting point of the sticking area and sliding area.

The difficulty is to define the boundary of the sticking area, i.e. value of l_p.

According to Shatla, et al. [101], the length of the sticking region was two times of the uncut chip thickness which is not the case if a large cutting depth is used.

3.4.4.4 Choice in the thesis

In this thesis, the workpiece material is Ti-6Al-4V, and the cutting tool is the carbide tool, thus a constant coefficient of friction 0.24 will be used according to [79].

3.5 Summary

According to the previous description, explicit method is more suitable for dynamic situation such as cutting process. Lagrangian description can be useful to describe the solid movement without severs distortion. Ls-dyna is used because its ability in describing dynamic problem.

Thus explicit method and Lagrangian description are adopted in the finite element simulation process. Ls-dyna is used as the finite element code.

Ti-6Al-4V is used for the workpiece material because its perfect physical property and widely use in the aerospace industry.

The Johnson–Cook constitutive model and damage model are employed because their accuracy to represent the workpiece property.

Physical method is used to simulate the chip separation because its connection with the work piece properties, thus more accurate in chip separation process.

Constant Coulomb's friction model is adopted according to the validation paper.

4 Modelling and simulation

4.1 Introduction

Modelling is the most important part of cutting process simulation in order to achieve acceptable results. In this chapter, the assumptions for building the model will be presented first. Then, the modelling of cutting tool, workpiece, and the cutting system will be discussed. Finally, the parameters used in the simulation process will be explained.

4.2 Assumptions for modelling

The metal cutting is a very complex process. It is nearly impossible to consider everything in one model. In order to investigate the influence of a specific variable such as cutting depth, cutting speed or wear, assumptions are needed to simplify the finite element model. Through the simplification process, the model becomes easier to build and the running time can be diminished to get a satisfied result. In this thesis, the assumptions in defining the problem are as follows:

- Plane strain assumption.

In plane strain problem, the dimension of the structure in one direction is much larger than that in the other two dimensions [79].

Under this assumption, orthogonal cutting model can be used.

- Machine base and fixture are both rigid in the cutting process.

In light cutting process, the oscillation of the base and fixture is quite small and can be ignored. Take the base and fixture as rigid can simplify the modelling process.

- Adiabatic thermal assumption.

Since the cutting time is very short, there is no heat conduction, heat convection and radiation between the cutting system and environment.

➢ Wear evolution process would be replaced by changing the tool geometry

With the sharp edge, a shear plane instead of the shear zone will appear in the deformation zone, which makes the model simpler [30]. Wear evolution needs the remeshing process to simulate the loss of material, which is not available in the Ls-dyna FEM method. The meshless method EFG would be more suitable for this kind of situation.

➢ The tool shank is rigid and cutting tool tied on it

Since the stress and strain distribution in the cutting tool need to be investigated, the tool cannot be a rigid body. In order to apply a constant cutting speed on the cutting tool, a tool shank is introduced and made rigid. The cutting tool is tied to the tool shank in Ls-dyna.

4.3 Cutting tool modelling

In order to validate the model, the cutting tool is regarded as rigid in the first place. Its geometry and properties are adopted from [79].

The geometric variables of the cutting tool are given in Table 6-1

Table 6-1 Geometric variables of the cutting tool [79]

Rake Angle, α (°)	Clearance Angle, c(°)	Edge radius, r (mm)
0	6	0

Tungsten carbide (WC) is used as tool insert. The properties of WC are given in Table 6-2.

Table 6-2 Physical properties of WC [79]

Physical parameters	Tungsten carbide insert
Density ($\mathrm{Kg/m^3}$)	11,900
Elastic modulus (Gpa)	534
Poisson's ratio	0.22
Conductivity (W/m K)	50
Specific heat (J/kg K)	400

Finite element mesh of tool is modelled with quadrilateral elements as the same as in [79] using 2808 nodes and 881 elements. There are more

elements in the contact area. Bias method is used to improve mesh density near the tool tip and contact face to obtain more accurate stress and temperature distribution results. This tool mesh design is shown in Figure 6-1.

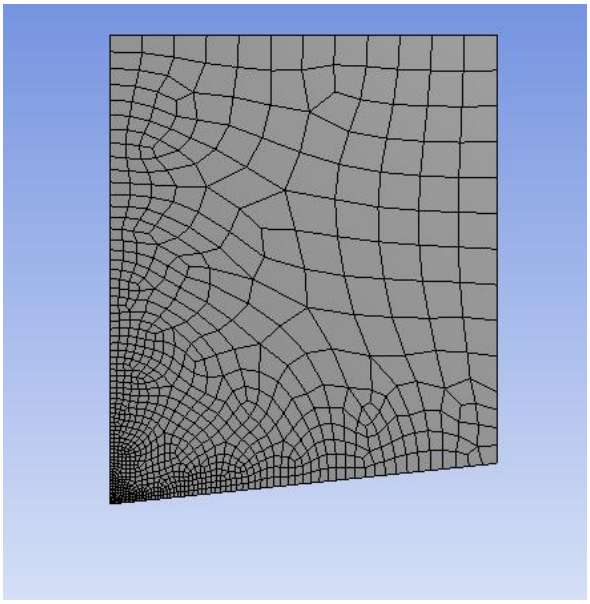

Figure 6-1 Cutting tool modelling

4.4 Workpiece modelling

In a finite element simulation system, the workpiece material plays a very important role. For the modelling process, it is vital to have a precise constitutive model and damage model. As mentioned in the last chapter, three constitutive models are frequently used in research area to represent the flow stress under high strain, strain rate and temperature. They are the Johnson–Cook (J-C) model, The Steinberg–Cochran–Guinan–Lund (SCGL) model and the Zerilli–Armstrong (Z-A) model.

According to the report by Banerjee [83], the Johnson-Cook model has the minimum average error when testing these flow stress models. So the Johnson-Cook model will be adopted in this modelling process.

There are six constants in the Johnson-Cook model, for Ti-6Al-4V, which is used as the workpiece material, Wang et al. [102] gave out a brief conclusion about the seven groups of parameters. Kay [103] obtained a new

group of J-C constants under both high and low strain rate based on the data of the other two models which is used in Zhang et al. [104]. Another model is mentioned by Liu [105] to simulate the high-speed machining of Titanium alloy.

In this literature, the J–C material constants are selected from Kay [103] and Liu [105]as shown in Table 6-3 which are already validated by experiments.

Table 6-3 Johnson-Cook constants

Model	A (Mpa)	B (MPa)	n	C	m	$\dot{\varepsilon}_0$ (s^{-1})	Reference
One	1098	1092	0.93	0.014	1.1	1	[103]
Two	860	683	0.47	0.035	1	1	[105]

The difference between these two model can be seen from the flow curves under different conditions.

Due to high strain, strain rate and temperature in metal cutting, the material flow stress data is represented by flow curves at 11 different strain (0.05, 0.5, 1, 1.5, 2, 2.5, 3, 3.5, 4, 4.5, 5), 4 different strain rates (1, 100, 10000, 100000 s^{-1}) and 6 different temperatures (20, 100, 300, 600, 900, 1200 ℃).

The flow curves can be seen as follows.

4.4.1 Flow stress curves for model one

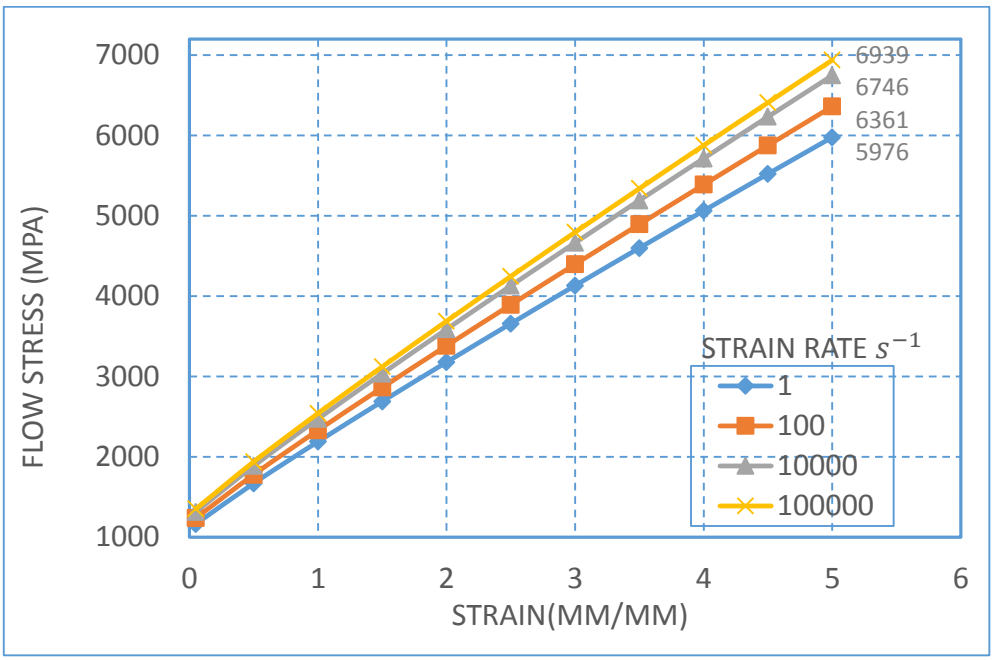

Figure.6-2 Ti-6Al-4V Johnson-Cook flow curve at T=20 ℃

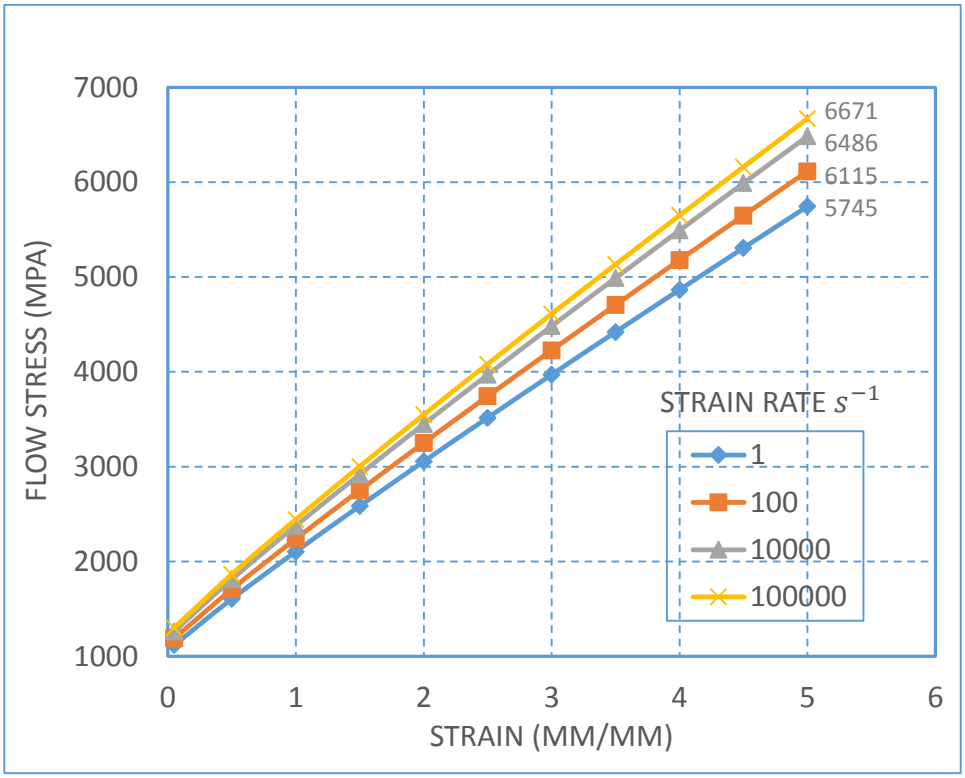

Figure 6-3 Ti-6Al-4V Johnson-Cook flow curve at T=100 ℃

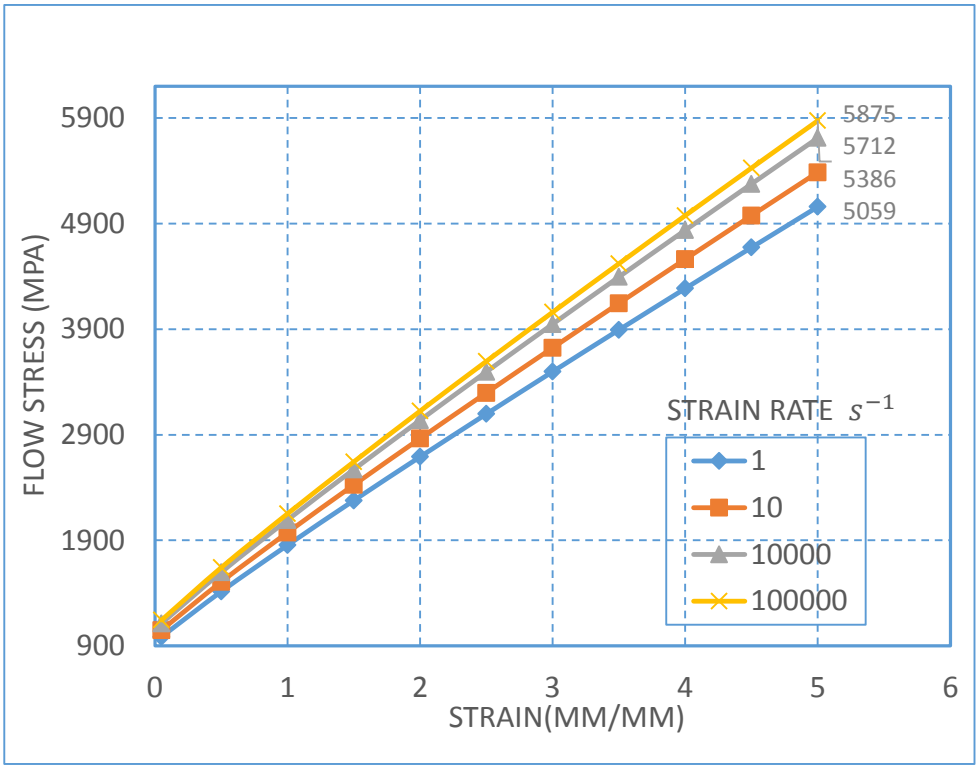

Figure 6-4 Ti-6Al-4V Johnson-Cook flow curve at T=300 ℃

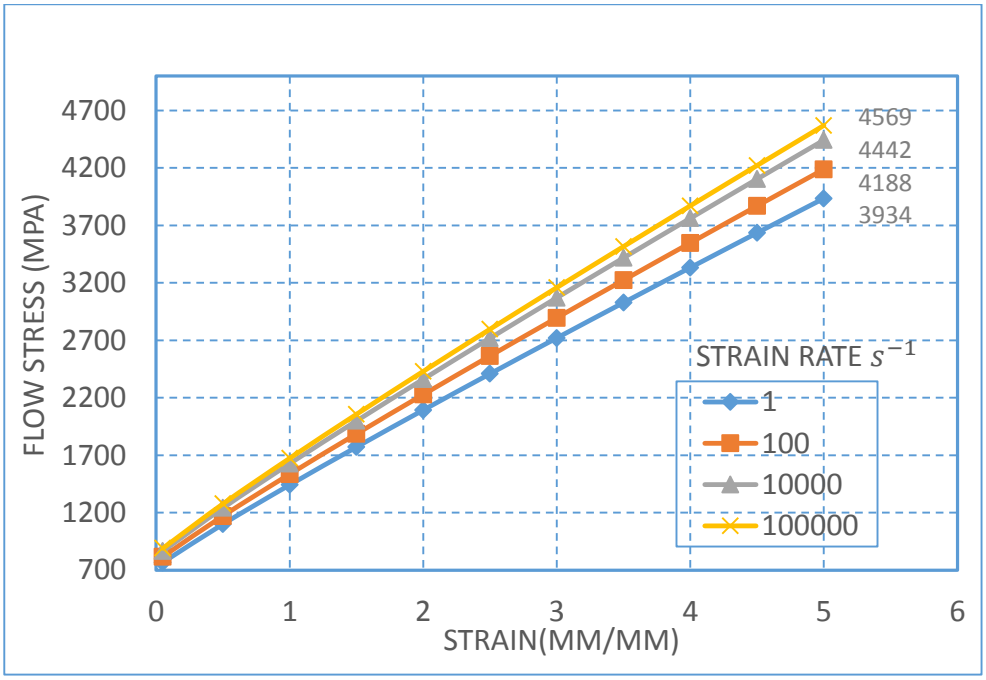

Figure 6-5 Ti-6Al-4V Johnson-Cook flow curve at T=600 ℃

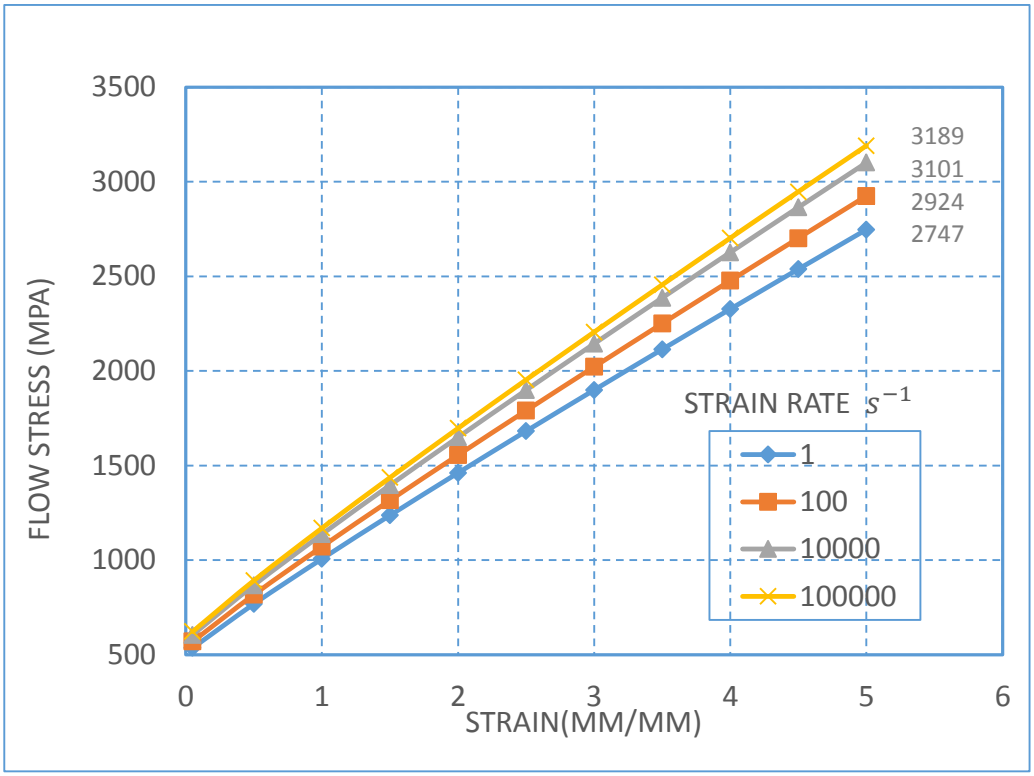

Figure 6-6 Ti-6Al-4V Johnson-Cook flow curve at T=900 ℃

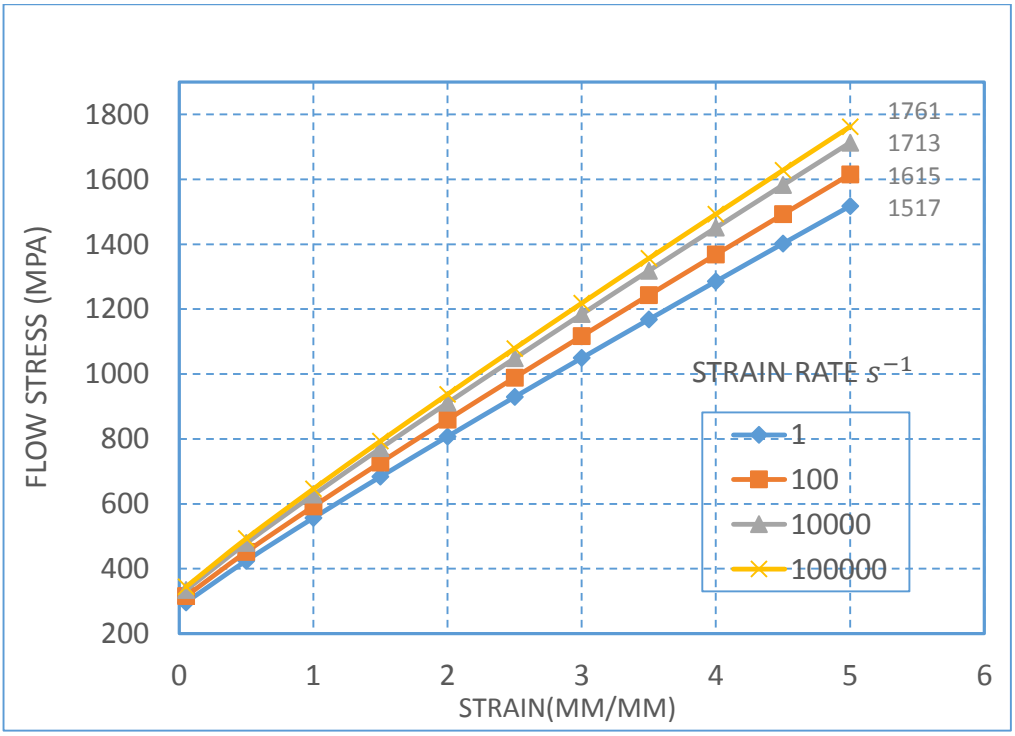

Figure 6-7 Ti-6Al-4V Johnson-Cook flow curve at T=1200 ℃

4.4.2 Flow stress curves for model two

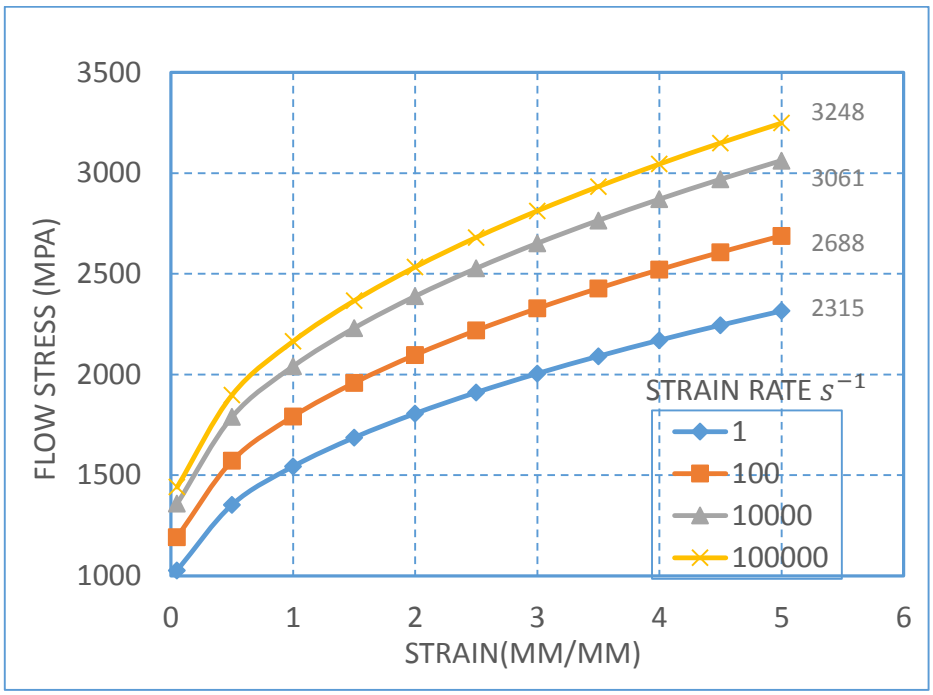

Figure 6-8 Ti-6Al-4V Johnson-Cook flow curve at T=20 ℃

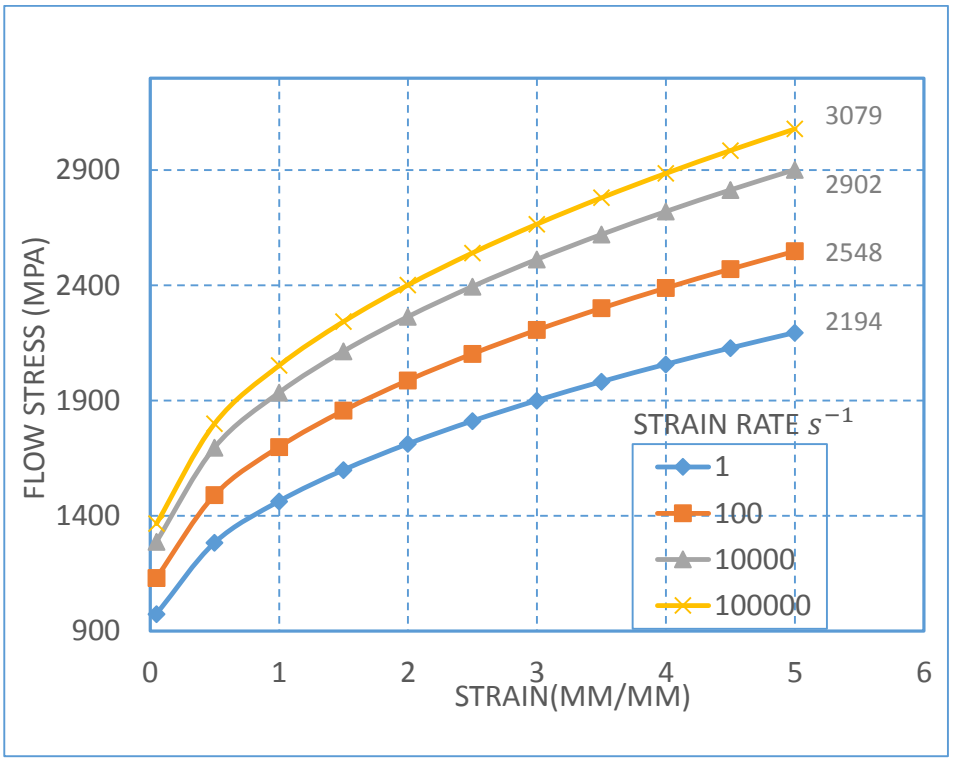

Figure 6-9 Ti-6Al-4V Johnson-Cook flow curve at T=100 ℃

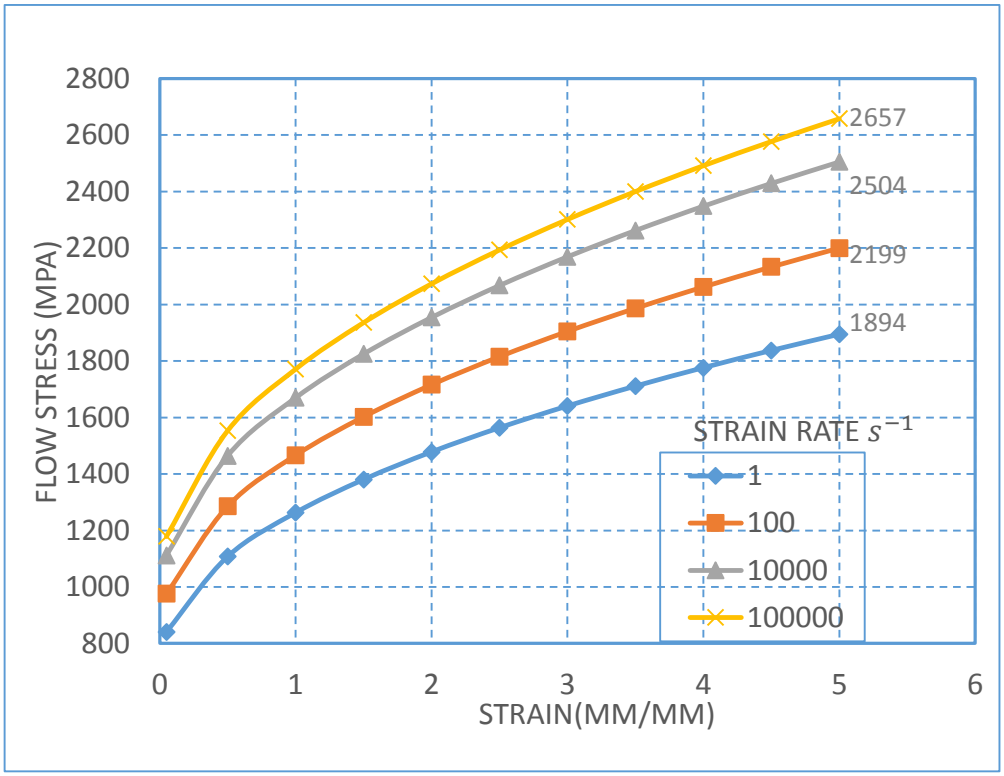

Figure 6-10 Ti-6Al-4V Johnson-Cook flow curve at T=300 ℃

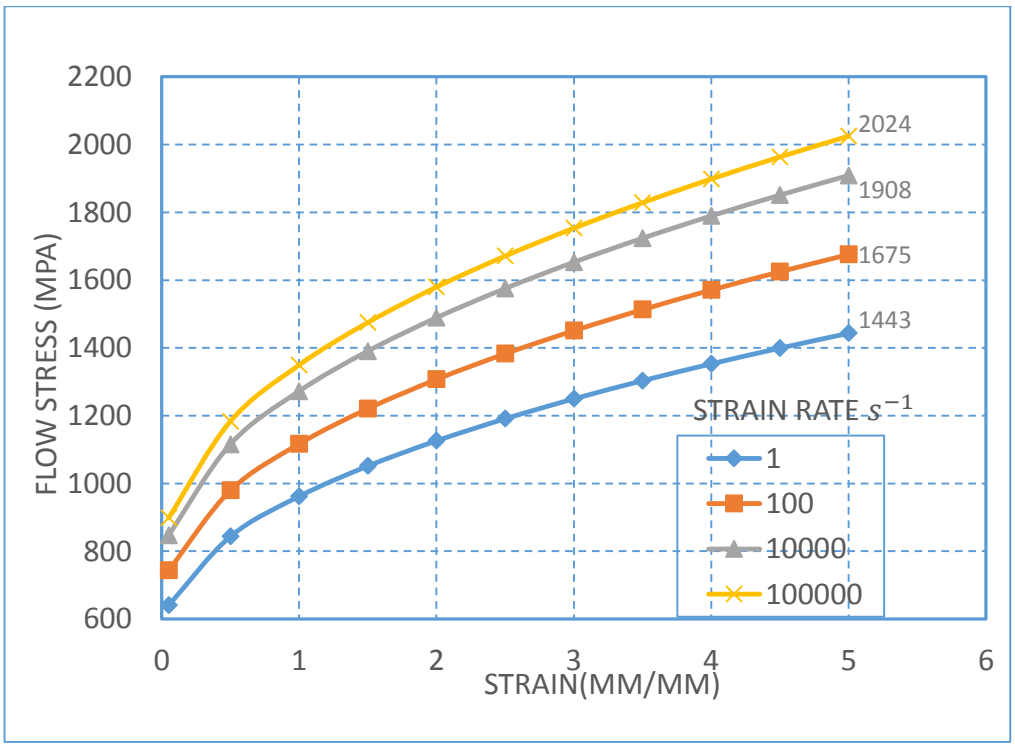

Figure 6-11 Ti-6Al-4V Johnson-Cook flow curve at T=600 ℃

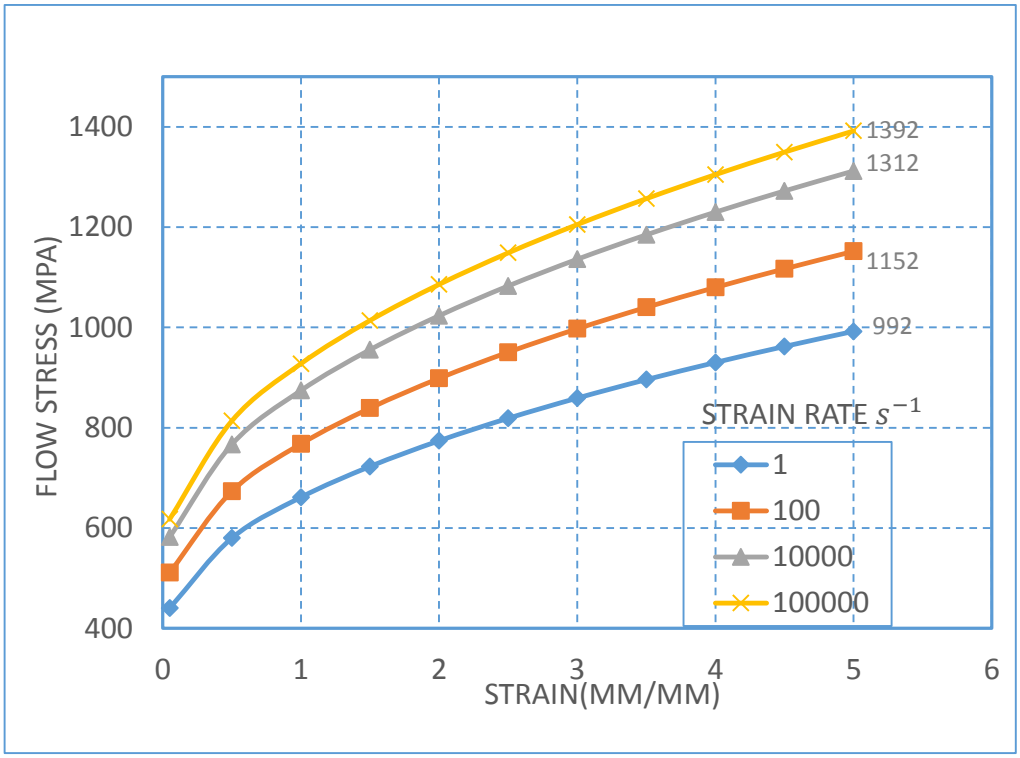

Figure 6-12 Ti-6Al-4V Johnson-Cook flow curve at T=900 ℃

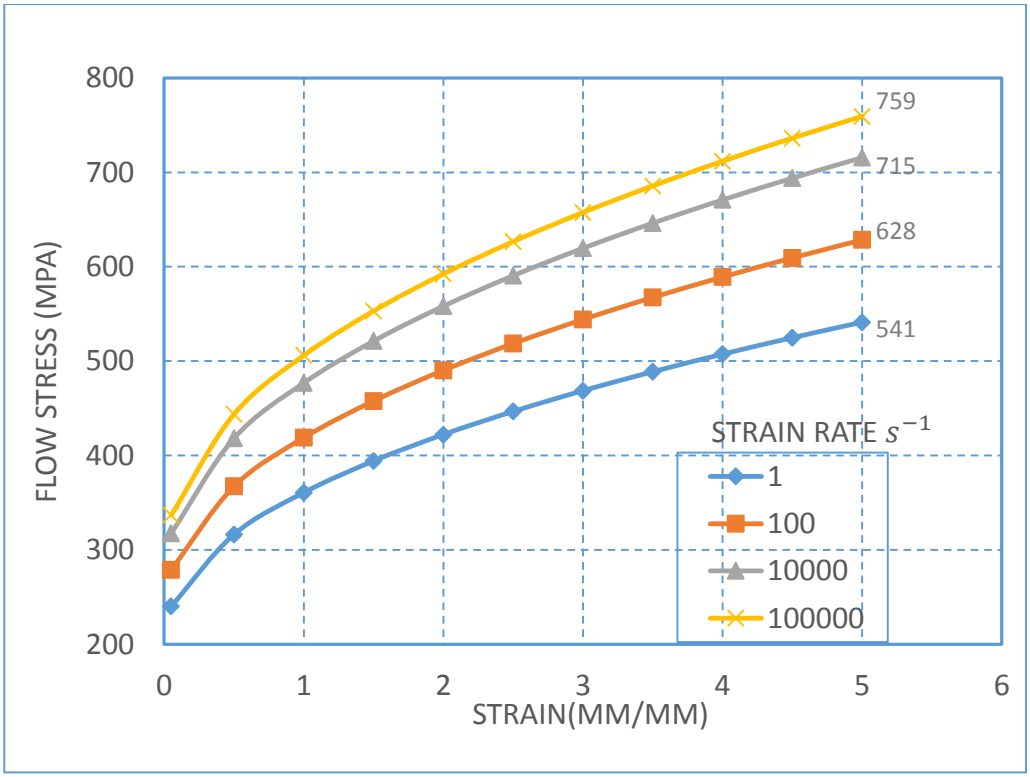

Figure 6-13 Ti-6Al-4V Johnson-Cook flow curve at T=1200 ℃

4.4.3 Difference between two constitutive models

The effects of strain, strain rate harden and thermal soften in two models are different. It can be concluded from the curves as follows:

4.4.3.1 Effect of strain rate

For model one, when keep the temperature and strain as constant, and strain rate varies from 1 to 100000, the change of stress is only 14.1%. While for the model two, the change of stress is 40.3%. As seen from Figure 6-14

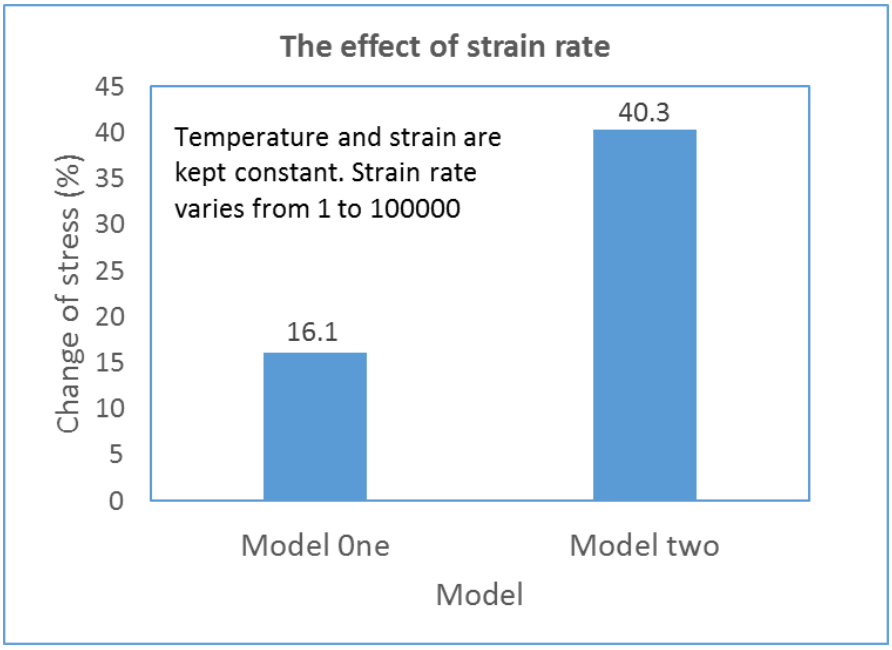

Figure 6-14 The effect of strain rate

4.4.3.2 Effect of strain

For model one, if the temperature and strain rate are not changed, and strain varies from 0.05 to 5, the change of stress is 413%. In the meantime, the change of flow stress in model two is 125%. As seen from Figure 6-15

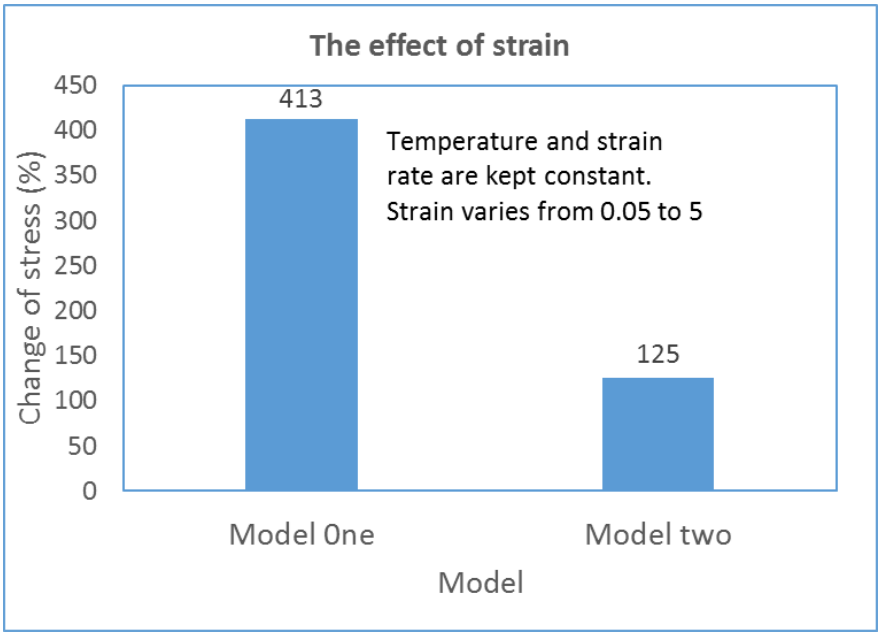

Figure 6-15 The effect of strain

4.4.3.3 Effect of temperature

For model one, when the strain and strain rate are regarded as constant, for each degree the temperature raises, the flow stress drop 4.3Mpa. However, the number in model two is just 1.4 Mpa. As seen from Figure 6-16

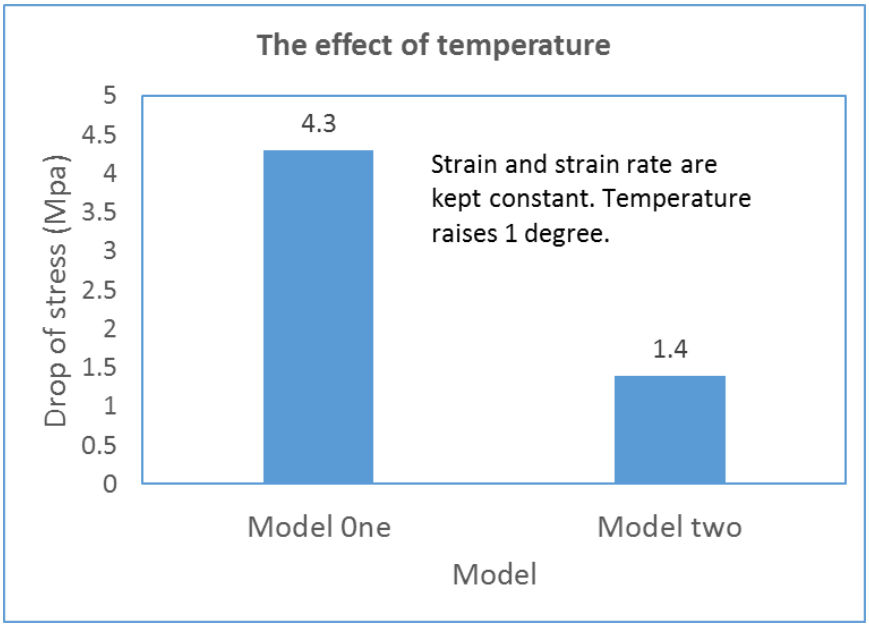

Figure 6-16 The effect of temperature

So there is an obvious strain harden and thermal soften effects in model one while the model two is focus on the strain rate harden effect.

The ductile Johnson-Cook damage model is used in this literature, which has already been introduced in the last chapter.

Five constants in the damage model are shown in Table 6-4

Table 6-4 Johnson-Cook damage model constants for Ti-6Al-4V [79]

d_1	d_2	d_3	d_4	d_5
-0.09	0.25	-0.5	0.014	3.87

The workpiece is modelled 5 mm long and 2 mm high. The physical parameters of the workpiece are show in Table 6-5

Table 6-5 Physical properties of Ti-6Al-4V [79]

Physical parameters	Workpiece (Ti-6Al-4V)
Density (kg/m^3)	4,430
Elastic modulus (Gpa)	109 (50℃) 91 (250℃) 75 (450℃)
Poisson's ratio	0.34
Conductivity (W/m K)	4.8 (20℃) 7.4 (100℃) 9.8 (300℃) 11.8 (500℃)
Specific heat (J/kg K)	611 (20℃) 624 (100℃) 674 (300℃) 703 (500℃)

Finite element mesh of the workpiece is modelled with quadrilateral elements using 12281 nodes and 4000 elements. The distribution of mesh on the workpiece is not uniform. There are more elements on the top than bottom, since only the top elements participate in the cutting process. There is no remeshing process in the cutting process, so the element in the cutting zone should be small enough to achieve a satisfied result.

This FE model of the workpiece is shown in Figure 6-17.

.

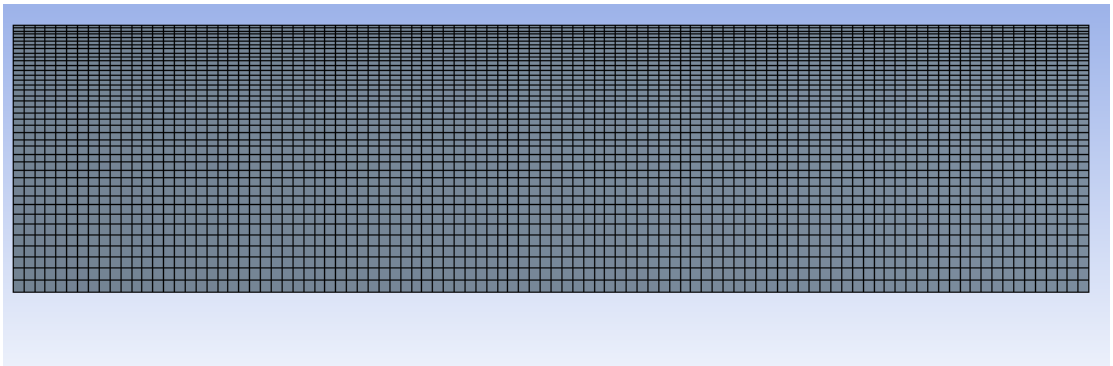

Figure 6-17 The workpiece modelling

4.5 System modelling

After modelling the cutting tool and the workpiece material, initial and boundary conditions will be discussed in the system modelling process.

The cutting system can be seen in Figure 6-18.

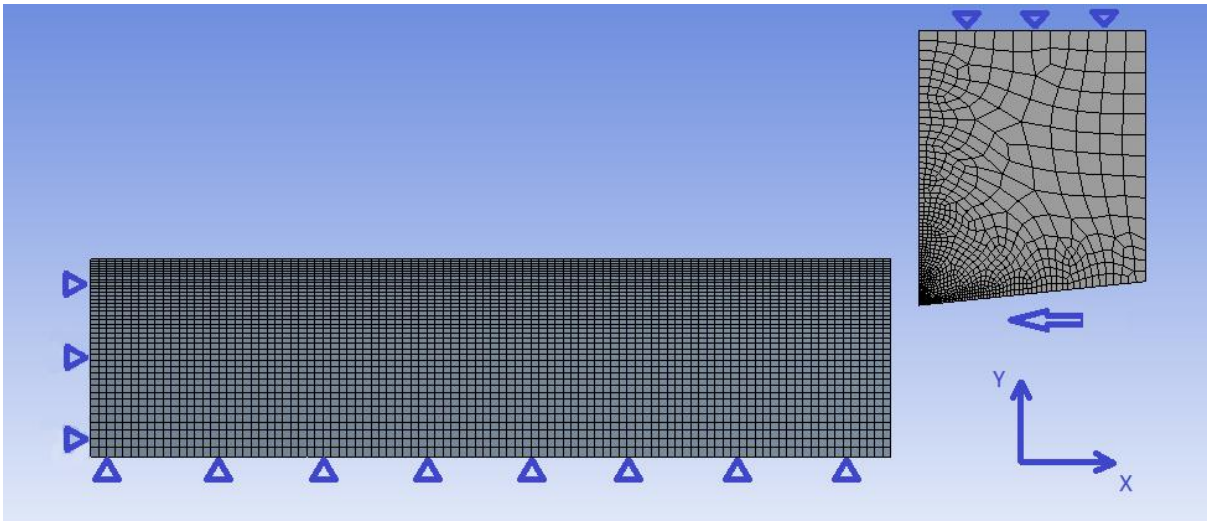

Figure 6-18. Cutting system

The cutting conditions are shown in Table 6-6

Table 6-6 Cutting conditions [79]

Cutting speed (m/min)	Cutting depth (mm)	Width of cut (mm)
4800	0.07	5

Displacement boundary conditions of the cutting system are shown in Figure 5-3 [79]. The left side and the bottom of the workpiece are fixed. The cutting tool is fixed at the Y direction and moves with a constant cutting speed along the negative X direction. Thus the cutting depth will not change in the whole cutting process.

The cutting system set as room temperature (25℃) at the beginning.

No coolant is applied in the cutting process.

In the cutting process, coolant can absorb the heat from the cutting zone, decrease the temperature in both workpiece and cutting tool. Furthermore, coolant can reduce the friction coefficient between the contact area. However, less and less coolant will be used in the future to protect the operators and environment.

So the cutting will perform without the coolant.

The contact between cutting tool and workpiece is thermal perfect, that is, a very large heat transfer coefficient for closed gaps is used. In this case, it is $10^7\ \mathrm{W/(m^2K)}$

There is no heat transfer between the cutting system and the environment due to the short cutting duration.

According to Shet [43], 85% to 95% of the plastic work converted into heat. So in this thesis, fraction of mechanical work converted into heat is set 0.9.

4.6 Parameters adopted in the cutting process

Throughout the simulation process, the workpiece material and cutting tool material will not change. Cutting speed, cutting depth and tool geometry may vary in different situations.

4.6.1 Validation model

In order to validate the model, all the conditions must be the same as the experiment settings mentioned in the literature. And all these parameters have been explained in the modelling process.

4.6.2 Effects of different cutting parameters

The situation in the validation model is not always the case. 4800m/min seems too high for most of the machines. In this thesis, the effects of different cutting parameters will be studied under low cutting speed condition and the effects of different wear types will be investigated in high speed cutting condition.

The common geometry rake angle=7°， clearance angle=6° is used according to [106] and [107].

In order to study the effect of cutting process parameters, 3 different cutting speed (5m/min, 15m/min, 30m/min), 3 different cutting depth (0.3mm, 0.5mm, 1mm), 3 different cutting tool edge radius (0mm, 0.05mm,0.1mm) were chosen. Thus 27 cases were studied. The process parameters for simulation are shown in Table 6-7 according to the reality in my company.

Table 6-7 The parameters for low speed cutting

Cutting speed (m/min)	5	15	30
Depth of cut (mm)	0.3	0.5	1
Tool edge radius (mm)	0	0.05	0.1

4.6.3 Effects of different wear types

The cutting tool geometry rake angle=7 °, clearance angle=6° is used. The cutting speed in this case is 240m/min when the cutting depth is 0.1mm according to the parameters used in my company. Cutting width is 1mm. The tool has a sharp edge and the inclination angle for the flank wear is 4°

according to [106], the flank wear shape of the cutting tool is shown in Figure 6-19.

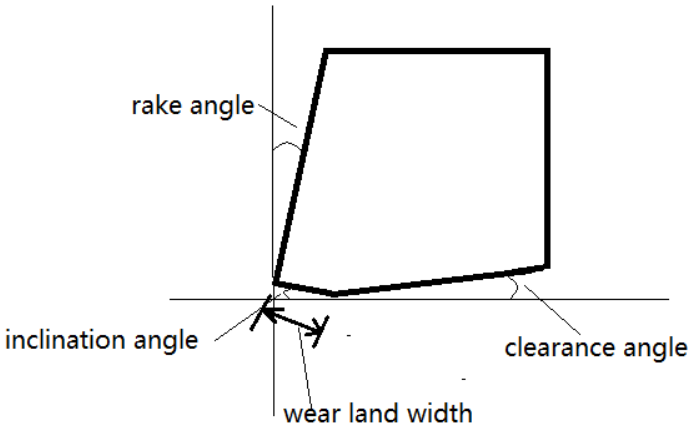

Figure 6-19 Flank wear land

For the flank wear, the wear land is chosen in Table 6-8

Table 6-8 Flank wear land

Flank wear (mm)	0	0.05	0.1	0.15	0.2	0.25	0.3

The crater wear geometry is shown in Figure 6-20

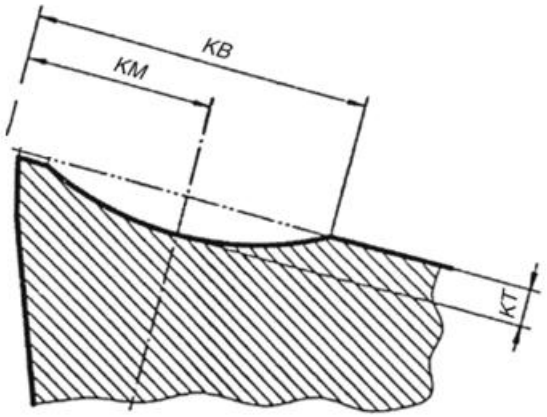

Figure 6-20 Crater wear land

There are two patterns of crater wear i.e., KB=2KM and KB<2KM. Both situations will be discussed. In titanium alloys machining process, temperature concentrates in a smaller area near the cutting edge comparing with the steel causing the crater wear on the rake face [107]. For steel, the distance from the cutting edge is 25μm [38], so in this thesis, the distance 10 μm is adopted. The maximum crater wear depth in [107] is around 40 μm,and the ration between crater wear length and depth is 5-15. The ration 10 is adopted.

The wear shape can be seen in Table 6-9 and Table 6-10.

Table 6-9 Crater wear when KB=2*KM

Case No.	KT (μm)	KB (μm)	KM(μm)
1	0	0	0
2	5	50	25
3	10	100	50
4	20	200	100
5	40	400	200

Table 6-10 Crater wear when KB<2*KM

Case No.	KT (μm)	KB (μm)	KM(μm)
6	5	60	35
7	10	110	60
8	20	210	110
9	40	410	210

5 Model validation

In this chapter, the simulation results will be presented. In the first place, the model will be validated through the experiment results from the published literature. Generally, the cutting force and the chip morphology will be used according to [79].

For Johnson-Cook model one, the chip breaks in the machining process. As shown in Figure 7-1.

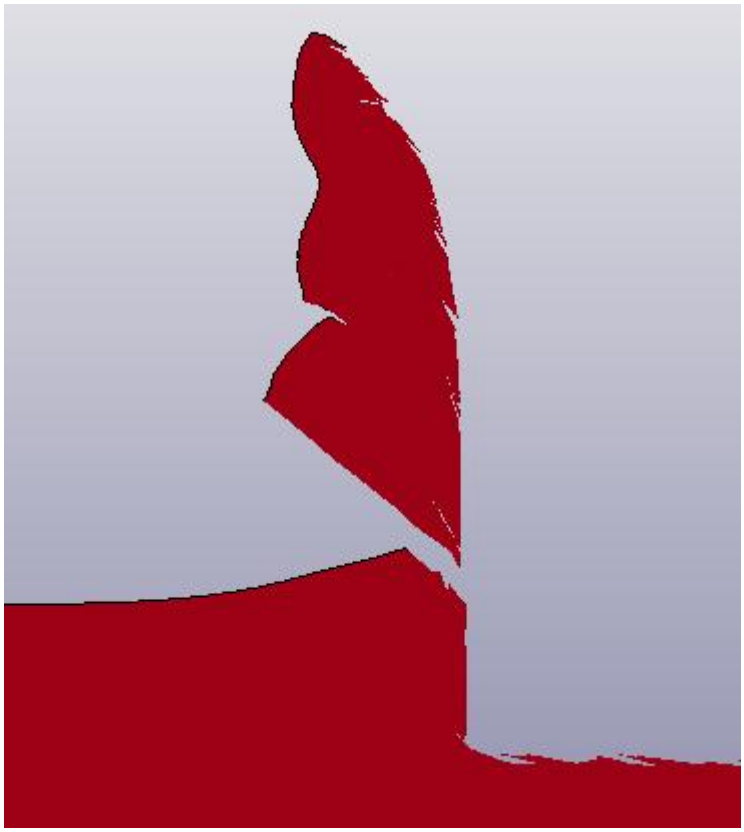

Figure 7-1 Chip formation for model one

For Johnson-Cook model two, segment chip is witnessed. As shown in Figure 7-2.

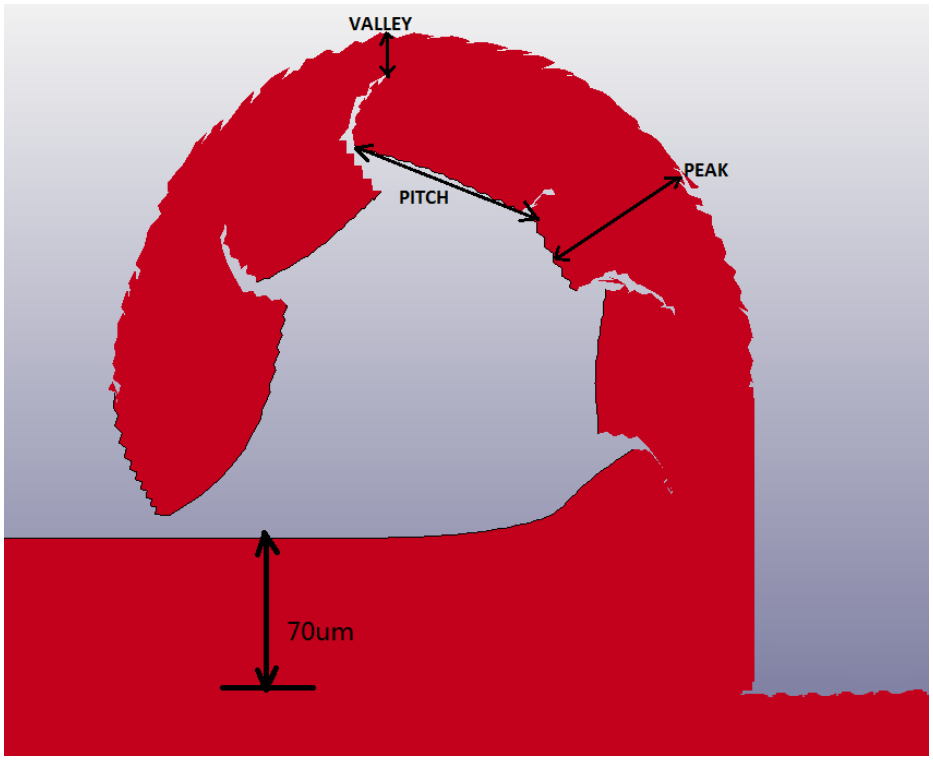

Figure 7-2 Segment chip formation for model two

The average peak is 84mm, the average pitch is 98mm.

The cutting force in this situation is shown in Figure 7-3.

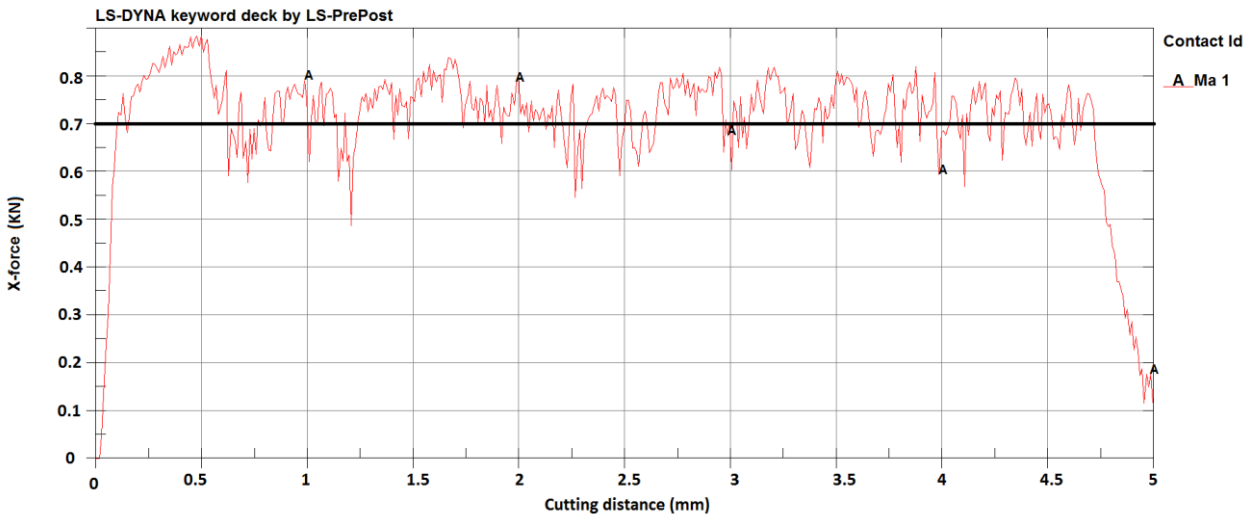

Figure 7-3 Cutting force for model two

Thus the average cutting force in stable state is 700N.

When comparing these data with the experiment results from the literature [79], the results can be seen from Table 7-1 and Table 7-2.

Table 7-1 Comparison of predicted chip morphology with experiment data

Chip morphology (μm)	Average peak	Average pitch
Experiment [79]	93	97.1
Simulation	84	98
Error	-9.7%	0.9%

Table 7-2 Comparison of predicted cutting force with experiment data

Cutting force (N)	
Experiment [79]	710
Simulation	700
Error	-1.4%

The predicted parameters have a good agreement with the experiments with absolute error within 10%.

Thus the model is validated with Johnson-Cook constitutive model two.

6 Results and discussion

After that, the variables related to the cutting tool such as cutting force, Von Mises stress and temperature distribution on the cutting tool will be investigated under different cutting conditions and tool geometry.

6.1 Effects of different process parameters on cutting tool

6.1.1 The effects of cutting speed

In this part of the study, effects of cutting speed on the cutting force, distribution of stress and temperature on the cutting tool are analysed. Different cutting depth and different cutting tool edge radius will be used.

6.1.1.1 The effect of cutting speed on the cutting force

The effects of different cutting speed on cutting force are shown in Figure 8-1, Figure 8-2. and Figure 8-3.

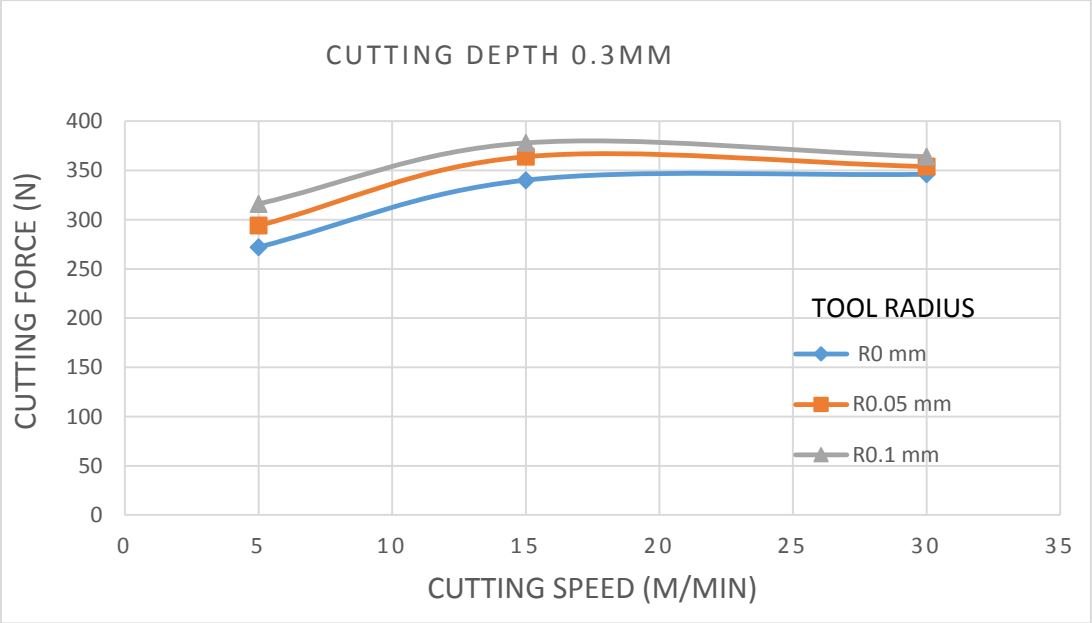

Figure 8-1 Relationship between cutting speed and cutting force when cutting depth is 0.3mm

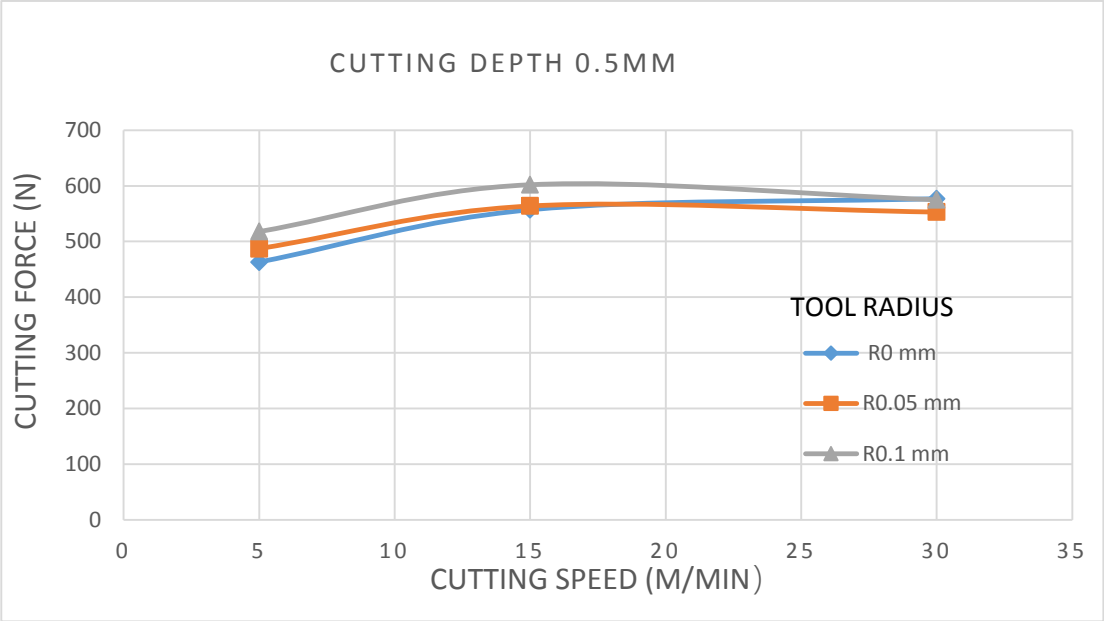

Figure 8-2 Relationship between cutting speed and cutting force when cutting depth is 0.5mm

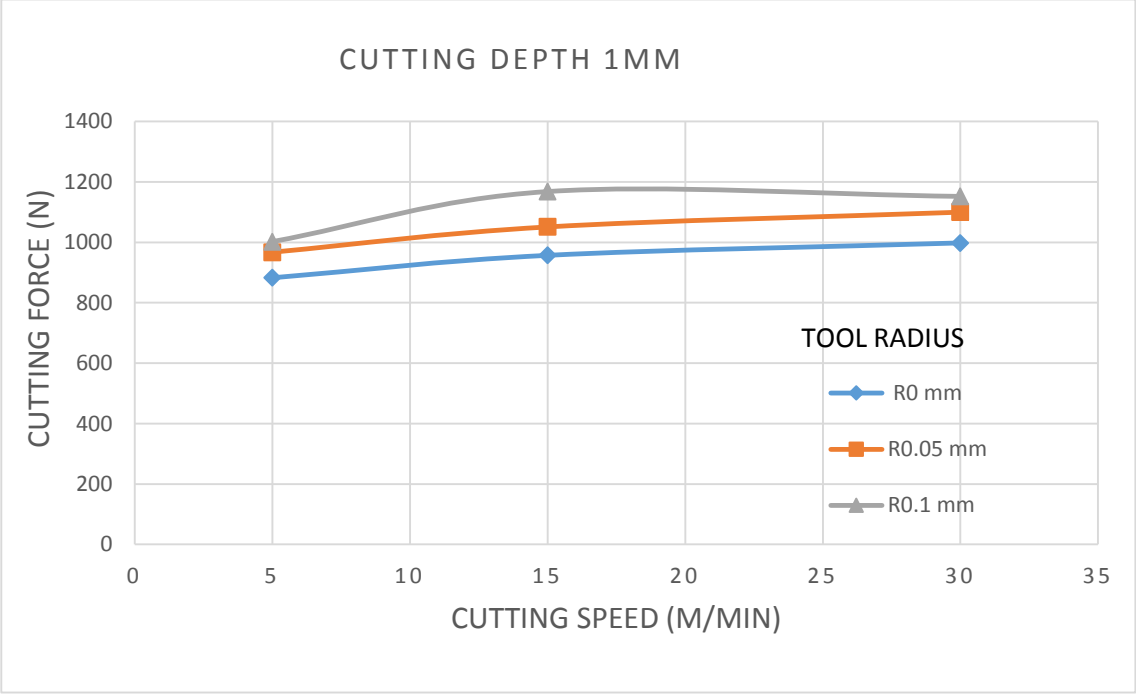

Figure 8-3 Relationship between cutting speed and cutting force when cutting depth is 1mm

These three figures show a similar trend of the relationship between cutting speed and cutting force. When the cutting speed increase from 5 m/min to 15 m/min, the cutting force increase more than that from 15 m/min to 30 m/min. This may distribute to the increasing of plastic deformation in the shear zone, the strain harden effect predominant in this stage. However, as the cutting force increase, the temperature in the contact region raises fast, causes the thermal soften effect in the plastic deformation zone. In some cases, the cutting force in 30m/min is even smaller than that in 15m/min which is also discovered by Nalbant et al. [108] when cutting Inconel 718 super alloys using coated cemented carbide tool.

6.1.1.2 The effect of cutting speed on the cutting tool maximum temperature

Cutting speed is an important parameter in the cutting process affecting the maximum temperature on cutting tool. The results are shown in Figure 8-4, Figure 8-5. and Figure 8-6.

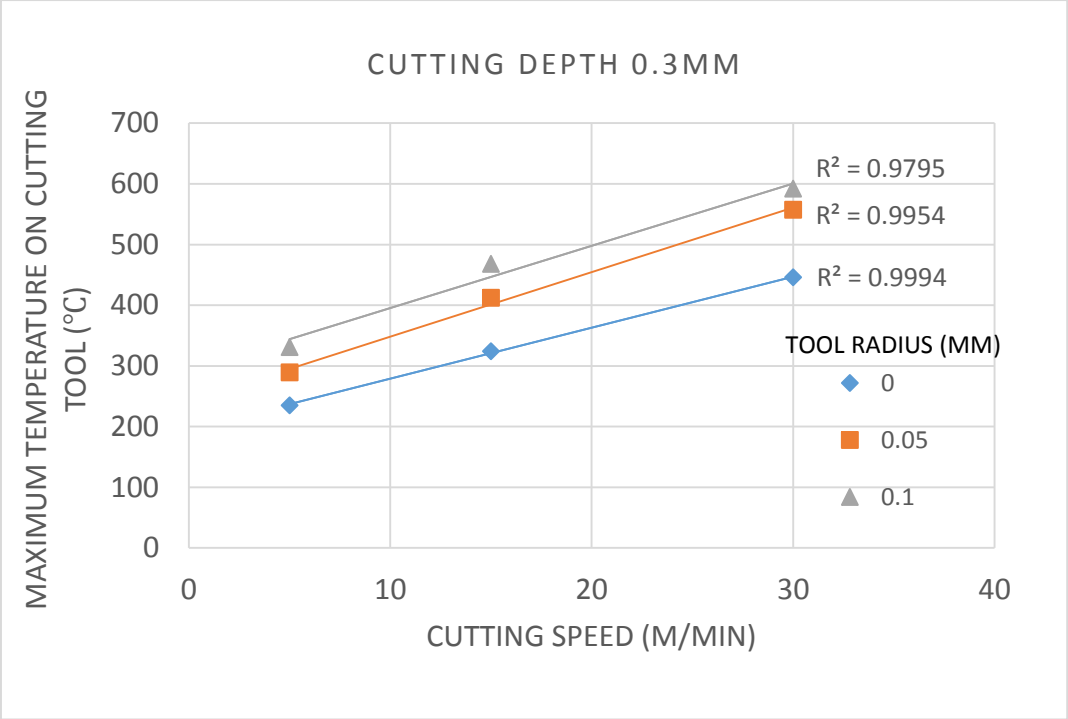

Figure 8-4 Relationship between cutting speed and cutting tool maximum temperature when cutting depth is 0.3 mm

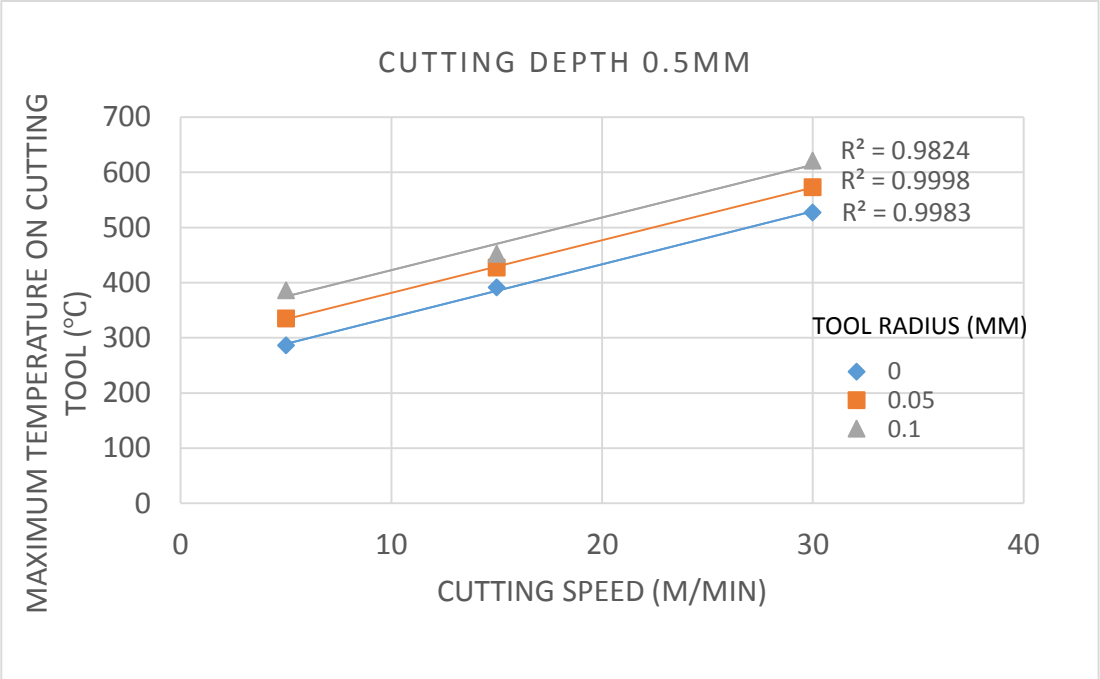

Figure 8-5 Relationship between cutting speed and cutting tool maximum temperature when cutting depth is 0.5 mm

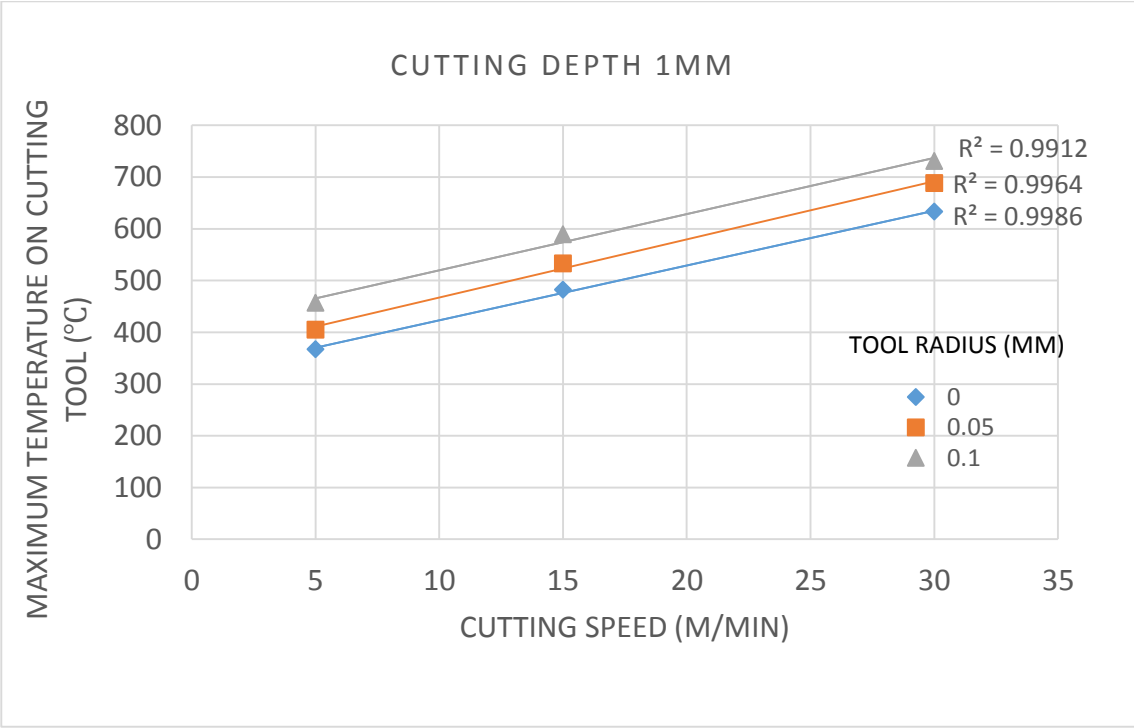

Figure 8-6 Relationship between cutting speed and cutting tool maximum temperature when cutting depth is 1 mm

A good linear relationship between cutting speed and maximum temperature on the cutting tool is shown.

From Figure 8-4, Figure 8-5, Figure 8-6, When the cutting speed increases from 5m/min to 30m/min, the maximum temperature on the cutting tool increases more than 200℃.The high temperature will weaken the strength of the cutting tool and cause the wear or damage. This is one of the reasons that low cutting speed is used in workshop when machining the Titanium alloy parts. Coolant is usually used in the Ti-6Al-4V cutting process, and thermal fatigue crack will be produced due to the thermal cycling condition [6].

6.1.1.3 The effect of cutting speed on the cutting tool maximum Stress

The change of cutting speed will not have a significant impact on the pattern of stress distribution. The maximum stress on the cutting tool changes with temperature in different cutting tool edge radius and cutting depth can be seen in Figure 8-7 to Figure 8-9.

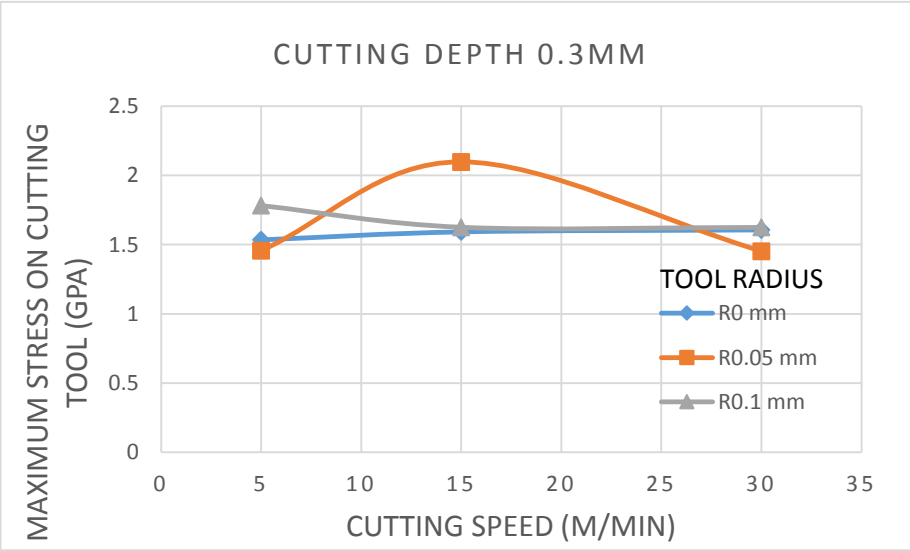

Figure 8-7 Relationship between cutting speed and cutting tool maximum stress when cutting depth is 0.3 mm

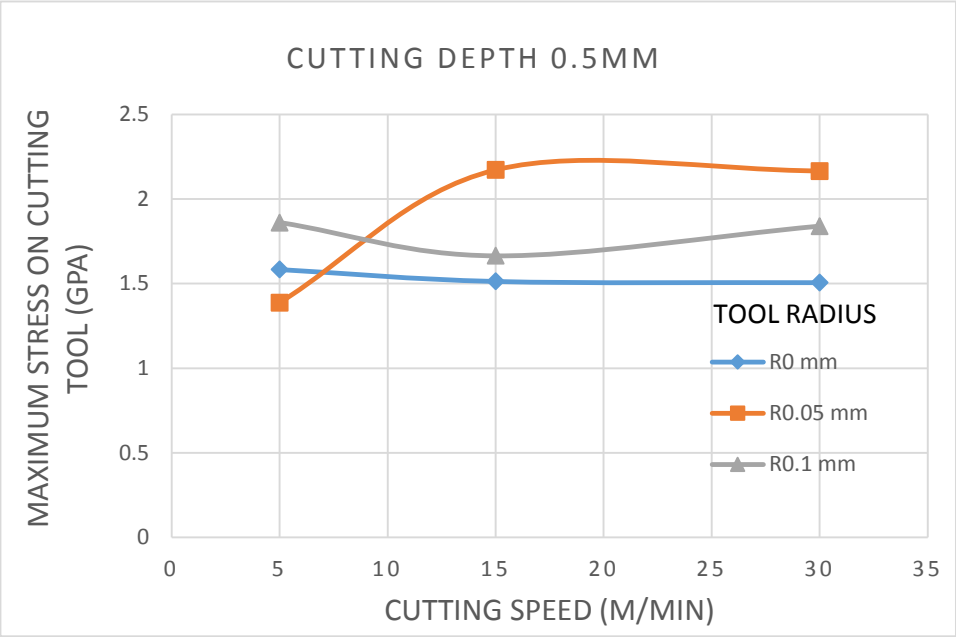

Figure 8-8 Relationship between cutting speed and cutting tool maximum stress when cutting depth is 0.5 mm

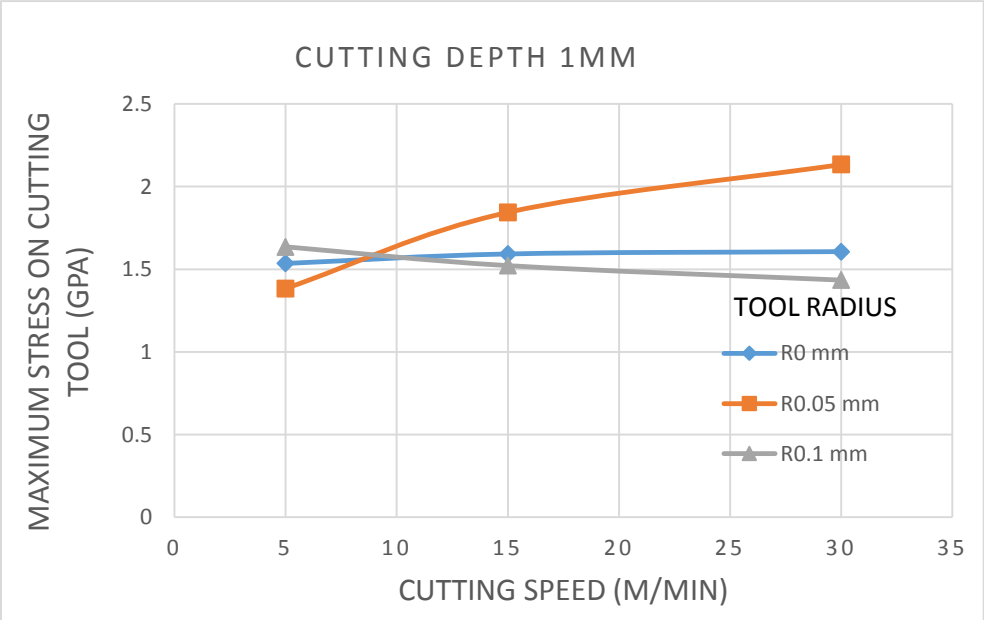

Figure 8-9 Relationship between cutting speed and cutting tool maximum stress when cutting depth is 1 mm

As the cutting speed increase, in some cases the maximum stress will increase at the beginning such as tool edge radius is 0.05. In other cases, the maximum stress on the cutting tool will only change in a narrow range. This may own to the combination of strain harden effect and thermal soften effect when the cutting speed goes up. For the orange curve, a sticking zone generated around the tool tips due to small cutting tool edge radius causing the increasing of maximum stress from 5 m/min to 15 m/min. This effect weakens in higher cutting speed especially for small cutting depth.

6.1.2 The effects of cutting depth

Cutting depth is a very important parameter in machining process. Increasing the cutting depth will improve the efficiency dramatically. However, there are some other aspects need to be considered such as the increasing of cutting force. The effects on the cutting force, maximum temperature and stress on the cutting tool will be presented.

6.1.2.1 The effect of cutting depth on the cutting force

The effect of cutting depth on the cutting tool is shown in Figure 8-10 to Figure 8-12.

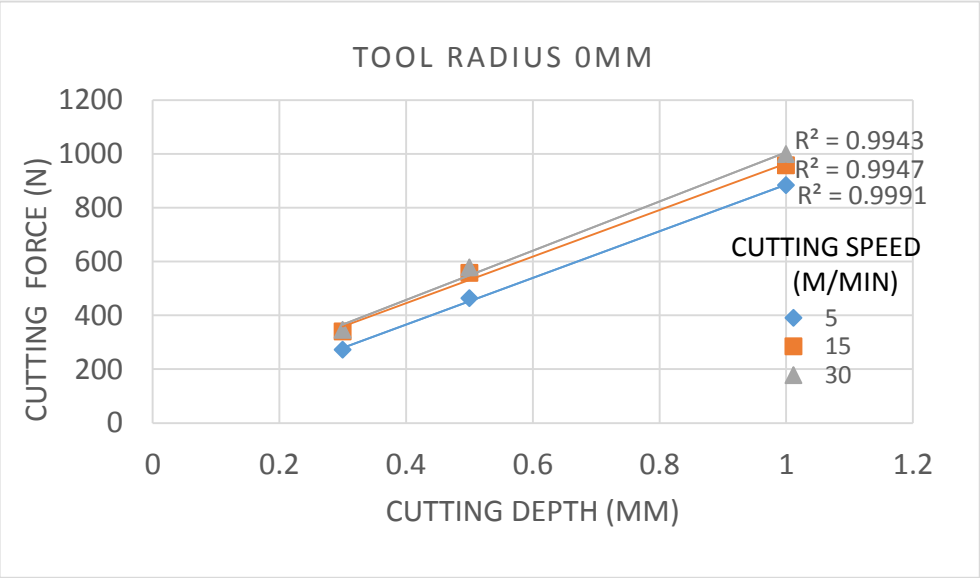

Figure 8-10 Relationship between cutting depth and cutting force when tool edge radius is 0 mm

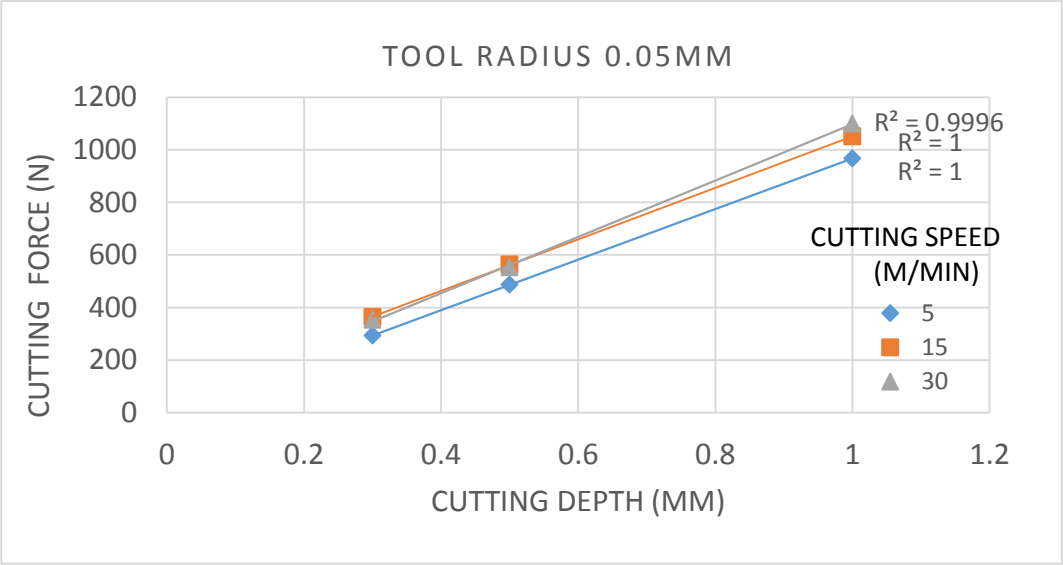

Figure 8-11 Relationship between cutting depth and cutting force when tool edge radius is 0.05 mm

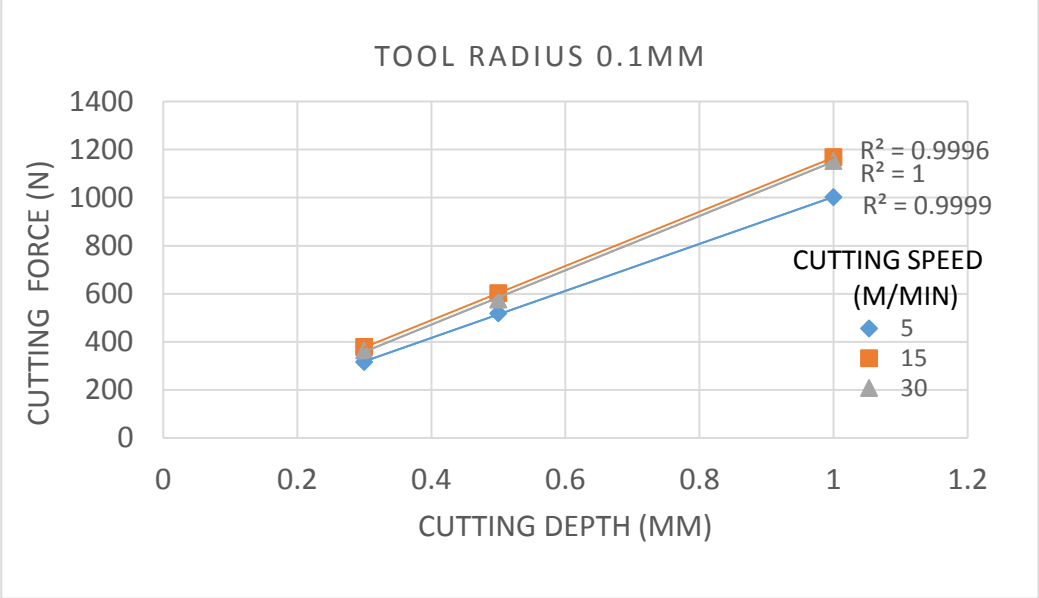

Figure 8-12 Relationship between cutting depth and cutting force when tool edge radius is 0.1 mm

Three figures show a similar trend. It can be concluded that the cutting force has a linear relationship with cutting depth when the cutting tool edge radius and cutting speed are kept constant. Asano [109] also found out a linear relationship between cutting depth and cutting force through the

experiments on AC8A alloy. The cutting force is almost 3 times when the cutting depth raises from 0.3mm to 1mm. It is a vital character for planners. When the cutting force for a certain cutting depth is measured, the force for all depth are known if other conditions are kept the same.

6.1.2.2 The effect of cutting depth on the cutting tool maximum temperature

The effects of cutting depth on the tool maximum temperature are shown in Figure 8-13 to Figure 8-15.

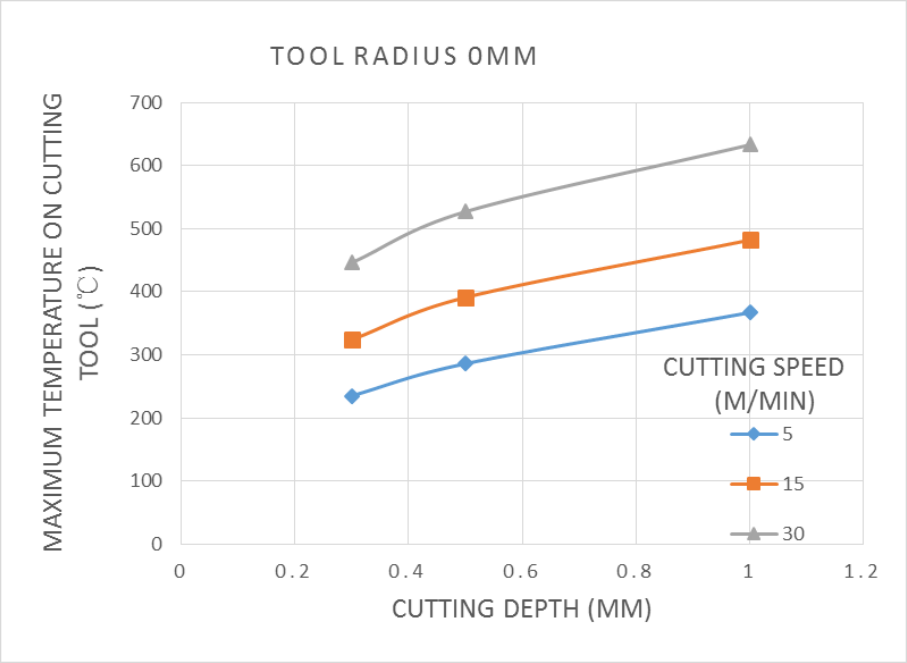

Figure 8-13 Relationship between cutting depth and cutting tool maximum temperature when tool edge radius is 0 mm

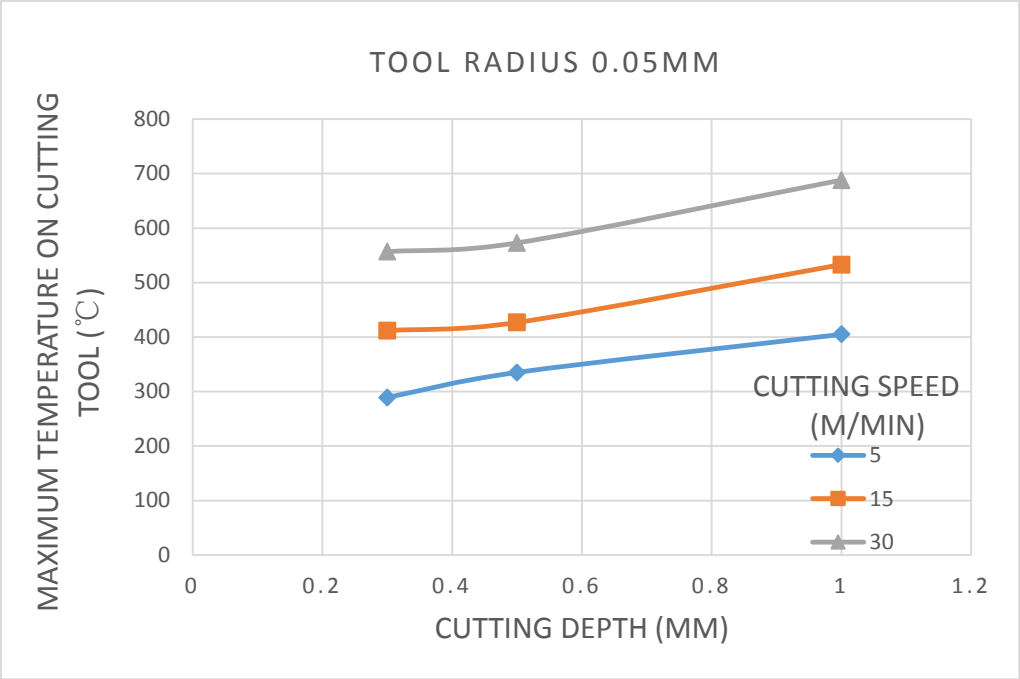

Figure 8-14 Relationship between cutting depth and cutting tool maximum temperature when tool edge radius is 0.05 mm

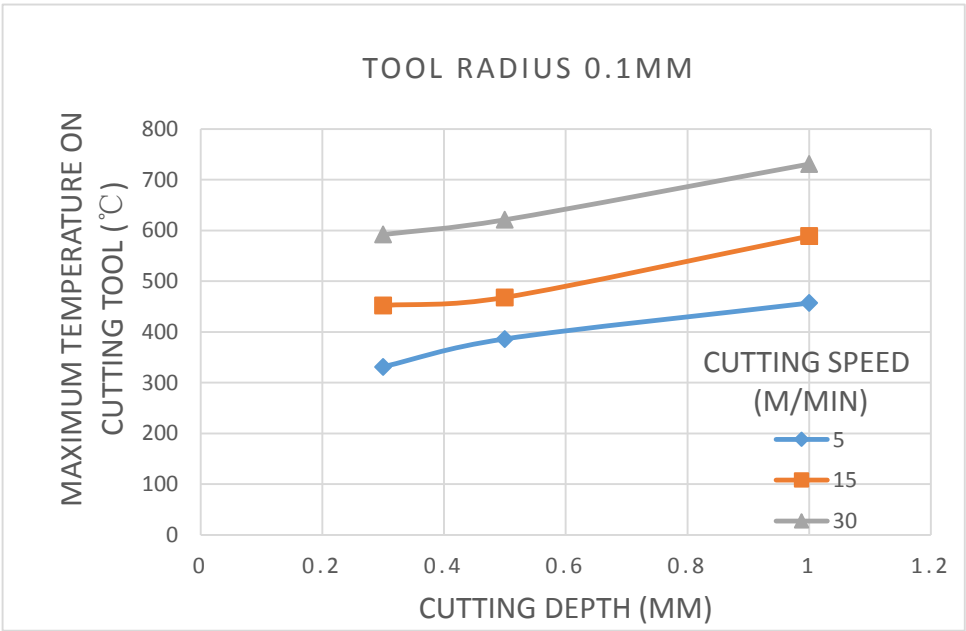

Figure 8-15 Relationship between cutting depth and cutting tool maximum temperature when tool edge radius is 0.1 mm

When the cutting depth raised from 0.3mm to 1mm, the increment of the temperature is around 120℃. The reasons for that are:

➢ As the increment of the cutting depth, more mechanical work is converted into heat in the deformation zone.

➢ Because of the low conductivity of Ti-6Al-4V, the heat generating in the cutting zone cannot diffuse

6.1.2.3 The effect of cutting depth on the cutting tool maximum Stress

The effects of cutting depth on the tool maximum stress are shown in Figure 8-16 to Figure 8-19.

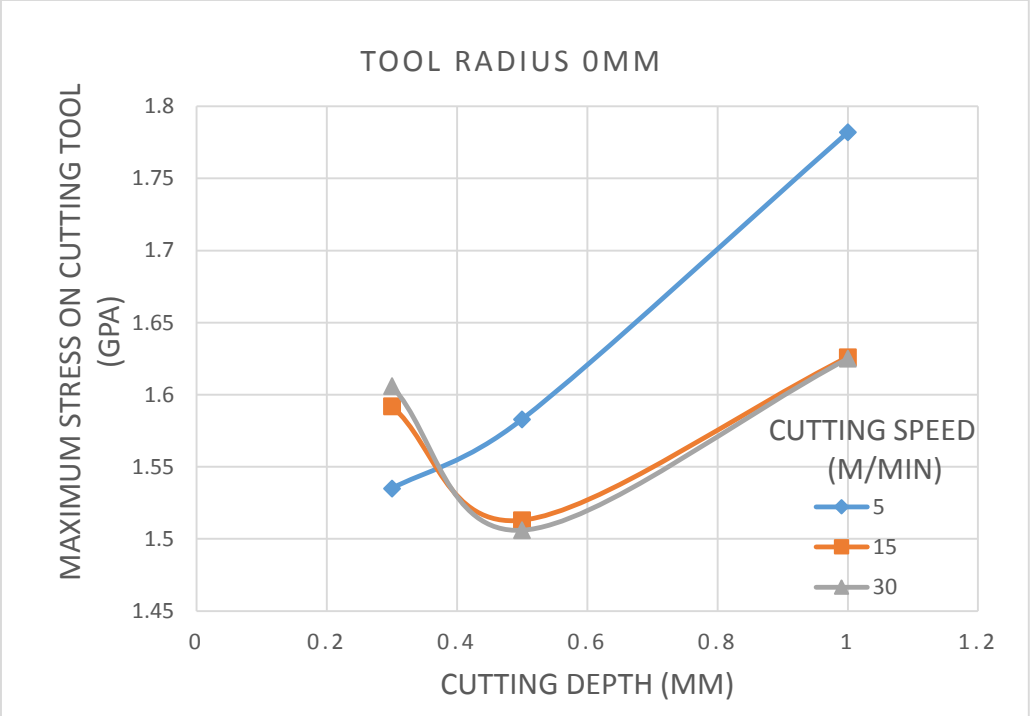

Figure 8-16 Relationship between cutting depth and cutting tool maximum stress when tool edge radius is 0 mm

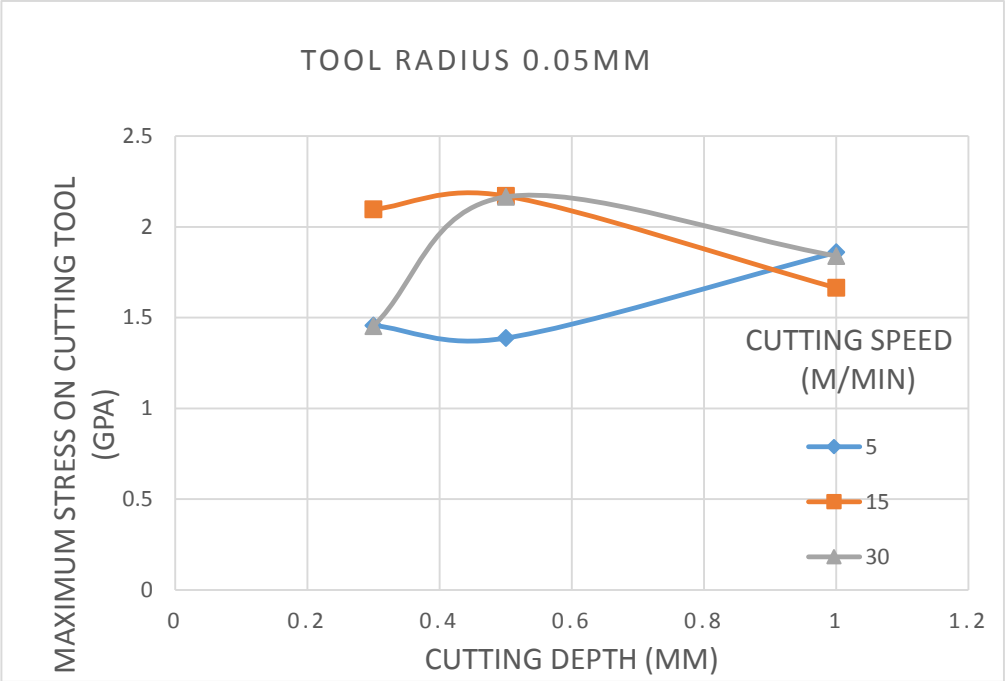

Figure 8-17 Relationship between cutting depth and cutting tool maximum stress when tool edge radius is 0.05 mm

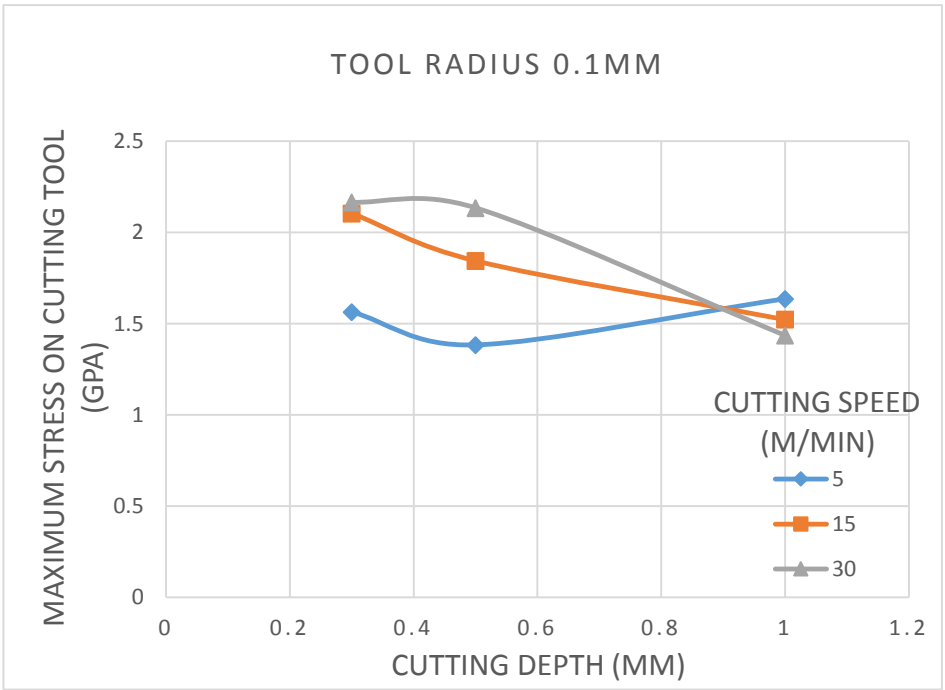

Figure 8-18 Relationship between cutting depth and cutting tool maximum stress when tool edge radius is 0.1 mm

There is no certain relationship between the cutting depth and the maximum stress on the cutting tool. One of the reasons may be when the depth of cut increases, the contact length between the chip and the cutting tool becomes longer. So the raising of the stress on the cutting tool becomes uncertain.

6.1.3 The effects of tool edge radius

The tool tip of a sharp tool is quite easy to break in the cutting process. The surface finishing is also poor when a sharp tool is used. In workshop, a cutting tool with a small cutting tool edge radius is normally used. In this part, the effect of cutting tool edge radius on the cutting force, maximum temperature and stress on the cutting tool will be presented.

6.1.3.1 The effect of cutting tool edge radius on the cutting force

The relationship between cutting tool edge radius and cutting force is shown in Figure 8-19 to Figure 8-21.

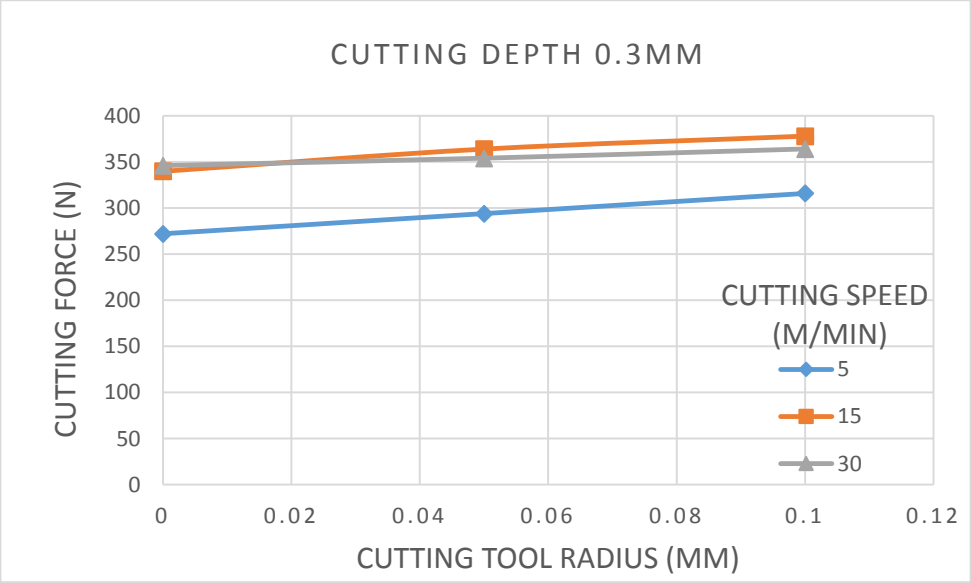

Figure 8-19 Relationship between cutting tool edge radius and cutting force when cutting depth is 0.3 mm

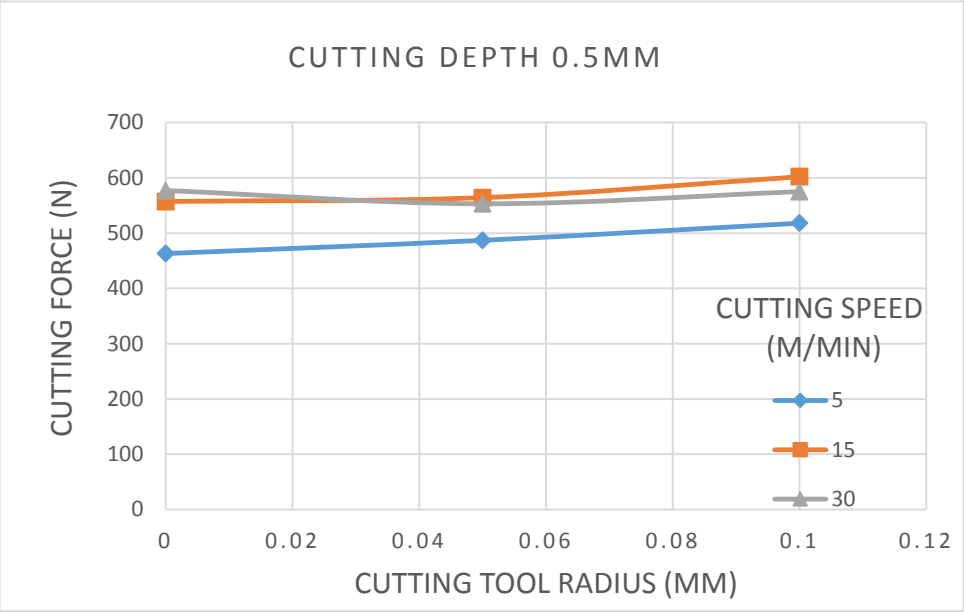

Figure 8-20 Relationship between cutting tool edge radius and cutting force when cutting depth is 0.5 mm

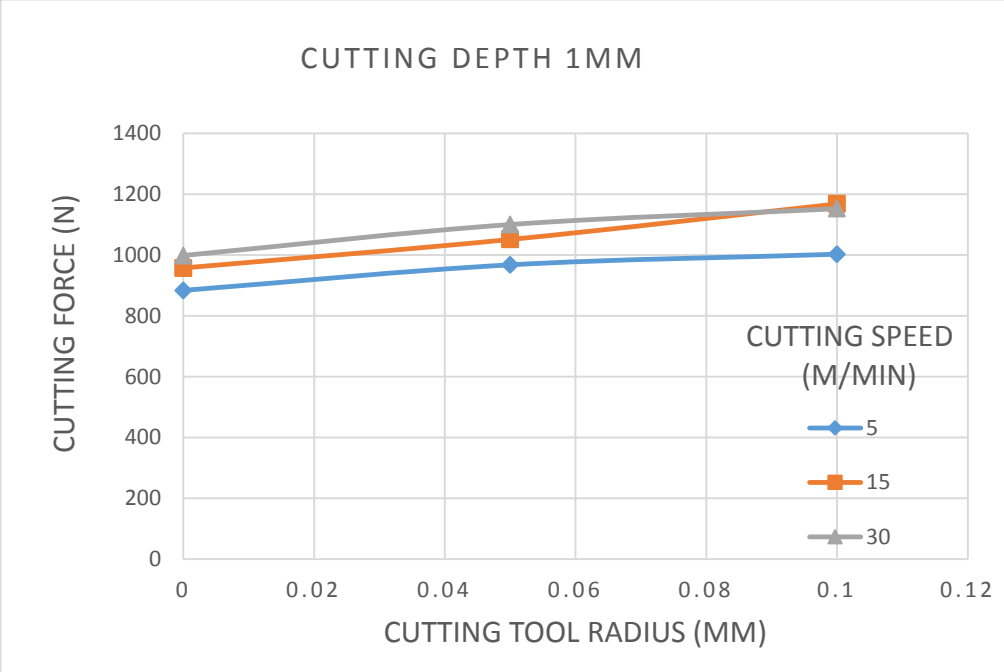

Figure 8-21 Relationship between cutting tool edge radius and cutting force when cutting depth is 1 mm

As the increasing of the cutting tool edge radius, the cutting force goes up. The increasing of cutting force is not significant when compares to the cutting depth. It is not clear if there is a proportion relationship. The increment of the cutting force is mainly due to the strain harden effect in front of the tool tip.

6.1.3.2 The effect of cutting tool edge radius on the cutting tool maximum temperature

The relationship between cutting tool edge radius and cutting tool maximum temperature is shown in Figure 8-22 to Figure 8-24.

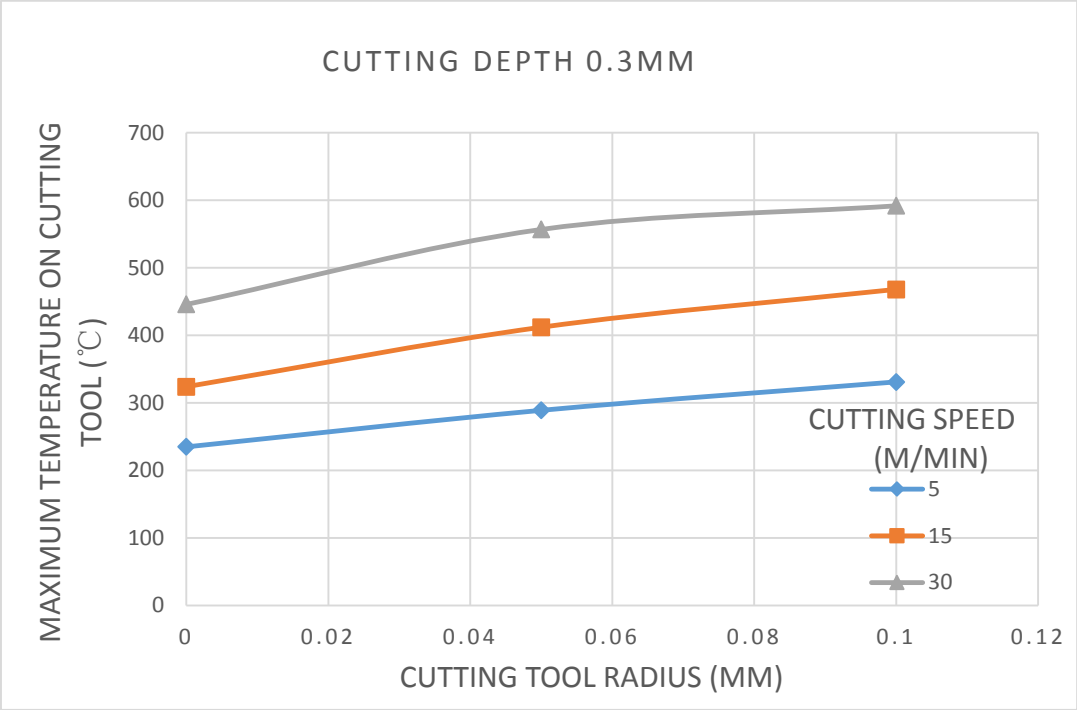

Figure 8-22 Relationship between cutting tool edge radius and cutting tool maximum temperature when cutting depth is 0.3 mm

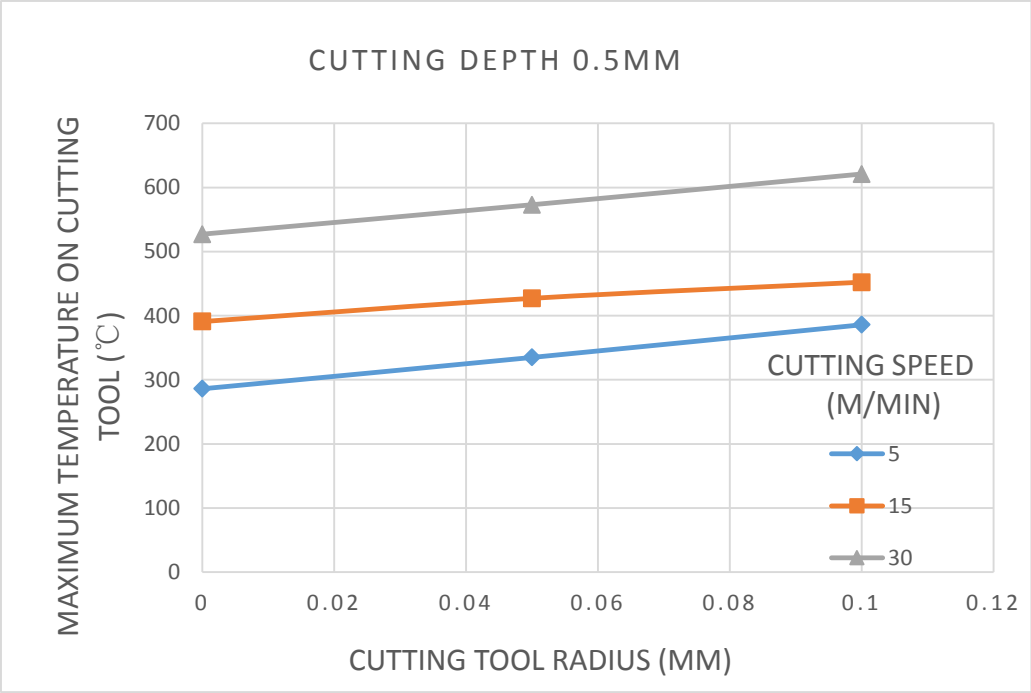

Figure 8-23 Relationship between cutting tool edge radius and cutting tool maximum temperature when cutting depth is 0.5 mm

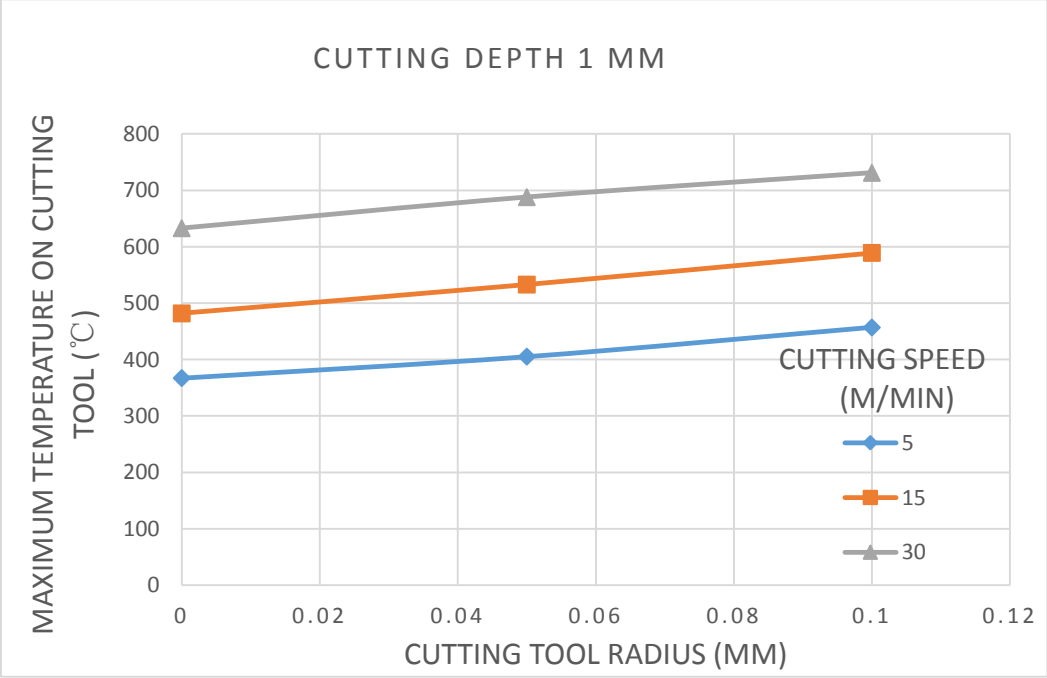

Figure 8-24 Relationship between cutting tool edge radius and cutting tool maximum temperature when cutting depth is 1mm

The maximum temperature increases with increased cutting tool edge radius. The increment is around 100℃ to 200 ℃ when the tool edge radius change from 0mm to 0.1 mm. The increased cutting tool edge radius will enlarge the contact area between cutting tool and workpiece. More friction work is done. Thus more heat is generated to conduct into the cutting tool.

Moreover, different edge radius changes the distribution of stress and temperature on the cutting tool. Which can be seen in Figure 8-25 and Figure 8-26.

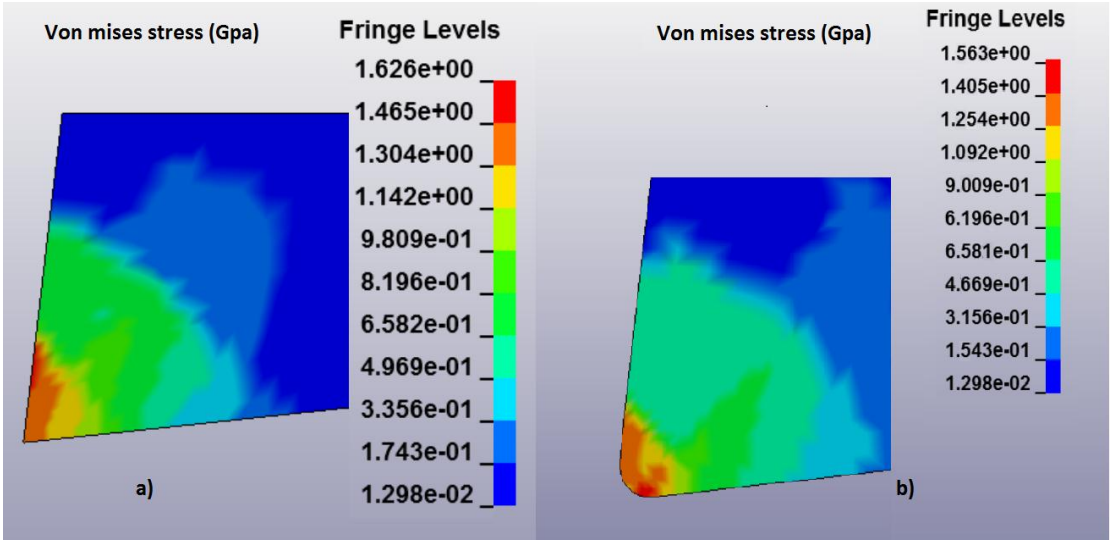

Figure 8-25 Von Mises stress distribution on the cutting tool

a) cutting speed 15m/min, edge radius 0mm, cutting depth 1mm;

b) cutting speed 5m/min, edge radius 0.1mm, cutting depth 0.3mm;

From a), the maximum stress on the cutting tool is on the rake face, a few distance from the tool tip. It may be caused by the sticking zone near the tool tip. When using a round edge tool, show in b), the maximum stress shift from the rake face to the flank face. This may own to the friction between the flank face with the workpiece.

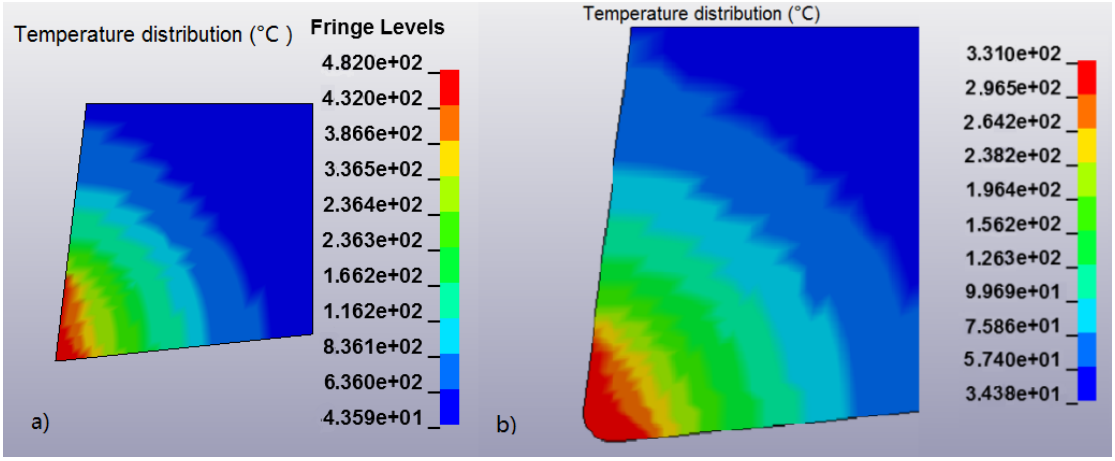

Figure 8-26 Temperature distribution on the cutting tool

a) cutting speed 15m/min, edge radius 0mm, cutting depth 1mm;

b) cutting speed 5m/min, edge radius 0.1mm, cutting depth 0.3mm;

From a), the maximum temperature on the cutting tool is near the cutting tool tip and diffusing along the rake face. From b), the maximum temperature extends to the flank wear which may cause the flank wear in the cutting process.

6.1.3.3 The effect of cutting tool edge radius on the cutting tool maximum Stress

The effects of cutting tool edge radius on the tool maximum stress are shown in Figure 8-27 to Figure 8-29.

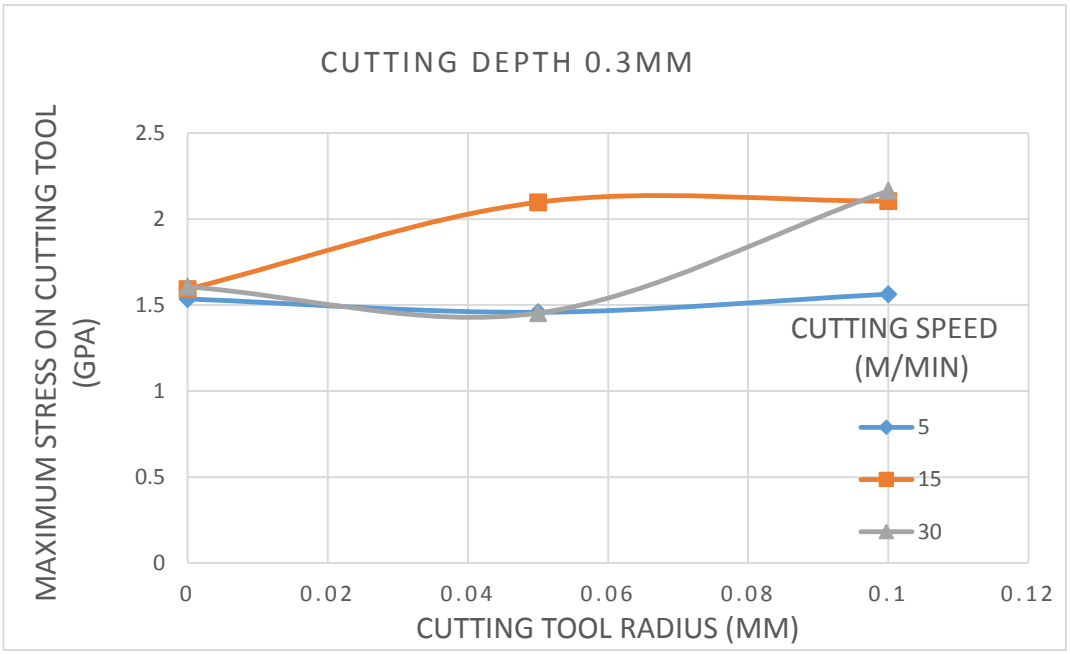

Figure 8-27 Relationship between cutting tool edge radius and cutting tool maximum stress when cutting depth is 0.3 mm

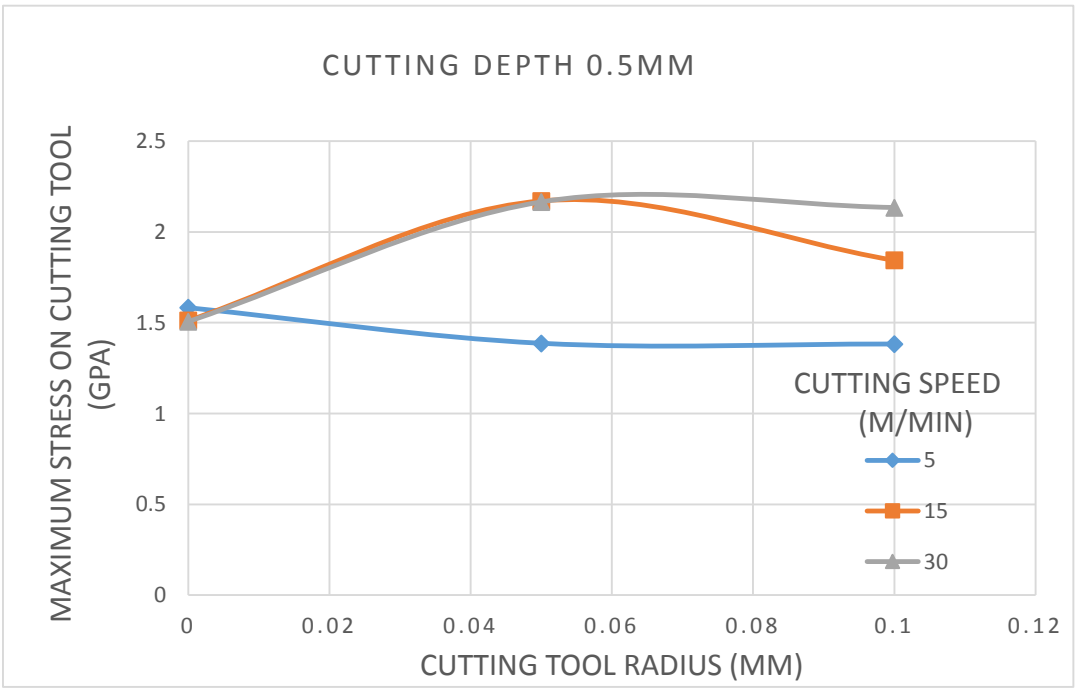

Figure 8-28 Relationship between cutting tool edge radius and cutting tool maximum stress when cutting depth is 0.5 mm

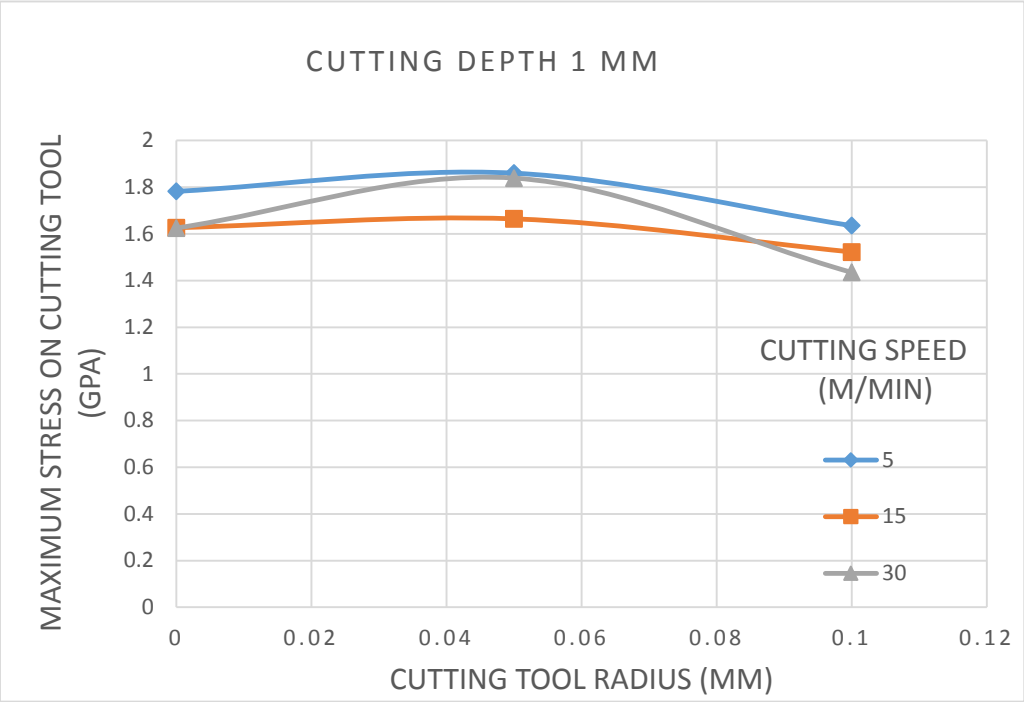

Figure 8-29 Relationship between cutting tool edge radius and cutting tool maximum stress when cutting depth is 1 mm

The cutting tool edge radius will change the stress distribution on the cutting tool as shown in Figure 8-25. However, there is no certain relationship between maximum stress and tool edge radius. When the cutting tool edge radius increases, the cutting force will increase. In the meantime, the contact length between the cutting tool and tool chip increases. So it becomes uncertain that the stress will increase or not.

6.2 The effects of flank wear

Flank wear is the most desirable wear in the cutting process mainly because its predictable. However, if the wear surpasses a criteria number, it may destroy the part and break the tool. So it is quite important to know the effect of the cutting tool flank wear on the cutting force, stress distribution on

the tool and temperature distribution. The simulation results for flank wear can be found in Appendix B.

6.2.1 The effect of flank wear on the cutting force

The relationship between flank wear and cutting force can be seen in Figure 8-30.

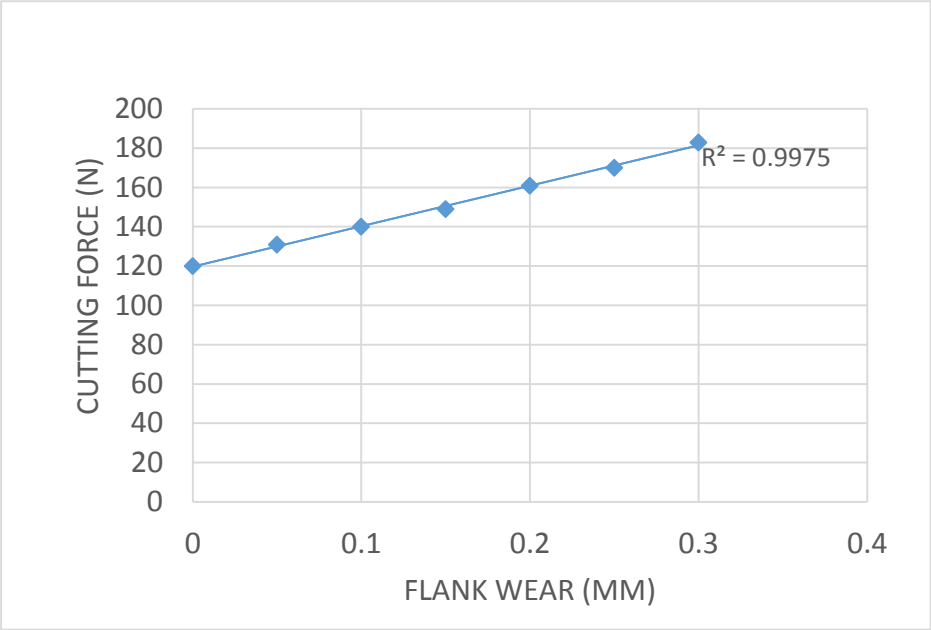

Figure 8-30 The relationship between flank wear and cutting force.

The R^2 measured for the relationship between flank wear and cutting force is 0.9975.

It can be concluded that the flank wear and cutting force has a linear relationship when the flank wear is less than 0.3. For every 0.05mm flank wear, the cutting force will increase about 10N. This phenomenon happens mainly because the friction force between the flank face and the workpiece.

On the other hand, the cutting power is related with cutting force in equation:

$$P=F*V \quad (6\text{-}1)$$

Where P is the machining power, F is the cutting force, V is the cutting speed. In this case, the cutting speed is a constant number. So the relationship between the machining power and flank wear is shown in Figure 8-31.

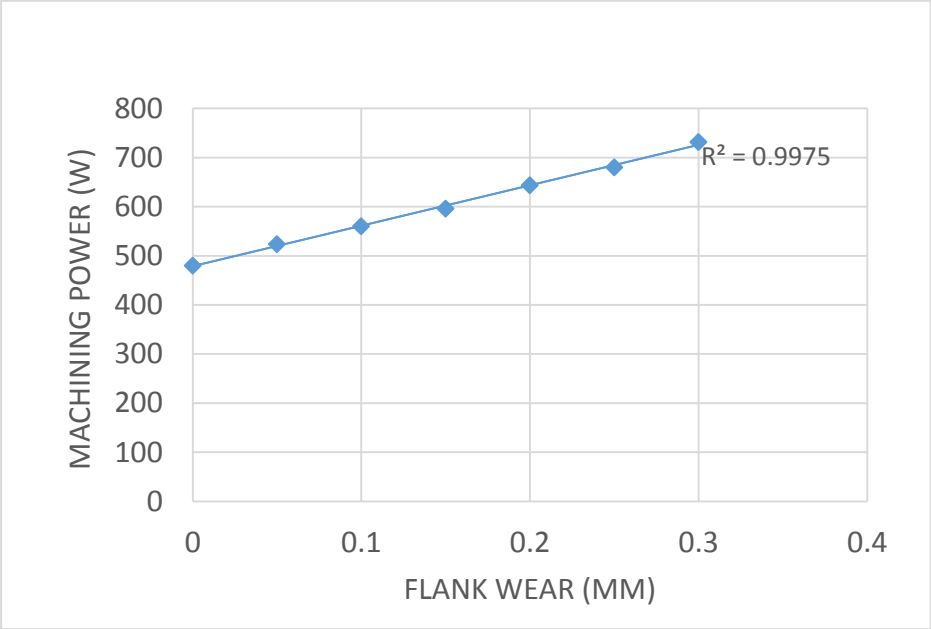

Figure 8-31 The relationship between flank wear and machining power

The Machining power can be easily read from the operation panel. Thus the operator can predict the cutting tool flank wear from the machining power. If the machining power reaches a critical value, for example 700W in this case, then the cutting tool should be changed before damaging the part or breaking the cutting tool.

6.2.2 The effect of flank wear on the cutting tool temperature distribution

The relationship between cutting tool flank wear and cutting tool maximum temperature is shown in Figure 8-32.

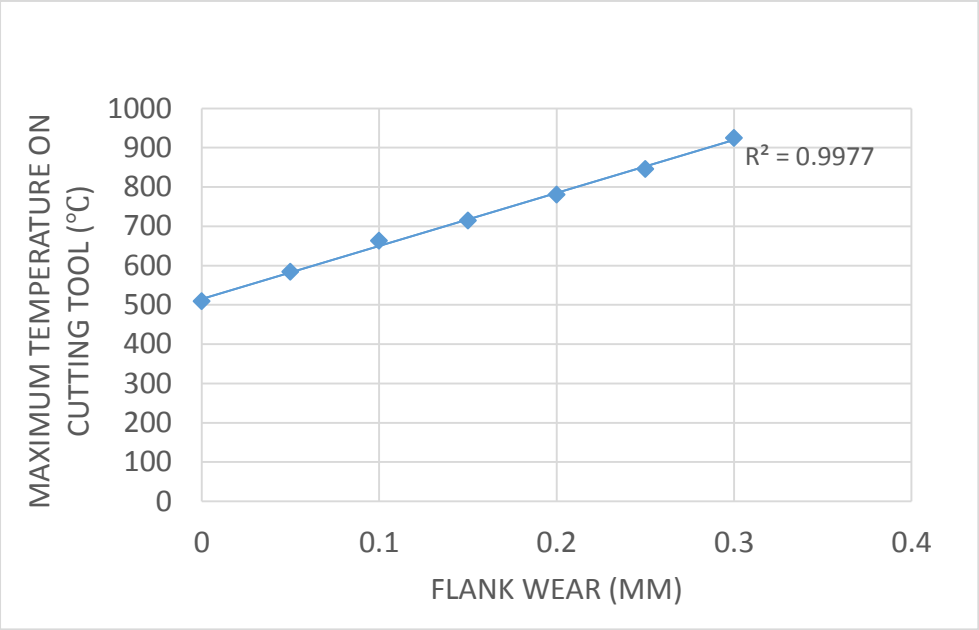

Figure 8-32 The relationship between cutting tool flank wear and cutting tool maximum temperature.

A linear relationship between flank wear and maximum temperature on cutting tool is witnessed. Sui and Feng [110] studied relationship between flank wear and cutting temperature, a similar trend is got when the flank wear is under 0.3 mm. Increasing the flank wear land will increase the contact length between cutting tool and workpiece. Thus, more machining energy converts into heat. When the flank wear land changes from 0 to 0.3mm, the maximum temperature on the cutting tool raises more than 400 ℃.

The wear land also changes the temperature distribution on the cutting tool. As shown in Figure 8-33 and Figure 8-34.

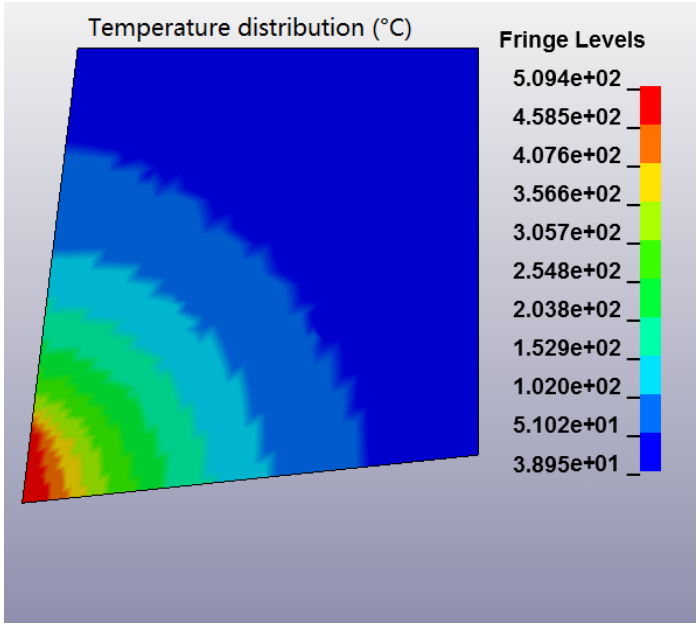

Figure 8-33 Temperature distribution with a new tool

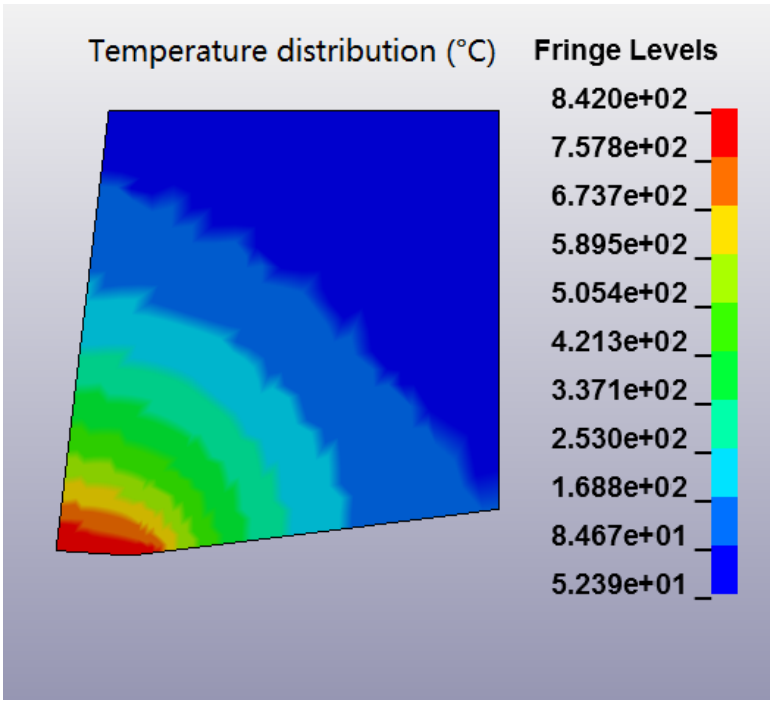

Figure 8-34 Temperature distribution when tool flank wear is 0.25mm

For Figure 8-33, the maximum temperature focus on the rake face, while in Figure 8-34, the maximum temperature is on the flank face.

6.2.3 The effect of flank wear on the cutting tool Stress distribution

The relationship between cutting tool flank wear and cutting tool maximum stress is shown in Figure 8-35.

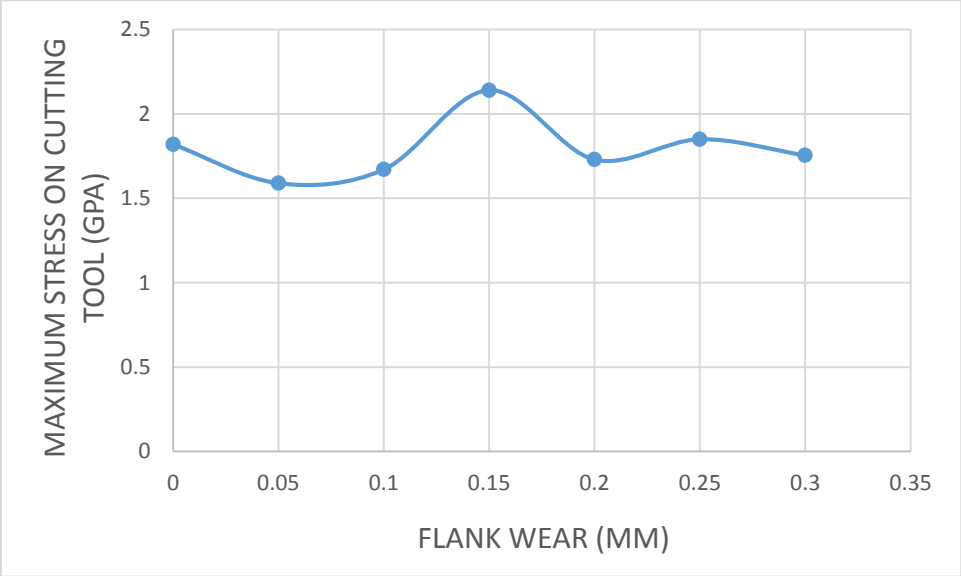

Figure 8-35 Relationship between flank wear and cutting tool maximum stress

There is no positive correlation or negative correlation between flank wear and maximum tool stress. However, the flank wear will change the stress distribution in the cutting tool. As shown in Figure 8-36 and Figure 8-37.

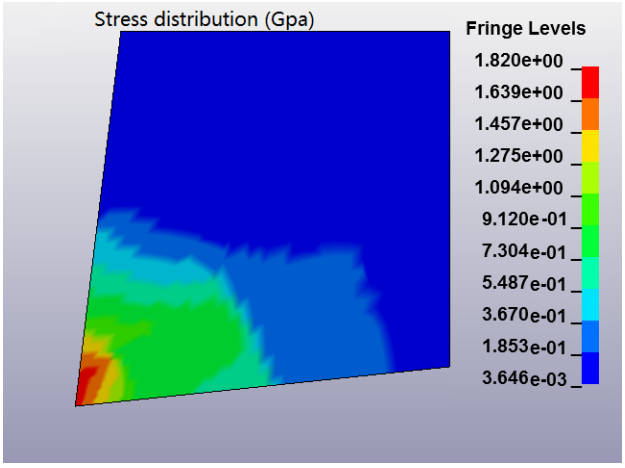

Figure 8-36 Stress distribution on a sharp tool

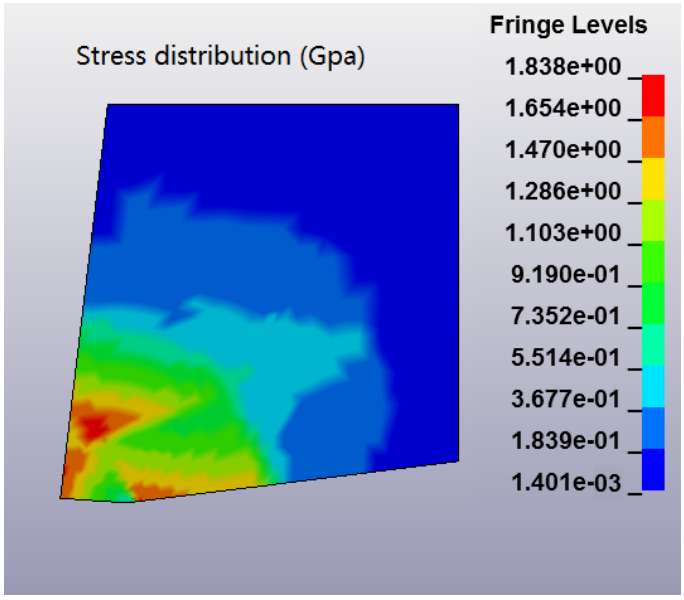

Figure 8-37 Stress distribution when the flank wear is 0.25mm

From the Figure 8-36, the stress is concentrate on the rake face, however, for a flank wear tool, the stress will not only focus on the rake face but also near the tip on the flank face.

6.3 The effects of crater wear

Crater wear is a result of abrasion (hard-particle grinding the tool face) and diffusion (atomic diffusion between the material and the cutting tool) wear mechanism. Due to the ductile property of Ti-6Al-4V, crater wear becomes a normal type of wear when machining Ti-6Al-4V. The effects of the crater wear will be investigated in the following sections. The simulation results for crater wear can be found in Appendix B.

6.3.1 The effect of crater wear on the cutting force

The effect of crater wear on the cutting force is shown as below

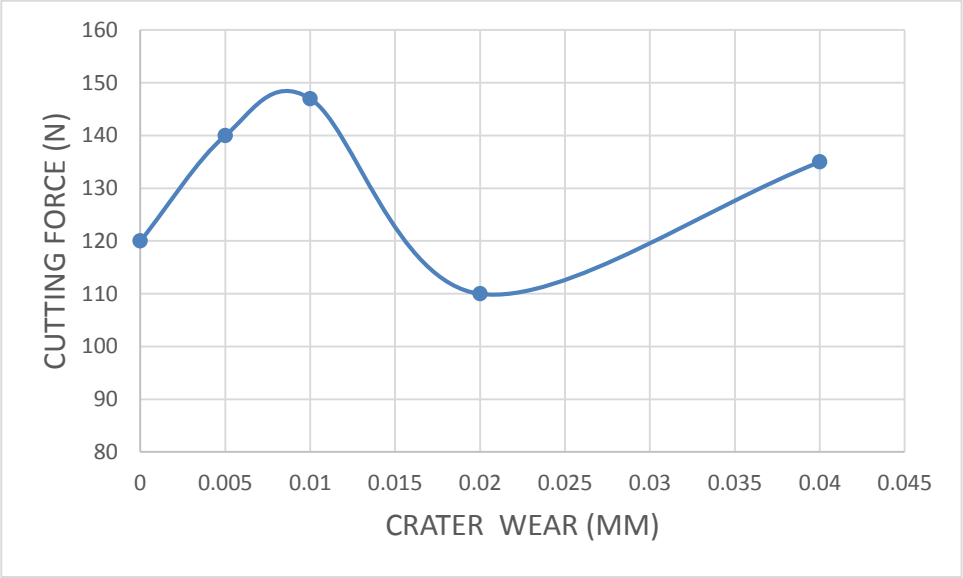

Figure 8-38 Cutting force Vs crater wear when the wear is from the tool tip

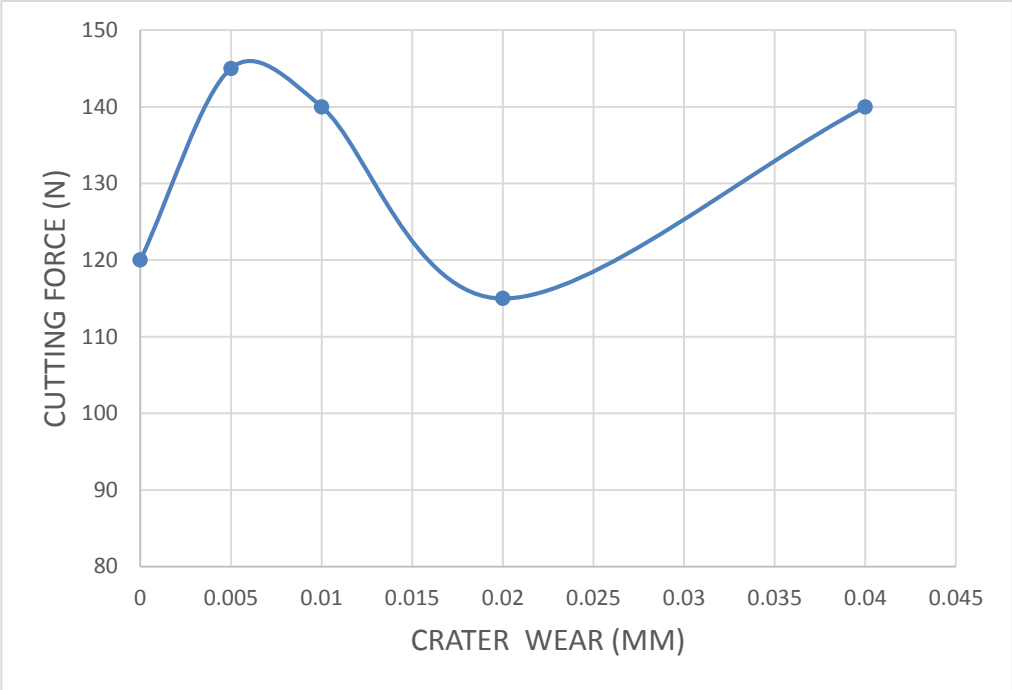

Figure 8-39 Cutting force Vs crater wear when the wear is 10 μm from the tool tip

From Figure 8-38 and Figure 8-39, The cutting force increases at the beginning. The material cannot flow smoothly when the defects is too small. When the crater wear becomes larger, the cutting force drops dramatically. This is mainly because the existence of the crater wear enlarges the rake angle of the cutting tool. However, after the crater wear land becomes even larger, the friction between the cutting tool and the chip dominates the effects. Chip breakage may be another reason for the decreasing of the cutting force. The crater wear plays a role as chip breaker. See Figure 8-40.

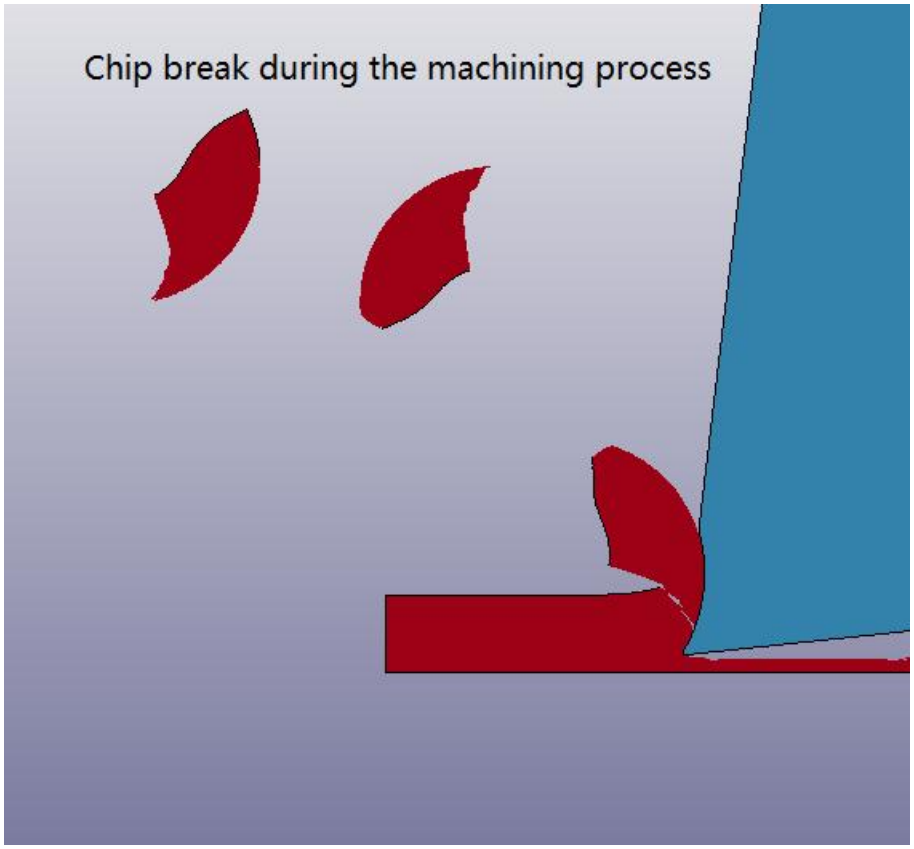

Figure 8-40 Chip breakage

6.3.2 The effect of crater wear on the cutting tool temperature distribution

The relationship between crater wear and cutting tool maximum temperature can be seen from Figure 8-41 and Figure 8-42.

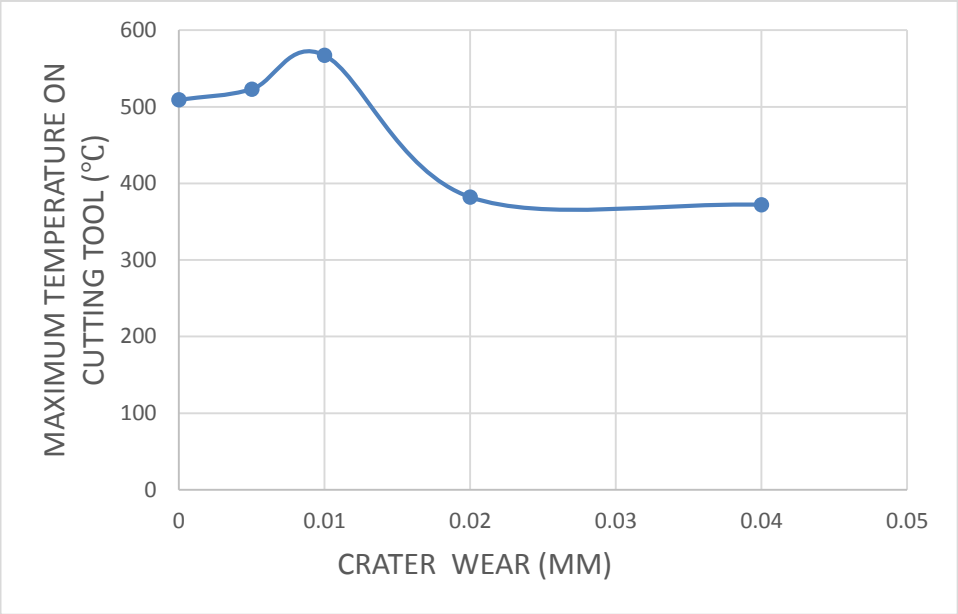

Figure 8-41 Maximum temperature on cutting tool Vs crater wear when the wear is from the tool tip

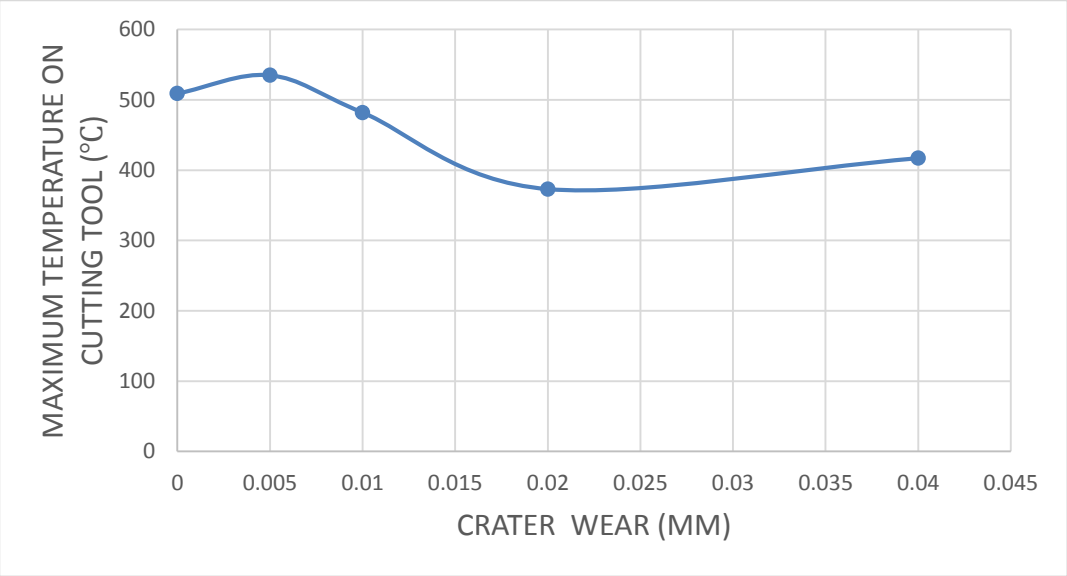

Figure 8-42 Maximum temperature on cutting tool Vs crater wear when the wear 10 μm from the tool tip

The maximum temperature on the cutting tool has the similar trend with the cutting force. The reason for the change of temperature is also the same as the cutting force.

The temperature distribution on the cutting tool can be seen from Figure 8-43.

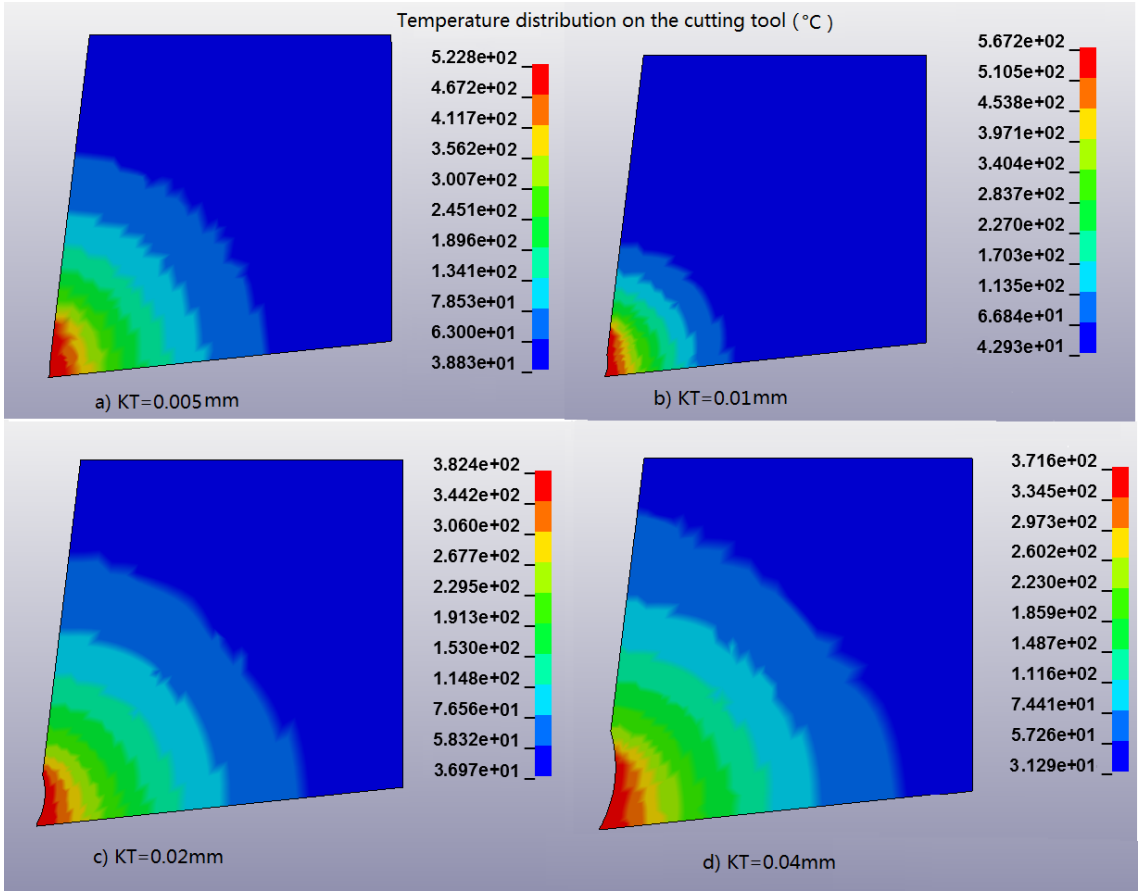

Figure 8-43 Temperature distribution in different crater wear sizes

The temperature mainly concentrates on the wear land as the increasing of the crater wear land.

6.3.3 The effect of crater wear on the cutting tool Stress distribution

The relationship between crater wear and cutting tool maximum stress can be seen from Figure 8-44 and Figure 8-45.

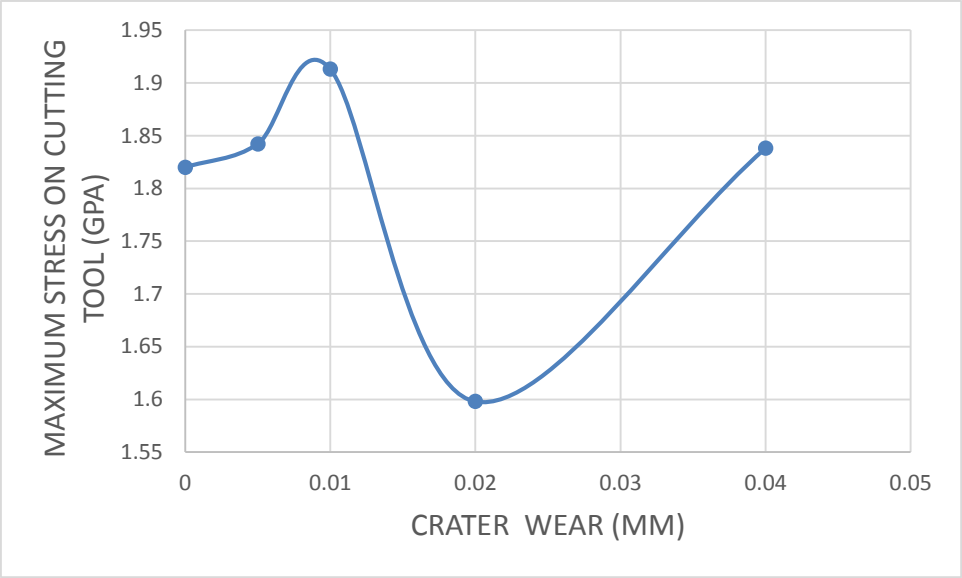

Figure 8-44 Maximum stress on cutting tool Vs crater wear when the wear is from the tool tip

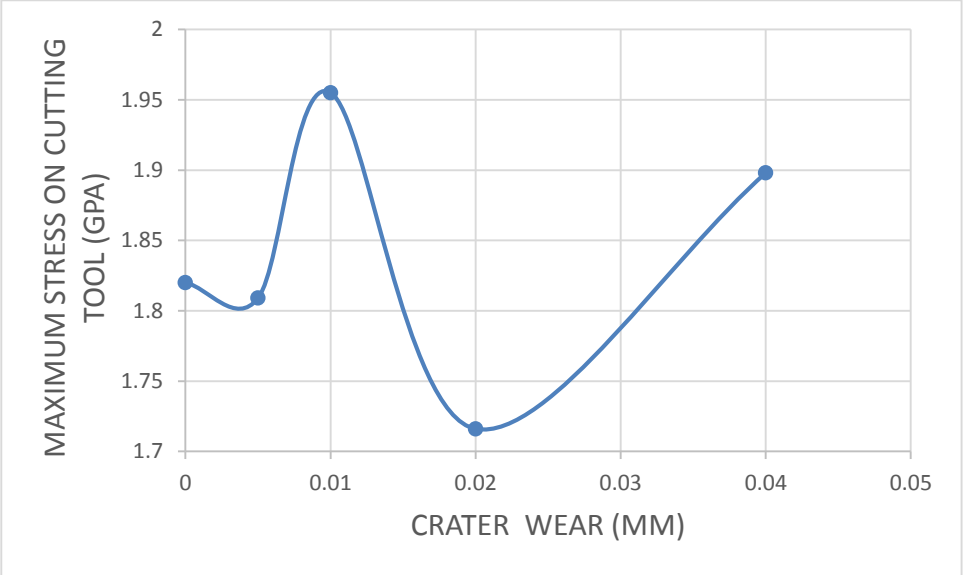

Figure 8-45 Maximum stress on cutting tool Vs crater wear when the wear 10 μm from the tool tip

The maximum stress on the cutting tool seems random. The stress distribution on the cutting tool can be seen from Figure 8-46.

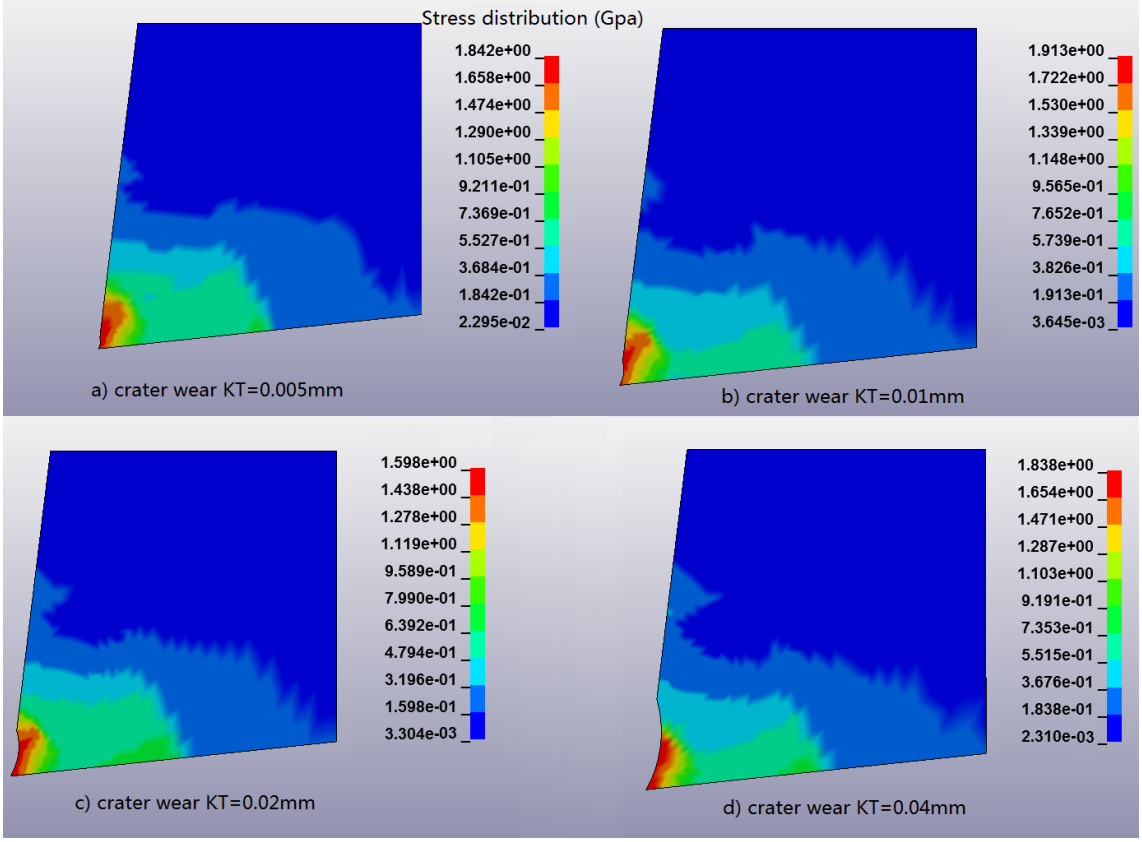

Figure 8-46 Stress distribution in different crater wear sizes

6.4 Limitation of the work

The limitation of the work can be concluded as follows:

- The workpiece constitutive model can be only used in a narrow area for some particular materials.
- The 2D model cannot represent the reality of the cutting process.
- The mesh has to be small enough because of the absence of the remeshing process.
- The time step has to be small enough to make sure the convergence of the result, so the computing time is enormous.

7 Conclusions and Future work

7.1 Conclusions

In this thesis, a thermo-mechanical model of plane strain orthogonal metal cutting with segment chip formation is presented. This model can be used to predict process parameters such as cutting force, temperature distribution, stress distribution and strain.

In the first part of this thesis, two groups of Johnson-Cook model constants are used to simulate the chip formation process and the results of these two models are compared with the experimental results published in the literature. Once the model is validated, one group of constants is adapted to investigate the effects of different kind of tool wear including the flank wear and crater wear on the cutting tool. The influence of different parameters such as cutting speed, cutting depth and cutting tool edge radius is also studied.

This thesis is mainly focused on the cutting process variables and wear characteristics on the cutting tool which is neglected by most of researchers. Machining power is adopted to predict the degree of flank wear which is convenient to use in the workshop.

From the statistics analysis, following conclusion can be draw:

- The flank wear land size has a positive correlation with the cutting force. A linear relationship is acquired through simulation when the flank wear is less than 0.3 mm.
- Machining power is a perfect indicator for changing tool if flank wear dominates in the wear type.
- Increasing the crater wear will decrease the cutting force in a suitable wear land.
- The existence of crater wear can break the chip.
- When the cutting speed reaches a critical value, the cutting force will decrease.

- All the investigated parameters such as cutting depth, tool edge radius, flank wear have a strong influence on the maximum temperature on the cutting tool.
- There is a linear relationship between cutting depth and cutting force in low speed cutting process.
- No obvious tendency between maximum stress and other studied parameters.
- When cutting tool edge radius increases, maximum stress and maximum temperature on the tool tend to move from rake face to flank surface which may cause flank wear.
- When a large flank wear is used in the cutting process, the maximum stress seems to move behind the formed tip on the flank face.
- The occurrence of the flank wear tends to transfer the maximum temperature and maximum stress from the rake face to flank face which may speed up the rate of flank wear.

7.2 Future work

There are also some points need to be investigated in the further work. The work can be divided into two parts: Model improvement and Application for the model.

There are three points in the model improvement area. Firstly, as no remeshing process is adapted in the model, the size of the element has to be small enough to get the accurate results. Thus the computing time is enormous. The longest simulation in this study is more than 16 hours. Thus it will be quite useful to adopt the remeshing process in the cutting process. Secondly, the simple orthogonal cutting model is used which should be changed into an oblique cutting model to represent the reality of the cutting process. Thirdly, because this model is only validated by Ti-6Al-4V, more materials should be applied to validate the effective of this Finite element model.

For the application part, there are mainly two aspects. Firstly, since the maximum stress, maximum temperature on the cutting tool are known, the tool design company may use the results to enhancing the weak point in different situations. For workshop, the relationship between the flank wear and the machine power can be adopted immediately when the critical machine power is decided. So the cutting tool can be replaced before its failure.

REFERENCES

[1] Rhodes, C. (2014). Manufacturing: statistics and policy, (01942), 12.

[2] Jablonowski, J., & Eigel-Miller, N. (2013). 2013 World Machine-Tool Output and Consumption Survey. Presentation, 32.

[3] Salonitis, K., & Kolios, A. (2014). Reliability assessment of cutting tool life based on surrogate approximation methods. International Journal of Advanced Manufacturing Technology, 71(5-8), 1197–1208. http://doi.org/10.1007/s00170-013-5560-2

[4] Wiklund, H. (1998) Bayesian and regression approaches to on-line prediction of residual tool life. Qual Reliab Eng Int 14(5):303–309

[5] Markopoulos, A. P. (2013). Finite Element Method in Machining Processes. http://doi.org/10.1007/978-3-319-02459-2

[6] Stephenson, D.A., Agapiou, J.S. (2006) Metal cutting theory and practice, 2nd edition. (Taylor & Francis, Boca Raton), p. 503.

[7] ISO (1993). ISO 3685: Tool-life testing with single-point turning tools.

[8] Wang, Q. Jane., Chung, Yip-Wah. (2013). Cutting Tool Wear and Failure Mechanisms. Encyclopedia of Tribology. C661-C677 http://doi.org/10.1007/978-0-387-92897-5

[9] Rabinowicz, E. (1965). Friction and wear of materials (Wiley-Interscience, New York). Chapters 6 and 7.

[10] Yen, Y.-C., Söhner, J., Lilly, B., & Altan, T. (2004). Estimation of tool wear in orthogonal cutting using the finite element analysis. Journal of Materials Processing Technology, 146(1), 82–91. http://doi.org/10.1016/S0924-0136(03)00847-1

[11] Sahin, Y., Kok, M., & Celik, H. (2002). Tool wear and surface roughness of Al_2O_3 particle-reinforced aluminium alloy composites. Journal of Materials Processing Technology, 128, 280 – 291.

[12] Arulkirubakaran, D., Senthilkumar, V., & Kumawat, V. (2015). Effect of micro-textured tools on machining of Ti–6Al–4V alloy: An experimental and numerical approach. International Journal of Refractory Metals and Hard Materials, 54, 165–177. http://doi.org/10.1016/j.ijrmhm.2015.07.027

[13] Li, B. (2012). A review of tool wear estimation using theoretical analysis and numerical simulation technologies. International Journal of Refractory Metals and Hard Materials, 35, 143–151. http://doi.org/10.1016/j.ijrmhm.2012.05.006

[14] Taylor, F.W. (1907). On the art of cutting metals. Trans A.S.M.E.28 38-43.

[15] Woldman, N.E. and Gibbons, R.C. (1951), Machinability and Machining of metals, McGraw-Hill, New York,47-53.

[16] Davis, J. R. (1995). Tool Materials. ASM Speciality Handbook, ASM International.

[17] Lo, S. P. (2000). An analysis of cutting under different rake angles using the finite element method. Journal of Materials Processing Technology, 105(1-2), 143–151. http://doi.org/10.1016/S0924-0136(00)00650-6

[18] Attanasio, A., Ceretti, E., & Giardini, C. (2013). Analytical models for tool wear prediction during AISI 1045 turning operations. Procedia CIRP, 8, 218–223. http://doi.org/10.1016/j.procir.2013.06.092

[19] Camargo, J. C., Dominguez, D. S., Ezugwu, E. O., & Machado, Á. R. (2014). Wear model in turning of hardened steel with PCBN tool. International Journal of Refractory Metals and Hard Materials, 47, 61–70. http://doi.org/10.1016/j.ijrmhm.2014.06.019

[20] Ceretti, E., Fallböhmer, P., Wu, W. T., & Altan, T. (1996). Application of 2D FEM to chip formation in orthogonal cutting. Journal of Materials Processing Technology, 59(1-2), 169–180. http://doi.org/10.1016/0924-0136(96)02296-0

[21] Felder, E., Montagut, J. L. (1980).Friction and wear during hot forging of steels. Tribology International. pp. 61-68.

[22] Takeyama, H., Murata, T. (1963). Basic investigations on tool wear. Trans. ASME J. Eng. Ind. 85. pp. 33–38.

[23] Usui, E., Hirota, A., Masuko, M. (1978). Analytical prediction of three- dimensional cutting process. Part 3. Cutting temperature and crater wear of carbide tool, Trans. ASME 100. pp. 222–228.

[24] Luo, X., Cheng, K., Holt, R., & Liu, X. (2005). Modeling flank wear of carbide tool insert in metal cutting. Wear, 259(7-12), 1235–1240. http://doi.org/10.1016/j.wear.2005.02.044

[25] Childs, T.H.C., Maekawa, K., Obikawa, T., Yamane, Y. (2000). Metal Cutting: Theory and Applications, Arnold, London, p. 77.

[26] Schmidt, C., Frank, P., Weule, H., Schmidt, J, Yen, Y.C., Altan, T. (2003). Tool wear prediction and verification in orthogonal cutting, in: Proceeding of Sixth CIRP International Workshop on Modeling of Machining Operations, Hamilton, Canada.

[27] Pálmai, Z. (2013). Proposal for a new theoretical model of the cutting tool's flank wear. Wear, 303(1-2), 437–445
http://doi.org/10.1016/j.wear.2013.03.025

[28] Ernst H, Merchant ME. (1941) Chip formation, friction and high quality machined surfaces. Surface treatment of metals. Am Soc Met 29:299–378

[29] Lee EH, Shaffer BW. (1951) The theory of plasticity applied to a problem of machining. Trans ASME—J Appl Mech 18:405–413

[30] Fang, N. (2003). Slip-line modeling of machining with a rounded-edge tool - Part II: Analysis of the size effect and the shear strain-rate. Journal of the Mechanics and Physics of Solids, 51(4), 743–762. http://doi.org/10.1016/S0022-5096(02)00061-3

[31] Arrazola, P. J., Özel, T., Umbrello, D., Davies, M., & Jawahir, I. S. (2013). Recent advances in modelling of metal machining processes. CIRP Annals -Manufacturing Technology, 62(2), 695–718. http://doi.org/10.1016/j.cirp.2013.05.006

[32] Abboud, E., Shi, B., Attia, H., Thomson, V., & Mebrahtu, Y. (2013). Finite Element-based Modeling of Machining-induced Residual Stresses in Ti-6Al-4V under Finish Turning Conditions. Procedia CIRP, 8, 63–68. http://doi.org/10.1016/j.procir.2013.06.066

[33] Arulkirubakaran, D., Senthilkumar, V., & Kumawat, V. (2016). Effect of micro-textured tools on machining of Ti–6Al–4V alloy: An experimental and numerical approach. International Journal of Refractory Metals and Hard Materials, 54, 165–177. http://doi.org/10.1016/j.ijrmhm.2015.07.027

[34] Chiappini, E., Tirelli, S., Albertelli, P., Strano, M., & Monno, M. (2014). On the mechanics of chip formation in Ti–6Al–4V turning with spindle speed variation. International Journal of Machine Tools and Manufacture, 77, 16–26. http://doi.org/10.1016/j.ijmachtools.2013.10.006

[35] Hadzley, A. B. M., Izamshah, R., Sarah, A. S., & Fatin, M. N. (2013). Finite Element Model of Machining with High Pressure Coolant for Ti-6Al-4V Alloy. Procedia Engineering, 53, 624–631. http://doi.org/10.1016/j.proeng.2013.02.080

[36] Kalyan, C., & Samuel, G. L. (2015). Cutting mode analysis in high speed finish turning of AlMgSi alloy using edge chamfered PCD tools. Journal of Materials Processing Technology, 216, 146–159. http://doi.org/10.1016/j.jmatprotec.2014.09.003

[37] Lei, S., Shin, Y. C., & Incropera, F. P. (1999). Thermo-mechanical modeling of orthogonal machining process by finite element analysis. International Journal of Machine Tools and Manufacture, 39, 731–750. http://doi.org/10.1016/S0890-6955(98)00059-5

[38] Li, K., Gao, X. L., & Sutherland, J. W. (2002). Finite element simulation of the orthogonal metal cutting process for qualitative understanding of the effects of crater wear on the chip formation process. Journal of Materials Processing Technology, 127(3), 309–324. http://doi.org/10.1016/S0924-0136(02)00281-9

[39] List, G., Sutter, G., Bi, X. F., Molinari, A., & Bouthiche, A. (2013). Strain, strain rate and velocity fields determination at very high cutting speed. Journal of Materials Processing Technology, 213(5), 693–699. http://doi.org/10.1016/j.jmatprotec.2012.11.021

[40] Liu, K., & Melkote, S. N. (2007). Finite element analysis of the influence of tool edge radius on size effect in orthogonal micro-cutting process. International Journal of Mechanical Sciences, 49(5), 650–660. http://doi.org/10.1016/j.ijmecsci.2006.09.012

[41] Mamalis, C., & Paulo Davim, J. (2010). Finite element modelling of machining of AISI 316 steel: Numerical simulation and experimental validation. Simulation Modelling Practice and Theory, 18(2), 139–156. http://doi.org/10.1016/j.simpat.2009.10.001

[42] Davim, J. P., Maranhão, C., Jackson, M. J., Cabral, G., & Grácio, J. (2008). FEM analysis in high speed machining of aluminium alloy (Al7075-0) using polycrystalline diamond (PCD) and cemented carbide (K10) cutting tools. International Journal of Advanced Manufacturing Technology, 39(11-12), 1093–1100. http://doi.org/10.1007/s00170-007-1299-y

[43] Shet, C., & Deng, X. (2003). Residual stresses and strains in orthogonal metal cutting. International Journal of Machine Tools and Manufacture, 43(6), 573–587. http://doi.org/10.1016/S0890-6955(03)00018-X

[44] Thepsonthi, T., & Özel, T. (2015). 3-D finite element process simulation of micro-end milling Ti-6Al-4V titanium alloy: Experimental validations on chip flow and tool wear. Journal of Materials Processing Technology, 221, 128–145. http://doi.org/10.1016/j.jmatprotec.2015.02.019

[45] Filice, L., Micari, F., Settineri, L., & Umbrello, D. (2007). Wear modelling in mild steel orthogonal cutting when using uncoated carbide tools. Wear, 262(5-6), 545–554. http://doi.org/10.1016/j.wear.2006.06.022

[46] Hosseinkhani, K., & Ng, E. (2013). Analysis of the Cutting Mechanics Under the Influence of Worn Tool Geometry. Procedia CIRP, 8, 117–122. http://doi.org/10.1016/j.procir.2013.06.075

[47] Kumar, V., Eakambaram, A., & Arivazhagan, A. (2014). FEM Analysis to Optimally Design End Mill Cutters for Milling of Ti-6Al-4V. Procedia Engineering, 97, 1237–1246. http://doi.org/10.1016/j.proeng.2014.12.402

[48] Salvatore, F., Saad, S., & Hamdi, H. (2013). Modeling and simulation of tool wear during the cutting process. Procedia CIRP, 8, 305–310. http://doi.org/10.1016/j.procir.2013.06.107

[49] Lin, Z.-C., & Lin, Y.-Y. (1999). Fundamental modeling for oblique cutting by thermo-elastic-plastic FEM. International Journal of Mechanical Sciences, 41, 941–965. http://doi.org/10.1016/S0020-7403(98)00067-8

[50] Liu, R., Melkote, S., Pucha, R., Morehouse, J., Man, X., & Marusich, T. (2013). An enhanced constitutive material model for machining of Ti–6Al–4V alloy. Journal of Materials Processing Technology, 213(12), 2238–2246. http://doi.org/10.1016/j.jmatprotec.2013.06.015

[51] Owen, D. R. J., & Vaz, M. (1999). Computational techniques applied to high-speed machining under adiabatic strain localization conditions. Computer Methods in Applied Mechanics and Engineering, 171(3-4), 445–461. http://doi.org/10.1016/S0045-7825(98)00220-5

[52] Özel, T. (2006). The influence of friction models on finite element simulations of machining. International Journal of Machine Tools and Manufacture, 46(5), 518–530. http://doi.org/10.1016/j.ijmachtools.2005.07.001

[53] Patil, S., Joshi, S., Tewari, A., & Joshi, S. S. (2014). Modelling and simulation of effect of ultrasonic vibrations on machining of Ti6Al4V. Ultrasonics, 54(2), 694–705. http://doi.org/10.1016/j.ultras.2013.09.010

[54] Umbrello, D. (2008). Finite element simulation of conventional and high speed machining of Ti6Al4V alloy. Journal of Materials Processing Technology, 196(1-3), 79–87. http://doi.org/10.1016/j.jmatprotec.2007.05.007

[55] Wang, Z., Nakashima, S., & Larson, M. (2014). Energy Efficient Machining of Titanium Alloys by Controlling Cutting Temperature and Vibration. Procedia CIRP, 17, 523–528. http://doi.org/10.1016/j.procir.2014.01.134

[56] Bil, H., Kılıç, S. E., & Tekkaya, A. E. (2004). A comparison of orthogonal cutting data from experiments with three different finite element models. International Journal of Machine Tools and Manufacture, 44(9), 933–944. http://doi.org/10.1016/j.ijmachtools.2004.01.016

[57] Klocke, F. (2010). Manufacturing Processes 1 Cutting. Springer-Verlag Berlin Heidelberg.

[58] Harewood, F. J. & McHugh, P. E. (2007). Comparison of the implicit and explicit finite element methods using crystal plasticity. Computational Materials Science, 39(2), 481–494. http://doi.org/10.1016/j.commatsci.2006.08.002

[59] Houcque, D. (2008). Applications of matlab: Ordinary differential equations (ode).Robert R. McCormick School of Engineering and Applied Science – Northwestern University, pages 1–12.

[60] Sun, J. S. Lee, K. H. & Lee, H. P. (2000). Comparison of implicit and explicit finite element methods for dynamic problems. Journal of Materials Processing Technology, 105(1-2), 110–118. http://doi.org/10.1016/S0924-0136(00)00580-X

[61] Yang, D. Y. Jung, D. W. Song, I. S. Yoo, D. J. & Lee, J. H. (1995). Comparative investigation into implicit, explicit, and iterative implicit/explicit

schemes for the simulation of sheet-metal forming processes. Journal of Materials Processing Technology, 50(1-4), 39–53. http://doi.org/10.1016/0924-0136(94)01368-B

[62] Shen R. Wu, Lei Gu, (2012). Introduction to the Explicit Finite Element Method for Nonlinear Transient Dynamics. Wiley-Blackwell.

[63] Rebelo, N. Nagtegaal, J.C. Taylor, L.M. (1992), Comparison of implicit and explicit finite element methods in the simulation of metal forming processes. Numerical Methods in Industrial Forming Processes.

[64] Hibbitt, Karlsson, (1997). ABAQUS Theory Manual Version 5.8.Hibbitt, Karlsson & Sorensen.

[65] Kim, J. Kang, Y.H. Choi, H.-H. Hwang, S.-M. Kang, B.S. (2002). The International Journal of Advanced Manufacturing Technology 20 (6) 407–413.

[66] Ghosh, S., & Kikuchi, N. (1991). An arbitrary Lagrangian-Eulerian finite element method for large deformation analysis of elastic-viscoplastic solids. Computer Methods in Applied Mechanics and Engineering, 86(2), 127–188. http://doi.org/10.1016/0045-7825(91)90126-Q

[67] Donea, J., Huerta, A., Ponthot, J., & Rodriguez-Ferran, A. (2004). Arbitrary Lagrangian–Eulerian Methods. Encyclopedia of Computational Mechanics Volume 1: Fundamentals, 413–436.

[68] Qiu, G., Henke, S., & Grabe, J. (2011). Application of a Coupled Eulerian-Lagrangian approach on geomechanical problems involving large deformations. Computers and Geotechnics, 38(1), 30–39. http://doi.org/10.1016/j.compgeo.2010.09.002

[69] Khoei, a. R., Anahid, M., & Shahim, K. (2008). An extended arbitrary Lagrangian–Eulerian finite element method for large deformation of solid mechanics. Finite Elements in Analysis and Design, 44(August), 401–416. http://doi.org/10.1016/j.finel.2007.12.005

[70] Pop B, Bianca A, Lobontiu M (2015). The finite element analysis approach in metal cutting [J]. Academic Journal of Manufacturing Engineering,13(1).

[71] Kilicaslan, C. (2009). Modelling and Simulation of Metal Cutting By Finite Element Method. Strain,86.

[72] Kohir, V , Dundur, S(2014). Finite Element Simulation to study the effect of flank wear land inclination on Cutting forces and temperature distribution in orthogonal machining, 1(1), 30–42.

[73] Zouhar, J., & Piska, M. (2008). Modelling the orthogonal machining process using cutting tools with different geometry. MM Science Journal, 49–52. Retrieved from http://scholar.google.com/scholar?hl=en&btnG=Search&q=intitle:MODELLING+THE+ORTHOGONAL+MACHINING+PROCESS+USING+CUTTING+TOOLS+WITH+DIFFERENT+GEOMETRY#0\nhttp://scholar.google.com/scholar?hl=en&btnG=Search&q=intitle:Modelling+the+orthogonal+machining+proces

[74] ASM International 10th Ed. (1990).Metals Handbook, Vol.2 - Properties and Selection: Nonferrous Alloys and Special-Purpose Materials.

[75] Brian Smith (2003).The Boeing 777.Advanced Materials & Processes, Volume 161, Issue 9, September 2003 (ASM International)

[76] Glbson, G.E. (Boeing) (2008), “Fracture Analysis for bondlines and interfaces of composite structures” 4th international conference of composite testing & model identification

[77] Carl T Olofson, Arnold F Gerds, Francis W Boulger, John A Gurklis, Battelle Memorial Inst Columbus Oh Defense Metals Information Center (1965). Machinability of titanium and its alloys relative to other selected materials.

[78] Johnson, G. R., & Cook, W. H. (1983). A constitutive model and data for metals subjected to large strains, high strain rates and high

temperatures. 7th International Symposium on Ballistics. http://doi.org/10.1038/nrm3209

[79] Chen, G., Ren, C., Yang, X., Jin, X., & Guo, T. (2011). Finite element simulation of high-speed machining of titanium alloy (Ti-6Al-4V) based on ductile failure model. International Journal of Advanced Manufacturing Technology, 56(9-12), 1027–1038. http://doi.org/10.1007/s00170-011-3233-6

[80] Sima, M., & Özel, T. (2010). Modified material constitutive models for serrated chip formation simulations and experimental validation in machining of titanium alloy Ti–6Al–4V. International Journal of Machine Tools and Manufacture, 50(11), 943–960. http://doi.org/10.1016/j.ijmachtools.2010.08.004

[81] Steinberg, D. J., Cochran, S. G., & Guinan, M. W. (1980). A constitutive model for metals applicable at high-strain rate. Journal of Applied Physics, 51(3), 1498–1504. http://doi.org/10.1063/1.327799

[82] Steinberg, D. J., & Lund, C. M. (1989). A constitutive model for strain rates from 10-4 to 106 s-1. Journal of Applied Physics, 65(1989), 1528–1533. http://doi.org/10.1063/1.342968

[83] Banerjee, B. (2005). An evaluation of plastic flow stress models for the simulation of high-temperature and high-strain-rate deformation of metals. arXiv:cond-mat/0512466.

[84] Hoge, K.G.; Mukherjee, A.K. (1977). The temperature and strain rate dependence of the flow stress of tantalum. Journal of Materials Science 12 (8): pp 1666–1672. http://doi.org/10.1007/BF00542818

[85] Orlikowski, D., Correa, A. a., Schwegler, E., Klepeis, J. E., Elert, M., Furnish, M. D., Nguyen, J. (2007). A Steinberg-Guinan Model for High-Pressure Carbon: Diamond Phase. AIP Conference Proceedings, 955, 247–250. http://doi.org/10.1063/1.2833022

[86] Armstrong, R. W., & Zerilli, F. J. (1988). Dislocation Mechanics Based Analysis of Material Dynamics Behavior. Le Journal de Physique Colloques, 49, C3–529–534. http://doi.org/10.1051/jphyscol:1988374

[87] Zerilli, F. J., Armstrong, R.W., (1993). Constitutive relations for the plastic deformation of metals. In: High-Pressure Science and Technology. American Institute of Physics, Colorado Springs, Colorado, pp. 989–992

[88] Zerilli, F. J. (2004). Dislocation Mechanics – Based Constitutive Equations. Metallurgical and Materials Transactions A, 35(September), 2547–2555. http://doi.org/8B48024755702CD66CE2185E9E2A7075

[89] Abed, F. H., & Voyiadjis, G. Z. (2005). A consistent modified Zerilli-Armstrong flow stress model for BCC and FCC metals for elevated temperatures. Acta Mechanica, 175(1-4), 1–18. http://doi.org/10.1007/s00707-004-0203-1

[90] LSTC. (2014). LS-DYNA Keyword User's Manual Volume II R7.1 (Vol. II).

[91] Mabrouki, T., Courbon, C., Zhang, Y., Rech, J., Nélias, D., Asad, M., … Salvatore, F. (2016). Some insights on the modelling of chip formation and its morphology during metal cutting operations. Comptes Rendus Mécanique, 344(4-5), 335–354. http://doi.org/10.1016/j.crme.2016.02.003

[92] Sui, S. C., & Feng, P. F. (2015). The influences of tool wear on Ti6Al4V cutting temperature and burn defect. The International Journal of Advanced Manufacturing Technology, 2–9. http://doi.org/10.1007/s00170-015-8093-z

[93] Hambli, R. (2001). Blanking tool wear modeling using the finite element method. International Journal of Machine Tools & Manufacture 41 (2001) 1815–1829, 41, 1815–1829.

[94] Toenshoff, H. K., & Denkena, B. (2013). Basics of Cutting and Abrasive Processes, 21–37. http://doi:10.1007/978-3-642-33257-9

[95] Chattopadhyay, A.K. (2005.). Machining Mechanism of chip formation.

[96] Astakhov, V. P., & Shvets, S.V., Osman, M. O. M. (1997). Chip structure classification based on mechanics of its formation. Journal of Materials Processing Technolog, 71, 247–257. http://doi.org/10.1016/S0924-0136(97)00081-2

[97] Hua, J., & Shivpuri, R. (2004). Prediction of chip morphology and segmentation during the machining of titanium alloys. Journal of Materials Processing Technology, 150(1-2), 124–133. http://doi.org/10.1016/j.jmatprotec.2004.01.028

[98] Calamaz, M., Coupard, D., & Girot, F. (2008). A new material model for 2D numerical simulation of serrated chip formation when machining titanium alloy Ti–6Al–4V. International Journal of Machine Tools and Manufacture, 48(3-4), 275–288. http://doi.org/10.1016/j.ijmachtools.2007.10.014

[99] Sun, S., Brandt, M., & Dargusch, M. S. (2009). Characteristics of cutting forces and chip formation in machining of titanium alloys. International Journal of Machine Tools and Manufacture, 49(7-8), 561–568. http://doi.org/10.1016/j.ijmachtools.2009.02.008

[100] Zone-Chin Lin, S.-P. Lo. (1997). Ultra-precision orthogonal cutting simulation for oxygen-free high-conductivity copper. Materials Processing Technology, 65, 281–291. http://doi.org/10.1016/S0924-0136(96)02416-8

[101] Shatla, M., Kerk, C. and Altan, T. (2001). Process Modelling in Machining. Part II: Validation and Applications of the Determined Flow Stress Data. International Journal of Tools and Manufacturing 41: 1659-1680.

[102] Wang, F., Zhao, J., Zhu, N., & Li, Z. (2015). A comparative study on Johnson-Cook constitutive modeling for Ti-6Al-4V alloy using automated ball indentation (ABI) technique. Journal of Alloys and Compounds, 633, 220–228. http://doi.org/10.1016/j.jallcom.2015.01.284

[103] Kay, G. (2003), U.S. Lawrence Livermore National Laboratory, ReportDOT/FAA/AR-03/ 57.

[104] Zhang, Y., Outeiro, J. C., & Mabrouki, T. (2015). On the selection of Johnson-Cook constitutive model parameters for Ti-6Al-4V using three types of numerical models of orthogonal cutting. Procedia CIRP, 31, 112–117. http://doi.org/10.1016/j.procir.2015.03.052

[105] Liu, S (2007) iFEM simulation and experiment research of cutting temperature and force in orthogonal cutting of titanium alloys (in Chinese). Dissertation, Nanjing University of Aeronautics and Astronautics, Nanjing.

[106] Filippi, E. (2015). Finite element prediction of the tool wear influence in Ti6Al4V machining, 31, 124–129. http://doi.org/10.1016/j.procir.2015.03.056

[107] Armendia, M., Garay, A., Iriarte, L. M., & Arrazola, P. J. (2010). Comparison of the machinabilities of Ti6Al4V and TIMETAL?? 54M using uncoated WC-Co tools. Journal of Materials Processing Technology. http://doi.org/10.1016/j.jmatprotec.2009.08.026

[108] Nalbant, M., Altin, A., & GÖkkaya, H. (2007). The effect of coating material and geometry of cutting tool and cutting speed on machinability properties of Inconel 718 super alloys. Materials and Design, 28(5), 1719–1724. http://doi.org/10.1016/j.matdes.2006.03.003

[109] Asano, K. (2015). Turning Machinability of Short Alumina Fiber Reinforced Aluminum Alloy Composite Using Carbide Tool, 56(7), 1120–1126.

[110] Sui, S., & Feng, P. (2016). Investigation on generation and features of burn defect in Ti6Al4V milling. The International Journal of Advanced Manufacturing Technology. http://doi.org/10.1007/s00170-016-8461-3

APPENDICES

Appendix A Simulation results for different process parameters

Table A-1 Simulation results using the sharp tool and 0.3mm cutting depth

Cutting speed (m/min) / Results	5	15	30
Cutting force (N)	272	340	346
Maximum temperature on cutting tool (℃)	235	324	446
Maximum von-miss stress on cutting tool (Gpa)	1.535	1.592	1.606

Table A-2 Simulation results using the sharp tool and 0.5mm cutting depth

Cutting speed (m/min) / Results	5	15	30
Cutting force (N)	463	557	577
Maximum temperature on cutting tool (℃)	286	391	527
Maximum von-miss stress on cutting tool (Gpa)	1.583	1.513	1.506

Table A-3 Simulation results using the sharp tool and 1mm cutting depth

Cutting speed (m/min) / Results	5	15	30
Cutting force (N)	883	957	998
Maximum temperature on cutting tool (℃)	367	482	633
Maximum von-miss stress on cutting tool (Gpa)	1.782	1.626	1.625

Table A-4 Simulation results using the R0.05 tool and 0.3mm cutting depth

Cutting speed (m/min) / Results	5	15	30
Cutting force (N)	294	364	354
Maximum temperature on cutting tool (℃)	289	412	557
Maximum von-miss stress on cutting tool (Gpa)	1.457	2.097	1.453

Table A-5 Simulation results using the R0.05 tool and 0.5mm cutting depth

Cutting speed (m/min) / Results	5	15	30
Cutting force (N)	487	564	553
Maximum temperature on cutting tool (℃)	335	427	573
Maximum von-miss stress on cutting tool (Gpa)	1.387	2.171	2.165

Table A-6 Simulation results using the R0.05 tool and 1mm cutting depth

Cutting speed (m/min) / Results	5	15	30
Cutting force (N)	883	957	998
Maximum temperature on cutting tool (℃)	367	482	633
Maximum von-miss stress on cutting tool (Gpa)	1.782	1.626	1.625

Table A-7 Simulation results using the R0.1 tool and 0.3mm cutting depth

Cutting speed (m/min) / Results	5	15	30
Cutting force (N)	316	378	364
Maximum temperature on cutting tool (℃)	331	452	592
Maximum von-miss stress on cutting tool (Gpa)	1.563	2.104	2.165

Table A-8 Simulation results using the R0.1 tool and 0.5mm cutting depth

Cutting speed (m/min) / Results	5	15	30
Cutting force (N)	518	602	575
Maximum temperature on cutting tool (℃)	386	468	621
Maximum von-miss stress on cutting tool (Gpa)	1.383	1.844	2.134

Table A-9 Simulation results using the R0.1 tool and 1mm cutting depth

Cutting speed (m/min) / Results	5	15	30
Cutting force (N)	1002	1168	1152
Maximum temperature on cutting tool (℃)	457	589	731
Maximum von-miss stress on cutting tool (Gpa)	1.635	1.522	1.435

Appendix B Simulation results for different tool wear

Table B-1 Simulation results for flank wear

FLANK WEAR (mm)	0	0.05	0.1	0.15	0.2	0.25	0.3
Cutting force (N)	120	131	140	149	161	170	183
Maximum temperature on cutting tool (℃)	509	584	663	715	781	846	925
Maximum stress on cutting tool (GPA)	1.82	1.59	1.671	2.14	1.73	1.85	1.755

Table B-2 Simulation results when crater wear is 10 μm from tool tip

Crater wear KT(mm)	0.005	0.01	0.02	0.04
Cutting force (N)	145	140	115	140
Maximum temperature on cutting tool (℃)	535	482	373	417
Maximum stress on cutting tool (GPA)	1.809	1.955	1.716	1.898

Table B-3 Simulation results when crater wear is from tool tip

Crater wear KT (mm)	0.005	0.01	0.02	0.04
Cutting force(N)	140	147	110	135
Maximum temperature on cutting tool (℃)	523	567	382	372
Maximum stress on cutting tool (GPA)	1.842	1.913	1.598	1.838